UNIVERSITEIT VAN PRETORIA
UNIVERSITY OF PRETORIA
YUNIBESITHI YA PRETORIA

Performance Measures of an Active, Small Scale Solar Basin Still in terms of Production Cost and Energy Efficiency

Emmanuel Adu-Awuku

Performance Measures of an Active, Small Scale Solar Basin Still in terms of Production Cost and Energy Efficiency

Author: Emmanuel Adu-Awuku

Supervisor: Mr PW Sonnendecker

Dissertation submitted in partial fulfilment of the requirements for the degree

Master of Engineering

(Chemical Engineering)

in the

Department of Chemical Engineering

Faculty of Engineering, Built Environment, and Information Technology

University of Pretoria

January 2024

Performance Measures of an Active, Small Scale Solar Basin Still in terms of Production Cost and Energy Efficiency

Abstract

The research investigated the characterisation of a cost-effective active solar still by implementing active solar still recommendations suggested by Marais (2018) and external condenser design improvements identified in the research work. Marais' (2018) still variation 3 was used to design a solar still to improve still productivity performance:

- By using an external condenser that will reduce the available condensation area and drive condensation away from the cover surface.
- By using active fluid flow to circulate humid air and, or water through the solar still.
- By reducing energy losses of the cover surface and energy accumulation of the back wall.

Meeting the main objective of improving still productivity involved selecting a cover surface more energy efficient than the 5 mm PMMA cover surface, characterising and improving performance of the external condensers, and field testing the active solar still fitted with the best performing external condenser.

The cover surface experiments were performed in a polystyrene solar still – this allowed quick and easy repeatability of experiments. The comparison between 4 mm thick single pane glass surface and polymethyl methacrylate surface (PMMA) showed single pane glass and double pane glass to give better performance; the single pane glass produced water at a rate of 4.58 $L.day^{-1}.m^{-2}$, and 2.38 $L.day^{-1}.m^{-2}$, respectively – 275 % and 95 % more than the PMMA surface. The double pane glass surface produced 4% higher water temperatures compared to single pane glass – concluding that using a double pane glass surface instead of the PMMA surface will reduce the energy loss experienced.

The external condensers were characterised in a controlled environment, by using a heated water bath. Forced convection cooling gave better yield performance than the natural cooling state. By using the heat sink with forced convection cooling as baseline, the tube banks showed a yield improvement range of between 140 % and 240 %. Tube banks with diameter of 9.5 mm outperformed the 12 mm diameter tube banks; for natural cooling, the performance gap was 14 % while for the forced convection cooling, the performance gap was 45 %. However, the 12.7 mm tube bank gave better steady state heat transfer and so was preferred for the active solar still experiments as reducing heat losses was one of the sub-objectives.

The double pane glass surface and the 12.7 mm tube bank under forced convection cooling were the best performing cover surface and heat exchanger, respectively, to be used on the active solar still. The active solar still was designed to implement internal humid-air circulation, induced by an air fan, to move humid-air through the external tube bank condenser, while a water pump is used to circulate the water body across the still backwall. The active solar still was run in both natural and forced convection cooling modes; the forced convection cooling mode showed faster condensation rates on all occasions. For the active solar still experiments, only forced convection cooling experiments were reported.

The active solar still experiments were run in three modes of circulation:

- **Humid air circulation** where only the external condenser air fan is operational,
- **Water circulation** where only the water pump is operational, and
- A combination of **humid air and water circulation** where both devices are operational.

The water circulation mode was able to show yield performance but was limited due to the rotating motion of the water body reducing the efficiency of solar absorption. The water circulation produced water at a rate of 1.61 $L.day^{-1}.m^{-2}$ compared to the rate of 4.91 $L.day^{-1}.m^{-2}$ for the reference still – the reference performed ~3 times better than the active solar still scenario with water circulation. The water circulation mode was excluded from experimentation.

A trial run of a heat exchanger fitted to the active solar still (no form of circulation) showed poor yield and energy efficiency performance. Implementing humid air circulation would have increased the energy loss across the active solar still and heat exchanger. The humid air circulation mode was also excluded from experimentation. The reference case produced a cheaper unit cost per litre value of R 0.52/l compared to R 2.20/l for the active solar still. The ~R 700 (40 %) cost investment resulted in a 3.00 $L.day^{-1}.m^{-2}$ (67 %) reduction in water productivity – the active solar still was economically unfavourable. The active solar still was cheaper than water market rates of R 4.40/l but not of municipal rates of 0.67 c/l.

The reference still also performed better than the benchmark still (Marais, 2018), producing water at R 0.40/l cheaper (45 %), 0.3 $L.day^{-1}.m^{-2}$ faster (10%), and ~40 % more energy efficient. The reference solar still was the best design for small-scale solar desalination of water.

Acknowledgements

The financial assistance from the University of Pretoria Chemical Engineering Department is hereby acknowledged. Opinions expressed and conclusions stated are those of the author and are not necessarily attributed to the UP Chemical Engineering Department.

The author would also like to express his gratitude and appreciation to:

My research supervisor Paul Sonnendecker for his support and guidance in putting together and simplifying a complex piece of work.

Mom, Dad, Eric, and Maggie for being an immense source of inspiration.

Contents

List of Figures

List of Tables

Nomenclature

A	area, m^2
c_p	specific heat capacity of a liquid, J/kg.K
c_v	specific heat capacity of a gas, J/kg
E	energy, J
h	convection heat transfer coefficient, $W.m^2.K$
he	external convection heat transfer coefficient, $W.m^2.K$
H	enthalpy of vapourisation, KJ/kg
k	thermal conductivity, W/m.K
m	mass flowrate, kg or average annual productivity, L
Nu	Nusselt number
Pr	Prandtl number
Q	heat flow, W
Re	Reynolds number
t	time, s
T	temperature, °C
U	internal energy, J
v	velocity, m/s

Greek symbols

α	absorptivity
Δ	difference between two end points
ε	emissivity factor
μ	viscosity, kg/m.s
ρ	density, kg/m^3
σ	Stefan-Boltzmann constant, $W/m^2.K^4$
τ	transmissivity
∞	ambient surroundings

Subscripts

cond	condensation, conduction
D	diagonal
e	exit
f	final
i	initial, inlet
ref	reflection
s, sur	surface
T	transverse
un	unaccounted energy

1. Introduction

Most African countries have rural or remote locations with a limited supply of clean water and reliable electricity (World Bank, 2017; Kuik, et al., 2011; Wohlgemuth, 2006). In cases where the resource is present, it is available only to a segment of the population, its supply is intermittent, or in extreme cases, there is no infrastructure to provide the resource to consumers (MIT, 2017; Wohlgemuth, 2006). The population of these locations are forced to rely on other, more expensive options to meet their water and electricity needs (Purvis, 2016).

Most rural locations in Africa experience arid or semiarid climate and have a high solar radiation potential (World Bank, 2020). The solar radiation can be converted into useful energy either on a micro (solar lamps) or mini scale (solar panels). There exists an opportunity to provide a distilled water solution to these rural locations that uses an abundantly available energy source – in this case, solar energy – to remain off-grid (Grimshaw & Lewis, 2010; Farooquee, 2017). Solar energy presents itself as a feasible energy source; it is readily available, will improve the sustainability of implementing a water purification solution, and is experiencing decreasing electricity conversion costs. This is also seen in literature where desalination units mainly operate on solar energy (Dehghan, et al., 2015; Rahbar & Esfahani, 2013; Xie, et al., 2015).

African countries register different levels of solar radiation potential based on their distance from the equator and on which side of the equator they fall. The top five global solar radiation locations, measured according to the average daily global horizontal irradiation, fall 30° north and south of the equator and are: 1. Yemen (6.47 kWh/m^2), 2. Namibia (6.40 kWh/m^2), 3. Sudan (6.32 kWh/m^2), 4. Oman (6.28 kWh/m^2), and 5. Niger (6.26 kWh/m^2) (ESMAP, 2020).

South Africa receives a daily average of 5.6 kWh/m^2 of solar radiation, with a minimum of 4.0 kWh/m^2 and a maximum of 6.4 kWh/m^2 (ESMAP, 2020). South Africa receives solar radiation > 5.0 kWh/m^2 across 75 % of the country with the north-western parts of the country receiving the highest solar radiation (ESMAP, 2020). 33 % of South

Africa's population is classified as rural, occupying 4.40 % of South Africa's land mass; it is important to note that the urban areas also cover 4.40 % of South Africa's land. This translates to a rural population density of 363 people/km^2 – significantly higher than Sub-Saharan Africa's density of 39 people/km^2 – with an average rural household of 4 people (World Bank, 2021; Statista, 2021). This is an important occurrence in the context of South Africa; a significant segment of South Africa's population lives in rural areas with limited water or electricity infrastructure but receive good quality solar radiation. South Africa's drought and desertification challenges have also increased the number of rural [and urban] water-stressed locations across the country (South African Government, 2015) The opportunity to implement a solar-powered water purification solution also applies to South Africa.

Literature presents passive and active basin solar stills as a method to produce clean water from saline or brackish water sources. The basin solar stills can reach a daily water production rate of between 3 and 10 L.m^{-2} (Emad, 2014; Khalifa, et al., 1999; Reddy, et al., 1983; Fath & Hosny, 2002) and energy efficiency between 15 and 25 % (Jones, et al., 2014). This is enough water to cater for just 2 % of the daily water needs of a rural South African household (GreenCape, 2019; United Nations, 2015; Statista, 2021). Ideally, the basin solar still should cater for the daily water needs of the consuming household – for personal hygiene and cooking. This translates to a daily production rate of between 200 to 400 L (GreenCape, 2019; United Nations, 2015). However, the maximum daily production rate that the basin still can theoretically achieve is 9.15 L.m^{-2}, where there are minimal energy losses and the still temperature corresponds to the maximum rate of condensation.

Marais' (2018) research on passive basin solar stills gave a daily average productivity of 2.6 L.m^{-2} and an average energy efficiency of 26 %. To improve the productivity of the solar still Marais (2018) suggests improving the energy utilisation of the solar stills:

- By using an external condenser that will reduce the available condensation area and drive condensation away from the cover surface.
- By using active fluid flow to circulate humid air and, or water through the solar still – making the solar still an active solar still (Fath & Hosny, 2002; Emad, 2014; Kumar, et al., 2016).

- By reducing energy losses of the cover surface and energy accumulation of the back wall.

This is the purpose of the active solar still research – linking directly from Marais' (2018) work, to determine if energy utilisation can be improved by attaching an external condenser surface and active fluid flow system on the passive solar still. While using an external condenser introduces an alternative condensation surface, implementing an active fluid flow system will circulate humid air through the external condenser and water through the solar still. This will keep the cover surface free from condensation, allowing a direct path for solar radiation to fall onto the base of the solar still. Using an external condenser reduces the available condensation area as the cover surface solely becomes an entry point for solar radiation.

Additionally, reducing energy losses of the cover surface and energy accumulation of the back wall will make more energy available for utilisation. Driving condensation away from the cover surface will reduce cover surface losses by reducing radiation, reflection, and scattering in the solar still (Jones, et al., 2014). There is also an opportunity to reduce energy losses of the cover surface through a material change of the cover surface. Comparing along the optical properties of the cover surface material, a lower emissivity means less energy is emitted as radiation, a higher transmissivity means more radiation is transmitted through the cover surface, and a lower absorptivity means less radiation is absorbed by the cover surface – using a cover surface material with a lower absorptivity, lower emissivity, and higher transmissivity of solar radiation will improve the energy utilisation of the solar still (Ibrahim, et al., 2015). Even as literature (Bhardwaj, et al., 2013; Jones, et al., 2014) shows a single pane glass surface to give a better performance than a polymethyl methacrylate (PMMA) surface, a PMMA surface was used to keep the still simple and durable in its operations. This is an important consideration as deploying the active solar stills in rural locations will mean its use by a low-skilled population and maintenance will not happen frequently. Investigating the cost-based performance of using a single pane glass surface, even with its fragility, might be beneficial to improving energy utilisation of the active solar still.

The energy accumulation of the back wall can be reduced by redirecting energy away from the back wall. Circulating water over the back wall presents an opportunity to simultaneously increase the energy content of the basin water and reduce the energy accumulation of the back wall. The active fluid flow system doubles up as an option to drive condensation away from the cover surface and to redirect energy accumulation from the back wall into the basin water.

The final objective statement reads – increasing the energy utilisation of a passive basin solar still by converting it into an active solar still, by using an external condenser surface and active fluid flow system. The main objective of the research paper was to build an external condenser and active fluid flow system to improve energy utilisation of the passive basin still, with sub-objectives:

1. To characterise the performance of the external condensers in a controlled environment, by using a heated water bath.
2. To improve the performance of the external condensers through physical modifications which included angle orientation of tubes, change in diameter size, exposed length of tubes, and number of tubes.
3. To field test the active solar stills with external condensers attached.
4. To use the active solar still to achieve a water production cost on par with current local municipal water rates of 0.67 c/l, or cheaper (City of uMhlathuze, 2021; Sol Plaatje Municipality, 2021). The water production rate will also be compared against the current distilled water market rate of R4.40/l (Checkers, 2021).
5. The further objectives of the research paper are to reduce:
    a. Energy losses of the 5 mm PMMA cover surface.
    b. Energy accumulation of the back wall.

The active solar still is a direct repurposing of Marais' (2018) work on the experimental optimisation of passive basin stills. The active solar still research transformed the passive basin by attaching an external condenser and implementing fluid flow across the external condenser or solar still. For this reason, the active solar still performance is be limited by the initial performance of Marais' (2018) passive still performance.

The external condensers used for experimentation had a few designs criteria to make them suitable for use on the active solar still:

- Aluminium was used as the major component due to its high conductivity, lightweight, and cost-effective compared to other metals.
- The fluid mover must be strong enough to pump fluid through the external condenser. For this reason, the external condenser must not be longer than 1.5 metres (m) as this would require a stronger, more expensive fluid mover.
- Air flow over the external condenser tubes could significantly impact the performance of the heat exchanger. The tubes were kept at an angle of 26° to promote condensate runoff and natural convection.

Quantifying the heated water bath experiments and active solar experiments is crucial in understanding the effect of the external condenser and fluid flow implementation. This limits the testing of the external condensers in a controlled environment where the only variable affecting performance is the external condenser. Once the external condensers are characterised, the test stills were baselined to give a comparative analysis of field testing of the active solar still experiments against a reference still case. This gives an indication of the cause and magnitude of any performance difference observed.

The capital and operational costs also limit the scope of the active solar still. Due to the need of the still to remain simple and durable, the cost invested in the solar still can only be justified by a performance improvement. The performance criteria – water productivity and energy efficiency – dictates how economically viable the solar still is. At all times, the design of the active solar still must be simple and durable, and cost-competitive to municipal water rates and market water rates.

2. Theory

2.1 Solar Radiation Potential in Africa

As previously noted, most rural locations in Africa occur in arid or semiarid climate and have a high solar radiation potential (showing a minimum daily solar radiation of 5.0 kWh/m^2); this is shown by Figure 1. Figure 1(a) shows the solar radiation distribution across Africa while Figure 1(b) shows the major climate regions across Africa. Although the tropical climate dominates, this is made up mostly of grasslands, semiarid, and desertified land. These locations show a minimum daily solar radiation potential of 5.5 kWh/m^2; as seen on Figure 1(a).

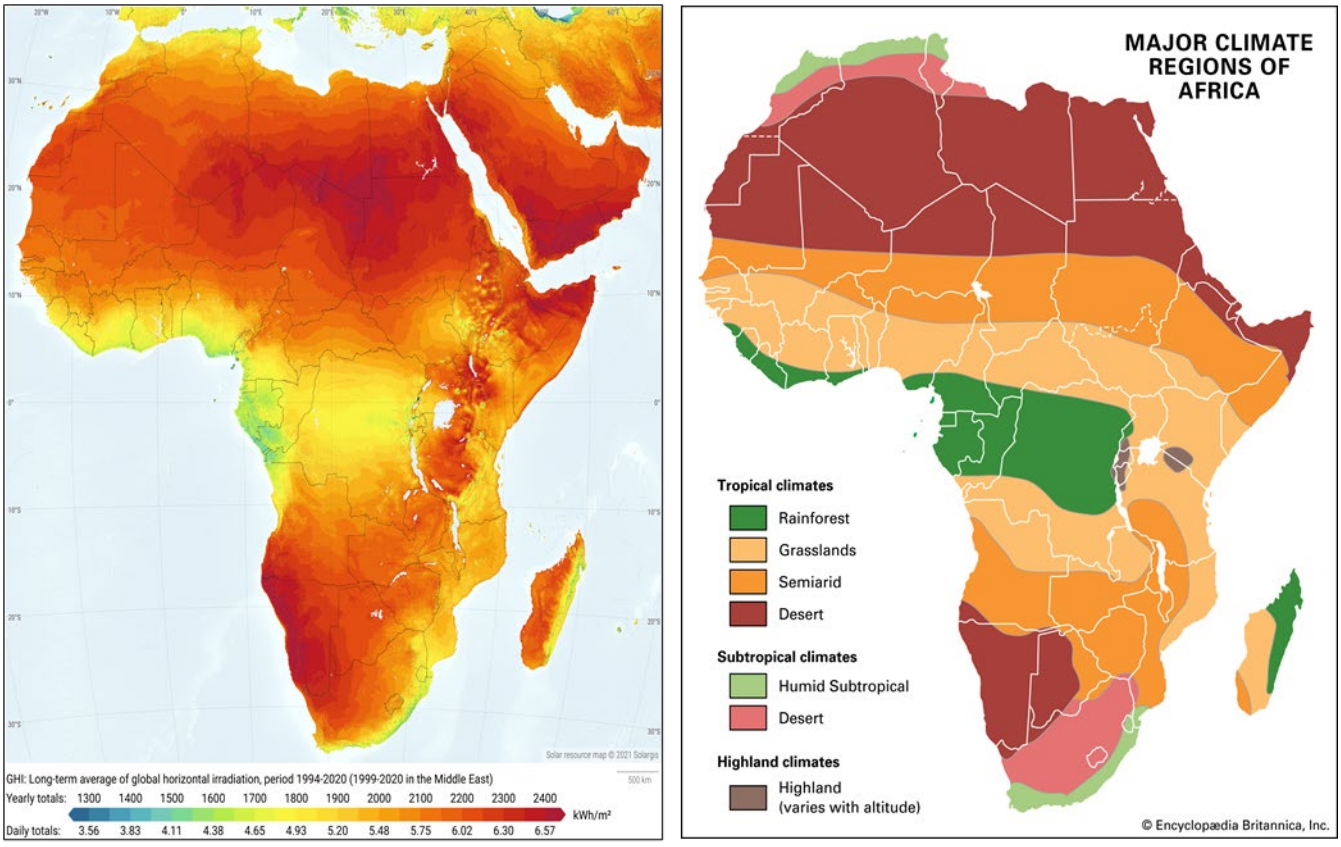

(a) (b)

Figure 1: Map of Africa showing (a) Climate regions and (b) Solar radiation potential (Global Horizontal Irradiation); (World Bank, 2020)

Figure 2 focuses on South Africa's solar radiation potential, showing the Global Horizontal Radiation distribution across the country. A comparative analysis showed that solar radiation > 6.0 kWh/m^2 is estimated to cover 12 to 18 % of the country,

mainly in the north-western parts of the country. This land area also fell into the desertified climate. Solar radiation between 5.6 and 6.0 kWh/m^2 is estimated to cover 28 to 33 % of the country, also falling into the desertified climate. Solar radiation between 5.0 and 5.6 kWh/m^2 is estimated to cover 15 to 23 % of the country; this land coverage included desertified regions and humid subtropical regions, closer to the coastline of South Africa (World Bank, 2020).

South Africa's climate is dominated by desertified climate, estimated to cover more than 80 % of the country while receiving a minimum solar radiation potential of 5.0 kWh/m^2. South Africa fits the hypothesis of having most of its rural locations experiencing arid or semiarid climate and having a solar radiation potential of at least 5.0 kWh/m^2 (World Bank, 2020). In view of rural and semiarid locations having abundant solar radiation, basin solar stills are a potential solution to address water cleanliness and water shortages in rural, semiarid locations.

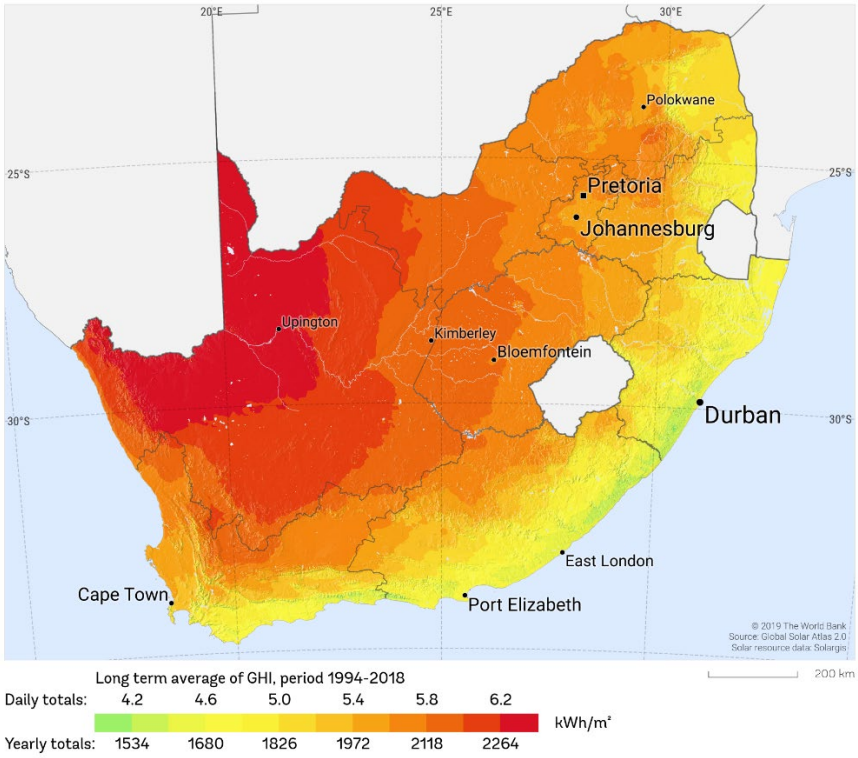

Figure 2: Solar radiation potential (Global Horizontal Irradiation) of South Africa (World Bank, 2020)

2.2 Simple Solar Basin Still

2.2.1 Context of the Simple Solar Basin Still Project

Marais (2018) investigated the experimental optimisation of a simple basin solar still to improve heat loss, evaporation rates, and condensation rates. Three still variations were designed to rate the performance of the solar basin stills based on the different components and features applied per still variation.

The still dimensions used by Marais (2018) were geometrically optimised from literature by:

- Using a ratio of length to width of 2 (Feilizadeh, et al., 2017, p. 163).
- Using the minimum, practical still front height that allowed inclusion of a water collection system and a sufficient angle of inclination for the cover surface condensation to run down (Feilizadeh, et al., 2017, p. 163).
- Using the latitude location of Pretoria as the angle of inclination. This is the location where experiments were run (Singh & Tiwari, 2004).

The solar basin still dimensions are shown below in Figure 3. The still was designed to have a cover surface area of 0.5 m^2.

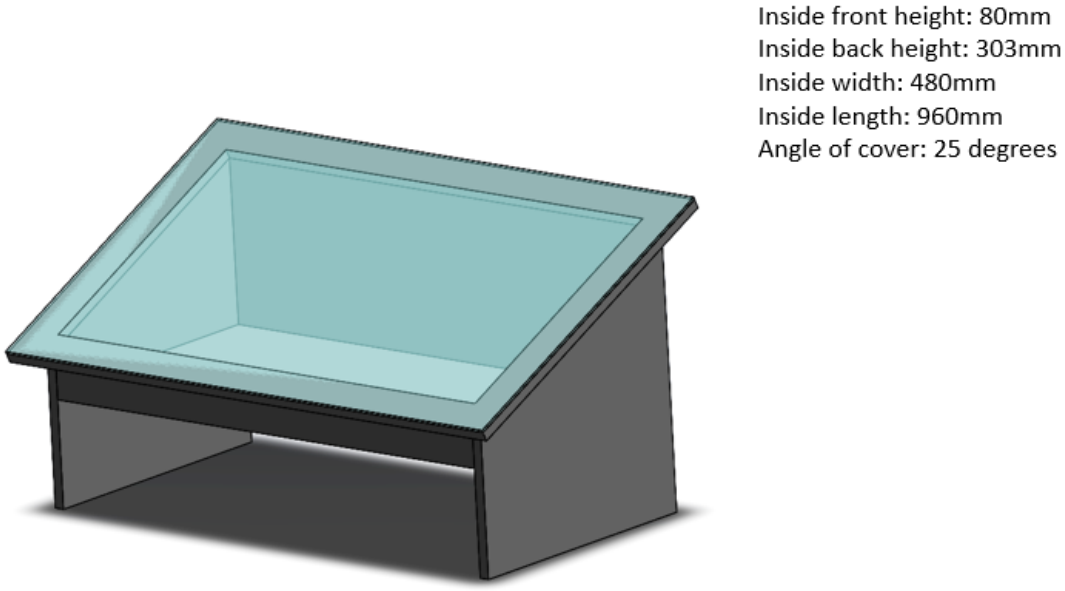

Figure 3: Geometry of Marais' (2018) passive basin solar still

The reference design variation and still variation 1 used 18 millimetres (mm) ShutterPly as still body, 5 mm PMMA as cover surface, polyurethane pond waterproofing sealant as a waterproofing barrier and 26 mm of closed-cell polyurethane for insulation. Additionally, the reference design variation had a PVC Tarpaulin layer added to absorb solar radiation. Still variation 2 was similar to the reference variation, except the polyurethane insulation was increased to 50 mm.

All three still variations were used for the experimental optimisation experiments, with the best features applied to still variation 3 as the most superior still. Still variation 3 used 40 mm extruded polystyrene (Isoboard™) as still body, 5 mm PMMA as cover surface, PVC Tarpaulin as absorber without waterproofing sealant, encased in 18 mm ShutterPly for rigidity and insulation. The final representation of still variation 3 is shown in Figure 4.

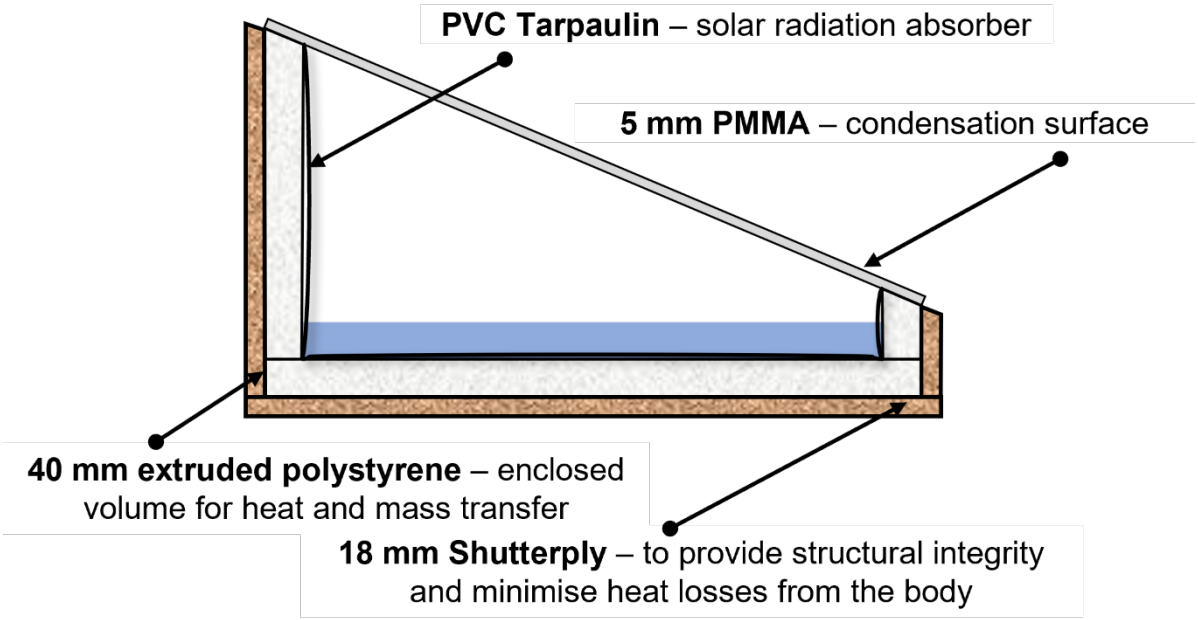

Figure 4: Base design of still variation 3 (Marais, 2018)

2.2.2 Cover Surface Observations

Figure 5 shows the energy balance for still variation 1 (Still 2) and still variation 3 (Still 4). At least 40 % of energy loss escapes through the cover surface in the form radiation, reflection, and convection. The is the largest energy loss term across the still and presents an opportunity to improve the driving force between the water basin

and the cover surface by keeping the cover surface cooler, leading to increased condensation yields.

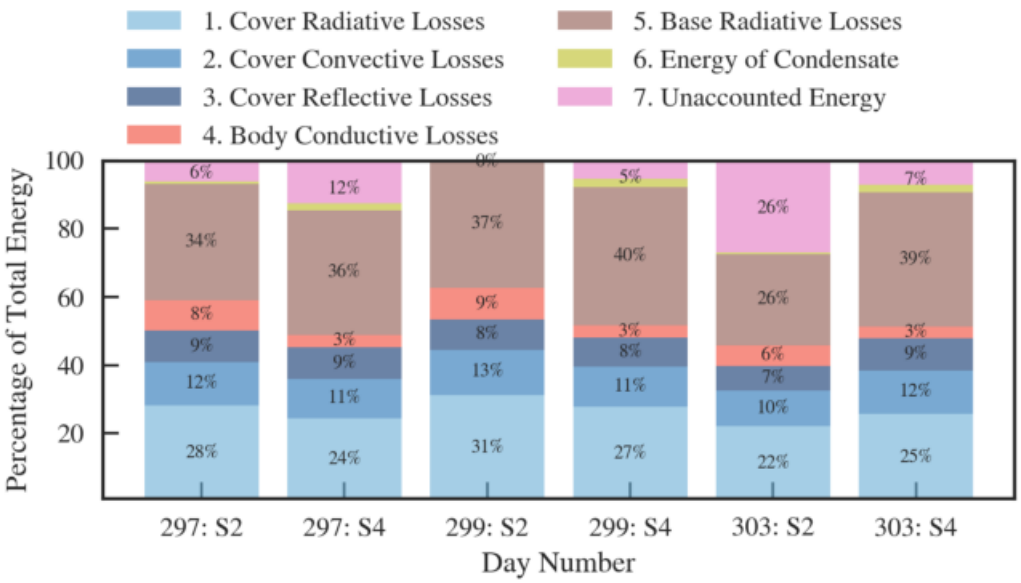

Figure 5: Energy balance analysis for still variations 1 and 3

2.2.2.1 Cover Surface Modifications for the Active Solar Still

Two forms of modifications proposed for the cover surface are:

- By directing condensation away from the cover surface and
- Changing the cover surface to a better performing material – better energy efficiency and condensation adhesion

The option to direct condensation away from the cover surface will be discussed in Sections 2.2.4.1 and 2.3.2. Choosing the appropriate cover surface material is important for the basin still for three reasons. The cover surface material dictates:

- The amount of solar radiation that reaches the base of the solar still,
- The resulting energy losses that occur through radiation, reflection, and convection, and
- The type of adhesion that forms between the cover surface material and the condensed water droplets.

Marais' (2018) did not perform cover surface tests comparing PMMA against other cover surface materials. Although literature shows us that a single pane glass gives a better performance over a PMMA cover surface, PMMA was used to keep the solar

still simple and durable to operate. This is an important consideration as the solar stills are meant for use in rural areas and remote areas which usually have a disconnected logistics network and a low-skilled population. Pilot scale initial tests comparing a 5 mm PMMA to a 4 mm single pane glass cover surface showed inconclusive results. This was the main reason cover surface modifications are discussed for the active solar still experiments, in the case that the cost-based performance improvement of using a single pane glass surface can be justified.

Literature showed that using different cover materials can have a positive effect on still performance; Table 1 shows that a glass cover surface gave the best improved performance of 27 % when compared against PET, Plexiglass, and thin film plastics; glass cover surfaces showed better properties of thermal conductivity and solar transmittance, absorbance, and emissivity.

Table 1: Cover surface modifications in Literature

Type of solar still	Author	Location	Daily yield (kgm^{-2})
CSS – Glass, Plexiglass, Plastic wrap	Jones et al. (2014)	Macon, USA (33°N, 84°W)	–
CSS – Glass and PET	Bhardwaj, ten Kortenaar & Mudde (2013)	–	– *+ 27 %*

Jones et al. (2014) compared the performance of glass, Plexiglass, and plastic wrap as cover surface materials. The glass cover surface showed the highest internal water temperatures and yield produced. The plexiglass cover performed the worst giving a yield 7 % lower than the plastic wrap.

Bhardwaj et al. (2013) showed a 27 % yield increase for a glass cover surface when compared with a polyethylene terephthalate (PET) cover surface. The main reason for this difference was that water droplets on the glass surface were flatter and had more contact area allowing more light to reach the still base compared to PET, which also

had the less-than-ideal scenario of water droplets not falling off the surface easily giving way for more condensation to occur.

Although the contact angle is the most important parameter for choosing a cover surface material, Marais (2018) optimised the cover angle to 26° and so changing the contact angle will not be considered for this study (Bhardwaj, et al., 2013).

2.2.3 Back Wall Observations

Marais (2018) noticed that a substantial amount of energy was trapped in the still back wall (body losses) – on average, body losses were 10 % of energy losses, shown in Figure 6; still 1 was modelled off the reference design variation. This presented an opportunity to improve the condensation yield and energy efficiency of the stills by reducing energy tapped in the still body.

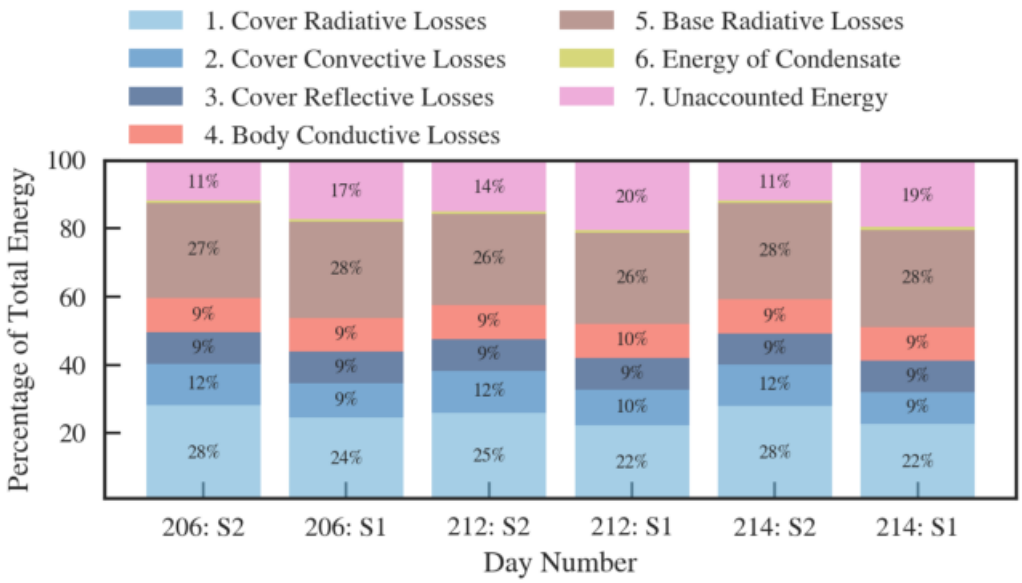

Figure 6: Energy balance of baseline still with no back wall reflectors attached

Marais (2018) experimented with aluminium back wall reflectors and immediately noticed an improvement in performance. The back wall temperatures decreased on average by 10 °C – shown by Figure 7 – resulting in a water temperature increase of 3 °C. However, the back wall reflectors lost their performance advantage the longer they stayed in the stills – starting from a 12 % yield increase to a 5 % yield increase while energy efficiency did not improve. The poor performance was due to

condensation that occurred on the surface of the reflectors and was lost to the solar still.

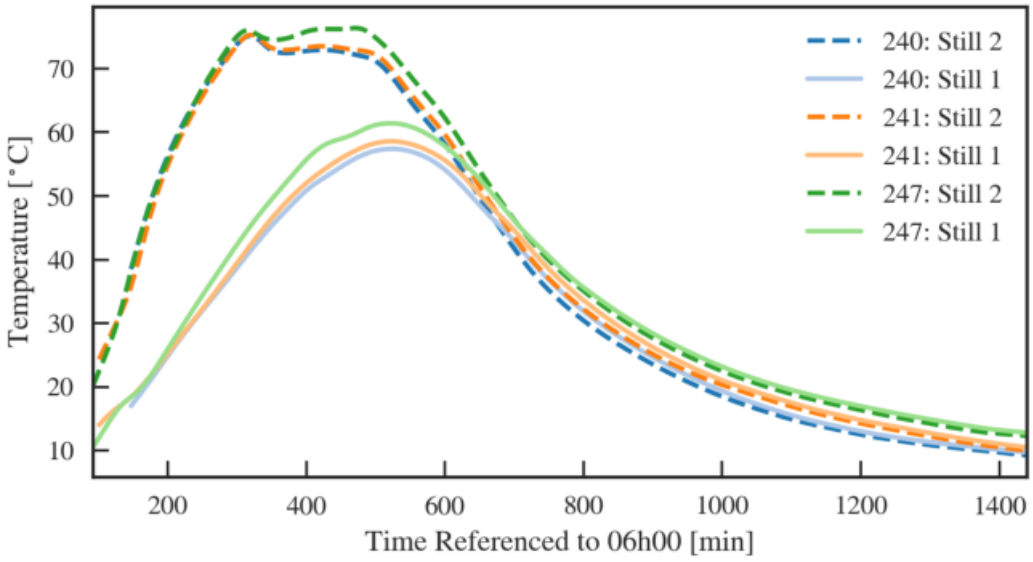

Figure 7: Back wall temperature profiles with back wall reflectors attached

Additionally, adding side reflectors to the solar still with back wall reflectors attached gave a still performance worse than the back wall reflectors case – with no improvement in energy efficiency of the side reflector case. Similar to the back wall reflectors case, the side reflectors case had a better performance initially before its performance deteriorated to below that of the baseline still – starting from a 15 % yield increase to a – 12 % yield increase.

Although Estahbanati et al. (2016) and Abdallah et al. (2008) suggested that adding internal reflectors to the still will increase performance, Marais' (2018) results did not agree. Estahbanati et al. (2016) observed a 16 % yield increase in summer and a 41 % yield increase in the winter, while Abdallah et al. (2008) showed a 32 % yield increase when compared to a conventional still in the summer. Estahbanati et al. (2016) included a comparison of front and side reflectors to back wall reflectors. Front and side walls showed an 18 % yield increase while back wall reflectors showed a 22 % yield increase; the back wall reflectors performed better than the front and side reflectors.

The back wall reflectors from Marais' (2018) results showed an improved yield between 8 – 12 % until the still performance deteriorated the longer the reflectors stayed in the still. For the back wall and side reflectors, there was a marginal performance improvement before the still performance deteriorated similar to the back wall reflectors scenario. Marais' (2018) results did not match the trends in literature.

2.2.3.1 Back Wall Modifications

The performance deterioration of the back and side wall reflectors prompts the need for an alternative method to remove or utilise the heat build-up in the back wall.

The water temperature profiles of the baseline still in Figure 7 showed peak temperatures of ~75 °C while water temperature profiles of the same baseline still showed peak temperatures of ~63 °C; this is shown in Figure 8. With $T_{water}<T_{back\ wall}$, energy from the back wall can be reused by running basin water over the back wall, preheating the basin water for evaporation.

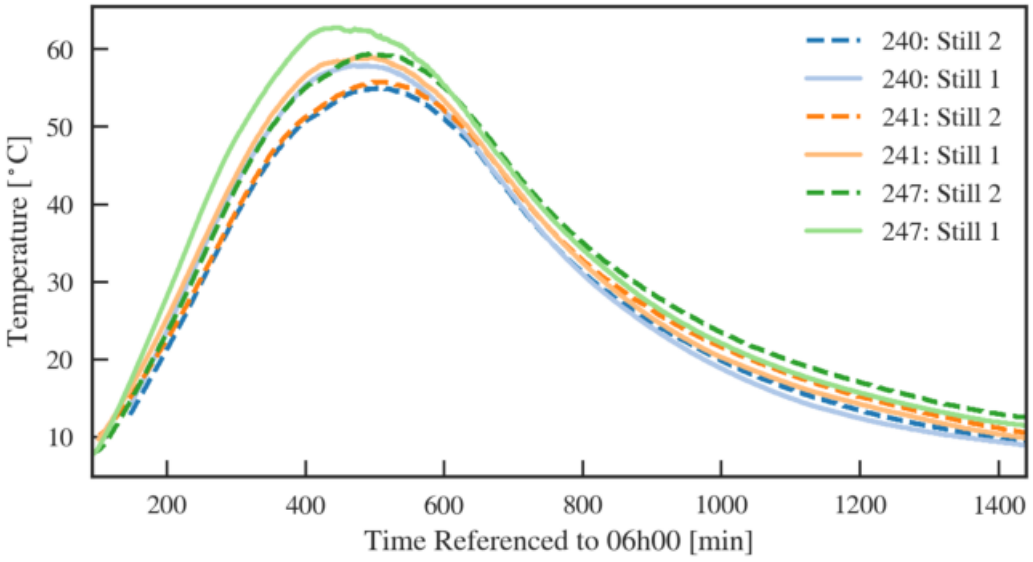

Figure 8: Water temperature profiles with back wall reflectors attached

There is limited commentary on circulating basin water over the back wall and so the potential performance increase of the back wall modification cannot be estimated. The purpose of the back wall modification is to capture as much of the ~10 % energy losses that sit in the back wall, using basin water to run down the back wall. The hypothesis is that preheating the basin water will improve condensation rates leading to higher

yields while the still becomes more efficient by reusing energy that would sit trapped in the back wall.

2.2.4 Additional Observations

2.2.4.1 Heat sink

External condensation area in the form of two aluminium heat sinks with surface area of 0.021 m^2 were attached externally to a portion of the cover surface. The still with the heat sinks attached experienced earlier onsets of condensation, higher condensation rates, and achieved on average 40 % higher condensation yields.

The improved solar still performance was due to the heat sinks' ability to remove energy from the cover surface by convection. The release of heat through the heat sinks reduced the cover temperature, increased the driving force for condensation between the basin water and the cover surface, and made the cover surface clearer from condensation. Keeping the cover cooler improved the still performance. At the same time, a cooler cover reduces radiative and convective losses while a clearer cover reduces reflective losses.

2.2.4.2 External tubes

Aluminium tubes were used to increase the external condensation area but had no effect on the still performance; only adding 0.02 kg to the yield at best. This was contrary to Rabhi et al. (2017) who showed a 32 % yield increase. The poor performance of the tubes was due to the lack of forced movement to direct the humid air into the cooler tubes.

2.2.4.3 Insulation Effects

Marais (2018) noted that increasing the insulation thickness of the solar still increased the thermal resistance of the solar still. This meant more solar energy was retained in the solar stills, leading to increased evaporation and condensation rates. After a certain point, increasing the thickness of the insulation reduced the performance benefit of the still.

Increasing the thermal resistance from 0.16 $K.W^{-1}$ to 1.1 $K.W^{-1}$ increased the condensate yield from 0.4 kg to 0.65 kg. This was a larger increase compared to the increase of 0.65 kg to 0.8 kg when the thermal resistance was increased from 1.1 $K.W^{-1}$ to 2.1 $K.W^{-1}$. Although the performance benefit and cost benefit of adding insulation diminished after the 1.1 $K.W^{-1}$ mark, the yield increased due to the heat retained in the insulation.

2.2.5 Conclusion

Still variation 3 was the best performing still, applying the best elements from the earlier still variations; and for this reason, it was used for the heated water bath and active solar still experiments. Table 2 summarises the performance of the still variations; still variation 1 was the worst performing still.

Table 2: Performance indication of still variations

Still variation	Daily condensation performance	Energy efficiency	Rank
Reference design	1.07 $L.m^{-2}$	13 %	3
Variation 1	0.99 $L.m^{-2}$ (-8 %)	12 %	4
Variation 2	1.30 $L.m^{-2}$ (22 %)	15 %	2
Variation 3	2.40 $L.m^{-2}$ (124 %)	26 %	1

2.3 Active Solar Basin Still

Marais (2018) showed that the passive solar basin still could benefit from active modifications that focus on increasing condensation rates and reducing energy losses in the still, specifically:

- Fluid flow modifications that could improve condensation rates by introducing fluid circulation.
- External condensation area modifications that could improve condensation yields by using air flow over the external condenser, and by directing condensation away from the cover surface and onto the external condenser.

2.3.1 Fluid Flow Modifications

Fluid flow modifications – any circulation of air or water within the still – were not considered by Marais (2018). Fluid flow creates a turbulent environment and increases the contact area between the air and the condensation surface, resulting in the increase of condensate yield. Stills with fluid flow induced by a moving device, for example a fan, are called active solar stills.

Fluid flow modifications are a direct fix to Marais' (2018) attempt in Section 2.2.4.2 to increase condensation rates by introducing an external condensation area. In that scenario, there was no driving force to direct the humid air into the cooler tubes. Using active fluid flow will allow stronger circulations through the solar still.

Literature in Table 3 shows that fluid flow modifications can result in a yield increase of up to 56 %.

Sethi & Dwivedi (2013) showed that a double slope active solar still under forced water circulation performed on par with a conventional solar still by producing yield between 1 $kg.m^{-2}$ and 3.5 $kg.m^{-2}$ daily with a still efficiency between 13 % and 31 % at water depths of 30 mm, 40 mm, and 50 mm.

Rahmani et al. (2015) showed that creating a natural circulation air convection loop through a thermo-syphon effect has a good effect on still performance. Ali (1993) studied the effect of placing a fan inside a conventional solar still and observed a 30 % yield increase. Mahian & Kianifar (2011) used a small fan and showed the improved air convection resulted in a 56 % yield improvement.

However, Fath & Elsherbiny (1993) also found that natural circulation of air contributed 75 % of the still productivity with a 50 % increase in efficiency. Lawrence & Tiwari (1990) recommend operating under natural convection to gain the advantages of simplicity, reliability, and cost-effectiveness.

Table 3: Fluid flow modifications in Literature

Type of solar still	Author	Location	Daily yield* (kgm^{-2})	Efficiency
Conventional single slope solar still (CSS)	Rahmani et al. (2015)	Oum El Bouaghi, Algeria (36°N, 7°E)	3.72 $kg.m^{-2}$ –	45 %
CSS – Air circulation	Ali (1993)	Tehran, Iran (36°N, 51°E)	– *+ 30 %*	–
CSS – Air circulation	Fath & Elsherbiny (1993)	Alexandria, Egypt (31°N, 30°E)	–	*+ 50 %*
CSS – Air circulation	Mahian & Kianifar (2011)	Mashhad, Iran (36°N, 60°E)	– *+ 56 %*	–
Double slope active solar still – Water circulation	Sethi & Dwivedi (2013)	Greater Noida, India (28°N, 78°E)	3.5 $kg.m^{-2}$ –	31 % (maximum)

* Percentage values in italics indicates the change in performance for the daily yield and efficiency.

2.3.2 External Condensation Area Modifications

Using an external condensation area on a passive solar basin still gives the option for:

- Additional condensation area and an external condensation surface to be coupled into one solution, and
- Condensation to solely occur on the external condensation area, keeping the cover surface cooler – creating a better driving force between the basin water and cover surface – and clear for solar radiation to enter the solar still unhindered.

Coupling fluid flow modifications – that will direct humid air through to the external condenser – with an external condenser will reduce cover losses and make more energy available for condensation.

2.3.2.1 External Condenser

Literature showed different types of condensers; built-in, internal (passive), and external (active), each with a different design and a different effect on still performance. Condensation surfaces featured in Marais' (2018) work but on a small scale as heat sinks attached to the cover surface and external aluminium tubes attached via the back wall.

For the cases where external condensers are used in literature, there is some form of fluid flow, either natural or induced, to carry the humid air past the condensation surface. Although this was also seen for passive condensers, induced fluid flow was a key feature of solar stills with external condensers. It is also possible that the use of an external condenser could drive condensation activity away from the cover surface entirely. Driving all heat and mass transfer action away from the cover surface will keep the cover surface cooler and clear from condensate. This will be tested and observed during the external condenser experiments.

Table 4 compares Marais' (2018) performance against literature, suggesting that there is scope to develop an active solar still with an external condensation surface to improve still performance. Marais' (2018) best results gave a 27 % yield improvement while the best yield improvement from literature was 60 %.

Marais' (2018) results shown in Table 4 were discussed in Section 2.2.4. Reddy et al. (1983) suggested incorporating dew point conditions in the optimum operating strategy on any still and showed a 15 – 25 % yield improvement when compared to a non-condenser still.

Kumar et al, (2016) studied the combined solution of an agitation effect with an external condenser. A shaft was used to agitate the water to break the boundary layer of water and increase the contact area with air. An exhaust fan was used to direct the humid air mixture into the external condenser. Kumar et al. (2016) saw a 39 % yield improvement from the combined agitation effect and external condenser solution. Fath & Elsherbiny (1993) showed a 42 % performance improvement when using a passive condenser.

Table 4: External condenser modifications in Literature

Type of solar still	Author	Location	Daily yield (kgm^{-2})	Efficiency
Simple basin still – Heat sink	Marais (2018)	Pretoria, South Africa (26°S, 28°E)	0.604 $kg.m^{-2}$ *+ 5 %*	–
Simple basin still – External tubes	Marais (2018)	Pretoria, South Africa (26°S, 28°E)	– *0 %*	–
CSS – Passive condenser	Fath & Elsherbiny (1993)	Alexandria, Egypt (31°N, 30°E)	– *+ 42 %*	*+ 50 %*
CSS – Passive condenser	Reddy et al. (1983)	New Delhi, India (29°N, 77°E)	4.45 $kg.m^{-2}$ *+ 15 – 25 %*	–
CSS – Active condenser with agitation	Kumar et al. (2016)	Kovilpatti, India (9°N, 78°E)	2.667 $kg.m^{-2}$ *+ 39 %*	*+ 13 %*
CSS – Active condenser with vacuum fan	Kabeel, et al. (2014)	Tanta, Egypt (31°N, 31°E)	– *+ 53 %*	–
CSS – Active condenser with vacuum fan	Monowe et al. (2011)	Botswana (25°S, 26°E)	– *+ 60 %*	–
CSS – Active condenser with vacuum pump	Ibrahim et al. (2015)	Cairo, Egypt (30°N, 31°E)	– *+ 16%*	*+ 30 %*

Literature has also shown the performance improvement when using a vacuum fan in tandem with an external condenser. Kabeel et al. (2014) showed a 53 % performance improvement while Monowe et al. (2011) gave a 60 % performance improvement. Ibrahim et al. (2015) showed a 16 % daily yield improvement and a 30 % energy efficiency improvement when incorporating a vacuum pump. The use of a vacuum fan/pump is a possible option to explore.

2.3.2.2 External Condenser Surface Air Flow

Air flow refers to the flow of air, either by natural or forced convection, over the external surface of the condenser, perpendicular to the flow of the external condenser. By this definition Marais (2018) condensation surfaces were implemented under natural convection.

Not much commentary exists on forced air flow over a condenser surface. However, using the hypothesis that increasing air flow over the condensation surface keeps the surface cool, more heat will be lost from the condenser due to the increased driving force between the humid air and the condenser surface. This scenario also aids heat loss from the condenser by increasing the convective heat transfer from the condenser surface to the air. The goal will be to use a “sub-optimally” designed external condenser that allows the right amount of heat loss without sacrificing overall still performance. Using an efficient external condenser will reduce the heat retention ability of the solar still, leading to a reduced performance. Section 2.2.4.3 shows how better heat retention leads to increased evaporation and condensation rates – using an inefficient external condenser will give better heat retention.

2.3.3 Annualised unit cost per litre of distilled water

The cost analysis is an economic analysis used on the solar stills to determine the feasibility of the modified still, based on the cost investment and resulting performance change. All the modifications described above require a cost investment, and to determine if the modified still is feasible, a cost analysis is applied.

The cost analysis uses financial data (lifecycle, interest rate, initial capital investment, etc), cost of still components, still runtime, and still daily yield to determine an annual cost of water production. The annual cost allows a uniform comparison between stills that have different financial data, different cost components, and were built for different locations (Ahsan, et al., 2013).

Although Marais (2018) mentioned the need to be cost-effective in the build of the solar still, no cost was reported for the passive basin still. The literature in Table 5 shows the various water production cost ranges considered acceptable for the type of

solar still considered. The water production method is considered viable if the cost per litre range lies between R 0.20/l and R 2.00/l (Esfahani, et al., 2011; Malaiyappan & Elumalai, 2015; Tiwari, et al., 2008; Ibrahim, et al., 2015; Kumar, et al., 2016). Falling outside this range indicates the economic unattractiveness of the solar still; either too much money was invested or there was not a significant performance improvement to justify the cost investment.

Table 5: Solar still water production cost ranges from Literature

Type of solar still	Author	Location	Cost range (R/l)*	Market rate (R/l)*
CSS – Active condenser with agitation	Kumar et al. (2016)	Kovilpatti, India (9°N, 78°E)	–	R 2.14/l (Rs 10/l)
CSS – Glass cover surface	Hassan & Abo-Elfadl (2017)	Assiut, Egypt (27°N, 31°E)	R 0.20/l ($ 0.0147/l) 11.4 % eff.	–
CSS – Passive condenser	Hassan & Abo-Elfadl (2017)	Assiut, Egypt (27°N, 31°E)	R 0.17/l ($ 0.0125/l) 16.1 % eff.	–
CSS	Jamil & Akhtar (2017)	Uttar Pradesh, India (27°N, 81°E)	R 0.53/l (Rs 2.64/l)	R 3/l (Rs 15/l)
CSS – Sub-atmosphere active condenser	Ibrahim et al. (2015)	Cairo, Egypt (30°N, 31°E)	R 0.52/l ($ 0.041/l)	–
CSS – Active condenser with thermoelectric cooling	Esfahani, Rahbar & Lavvaf (2011)	Semnan, Iran (35°N, 53°E)	R 0.94/l ($ 0.13/l) 13 % eff.	–

* Conversion in Rands considers the relevant exchange rates at the time of publishing of respective articles

Jamil & Akhtar (2017) and Hassan & Abo-Elfadl (2017) reported the unit cost of conventional solar stills to be R 0.53/l and R 0.20/l, respectively. Kumar et al (2016) did not give a unit cost for their active condenser but noted a market price of R 2.14/l. This market price of distilled water is important to consider as it gives a first mark of how well the economics of any still should perform, i.e. below the market price.

The passive condenser still of Hassan & Abo-Elfadl (2017) had a unit cost of R 0.17/l which was lower than the R 0.20/l of the CSS. This was one of the lowest prices seen in literature. The low price might have been due to the low capital cost of using a passive condenser and the 39 % performance improvement the passive condenser created.

Ibrahim et al. (2015) studied a solar desalination system working at sub-atmospheric pressure. This still was complex and involved using an evaporation chamber, a condenser with copper fins, an isolating valve, and the fabrication cost. This resulted in a 39 % cost increase but resulted in a 16 % performance increase. The net effect was a unit cost of R 0.52/l, on par with Jamil & Akhtar's (2017) CSS.

The aim of this research is to produce water at the local municipal rates of 0.67 c/l, or cheaper. The cost of 0.67 c/l is inclusive of transport and distribution costs (City of uMhlathuze, 2021; Sol Plaatje Municipality, 2021). The water production rate will also be compared against the current distilled water market rate of R4.40/l (Checkers, 2021). The equations used in the cost analysis are detailed in Section 2.6.

All references shown in Table 5 used a lifecycle period of 10 years in their economic analysis. Increasing the lifecycle period beyond 10 years will reduce the water production costs however, this might not be a feasible option to reduce the water production costs as the stills will use complex designs and components, leading to an increased capital investment.

It is more likely that the lifecycle period of the solar stills is closer to 5 years than 10 years. A lower lifecycle period could be an advantage in terms of reducing the capital investment required and using cheap components and simple still designs, avoiding the need to use more expensive components to improve the lifecycle of the still. This

also creates an economic benefit by creating low skills jobs to manufacture the simple basin solar stills.

2.3.4 Performance Improvement

Marais' (2018) research showed three main barriers to improved still performance:

1. Heat build-up in the body and back wall.
2. Large energy losses through the cover surface.
3. The simple passive still produces low yields due to the inefficient modes of condensation.

The active solar still modifications suggested will investigate solutions to the barriers mentioned by:

1. Using back wall modifications to circulate basin water over the back wall.
2. Using a better performing cover surface material.
3. Using fluid flow modifications to induce stronger circulations of humid air and or basin water.
4. Using external condensation modifications to reduce the condensation area and to drive condensation solely to the external condenser.

Literature suggests that using the modifications mentioned to transform the passive basin still into an active solar still will lead to improved still performance. Table 6 shows the best individual modification improvements from literature; the external condenser modifications showed the best daily yield and efficiency improvement of 60 % and 50 %, respectively. The active stills lie in the cost per litre range of R 0.52/l – R 0.94/l indicating a viable method of water production.

Although simple and complex designs are suggested with the modifications, the complex designs will not be investigated; for example, use of a vacuum fan and cover surface agitation. It is possible that some of these complex designs will give a significant performance improvement, however the active solar still needs to remain simple in design and operation, and cost-effective as modifications are made.

Table 6: Best performance improvement per modification

Modification	Performance improvement (%)	
	Daily yield	Efficiency
Cover surface modifications	+ 27 %	–
Back wall modifications	–	–
Fluid flow modifications	+ 56 %	+ 50 %
External condenser modifications	+ 60 %	+ 50 %

This is an important consideration as the stills are designed to be used off-grid, in remote locations. Keeping the still simple and cost-effective means that the still can be operated with a low level of skill and still components can be replaced and maintained easily and cheaply in off-grid or remote locations.

2.4 Mechanisms of Heat and Mass Transfer in an Active Solar Basin Still

The energy pathways of a solar still are shown in Figure 9. The mechanisms of evaporation, condensation, diffusion, and to a lesser extent convection, result in mass transfer in a basin solar still.

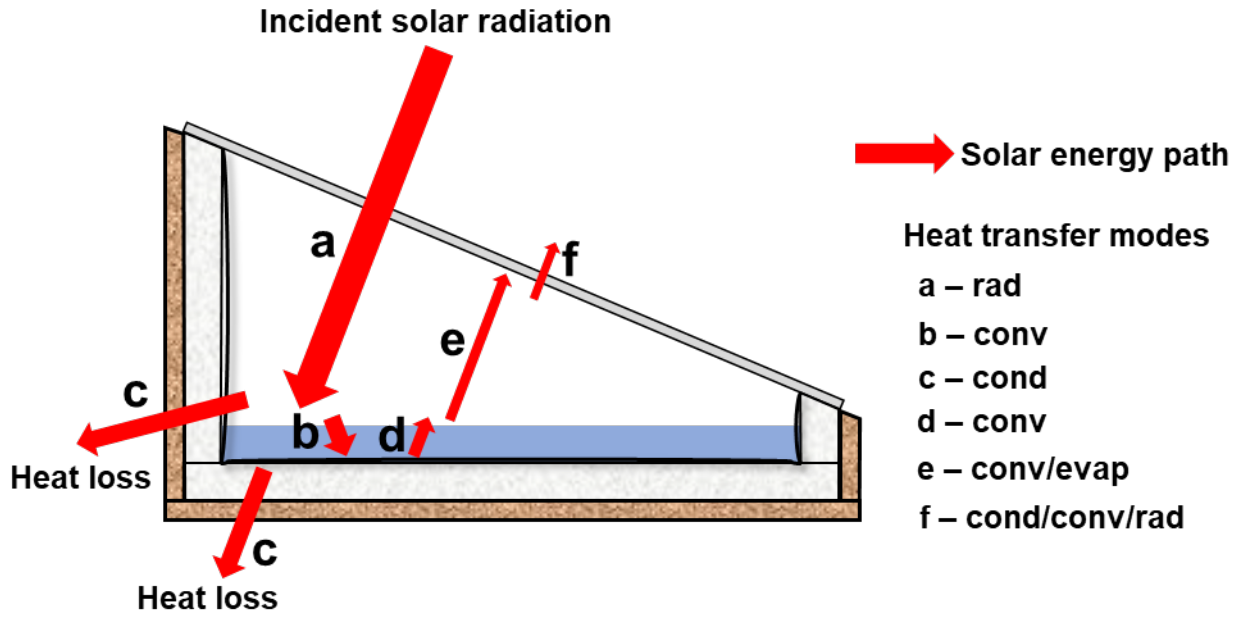

Figure 9: Heat transfer pathways in a basin still (Bhardwaj, et al., 2015, p. 483)

For active fluid flow circulation, the energy interactions remain the same. However, the external condenser surface area creates another heat transfer point where the modes of conduction and convection act. Further to the external condenser, the fluid movers also create two new energy transfer points. Active fluid flow is a mode of momentum transfer that enables heat transfer, i.e. fluid flow can act as a heat sink or a heat source (Çengel & Ghajar, 2015, p. 835; Webb & Kim, 2005, p. 689). The energy modes are shown in Figure 10.

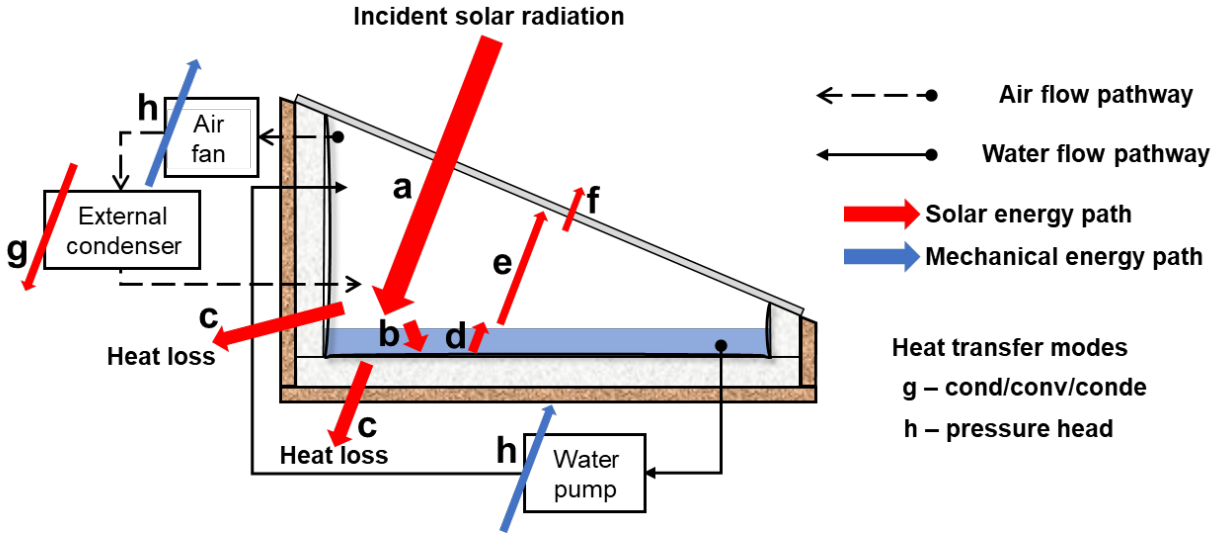

Figure 10: Heat transfer pathways in an active solar still

Figure 11 shows the mass movements across the active solar still. The mass transfer modes initially mentioned are depicted along with the bulk fluid flow of the active solar still. The primary driving force for fluid flow is pressure difference, whereas for mass transfer it is concentration difference (Çengel & Ghajar, 2015, p. 835).

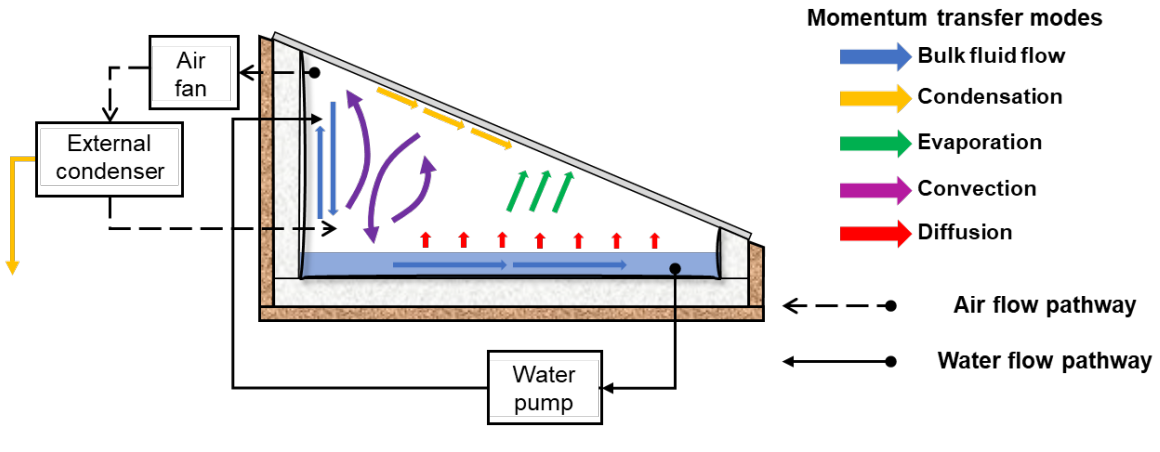

Figure 11: Momentum transfer pathways in an active solar still

2.4.1 Mathematical Model

The mathematical description of the system requires continuity and energy balance equations, and in applying these balances, the following assumptions are made:

- Minute by minute steady state conditions.
- Uniform temperature across the different surfaces of the solar still.
- Approximated properties at phase change boundaries are accurate.
- Heat transfer through the piping system is neglected.
- Energy input required to drive the air fans and water pump is neglected.
- The flow frictional losses are also assumed negligible (Ibrahim & Elshamarka, 2015, p. 402).

For an active solar still, water production of the still is equal to the amount of condensed water under the cover surface and from the external condensation surface. This is based on the energy balances and assumes a steady state condition of operation (Feilizadeh, et al., 2016, p. 176). The data discretisation through finite difference approximation also models the system as steady state.

2.4.2 Simultaneous Heat and Mass Transfer

Considering the active solar still will experience both heat and mass transfer, the system is modelled by simultaneous heat and mass transfer; this is termed the simultaneous transfer phenomena (Çengel & Ghajar, 2015, p. 882).

The analogies that exist between the heat and mass transfer phenomena hold true because of the similarity in their mechanisms. The existence of the analogies requires the following conditions to exist within the system:

- There is no homogeneous reaction occurring.
- There is no viscous dissipation.
- There is a low flowrate of mass transfer to not affect the velocity profile.
- The physical properties are constant (Welty, et al., 2015, p. 519).

2.5 Performance Indices of an Active Solar Still

The three main categories of performance factors affecting a solar still are shown in **Table 7** (Jamil & Akhtar, 2017, p. 75; Ibrahim, et al., 2015, p. 61).

Table 7: Performance factors of a solar still

Meteorological Parameters	Design Parameters	Operational Parameters
Humidity	Still dimensions	Location of still
Sky clearness	Insulation features	Orientation of still
Wind velocity	Condenser features	Saline water depth
Wind direction	Cavity aspect ratio (A_R)	Feed water temperature
Solar radiation	Flow energy input	
Ambient temperature	Evaporation process	
Atmospheric pressure	Condensation process	
	Active fluid flow setup	
	External condenser area	

Meteorological conditions cannot be controlled and thus emphasis is placed on the design and operation of the solar still to augment its performance. The operational parameters of the active solar still will be kept as uniform as practically possible. The design features implemented for the active solar still will be ranked by the daily productivity (yield), energy efficiency, and energy balance analysis of the solar still. Measuring the performance adjustments of the design allow a coherent analysis for any type of change made, as well as for comparison against the reference basin solar still. This method also eliminates the need to report on incremental performance variables, such as a cooler condenser surface or less radiation losses.

2.5.1 Daily Productivity

The daily productivity, or yield, is based on the mass of condensate collected from the cover surface and from the external condenser over a time period, *t*, normalised over the total condensation area. This is shown in Equation (1) (Bhardwaj, et al., 2015, p. 483; Ibrahim & Elshamarka, 2015, p. 403).

$$Productivity = \frac{m_{total}}{(A_{cond} + A_{surf})t};\ m_{total} = m_{cond} + m_{surf} \quad (1)$$

2.5.2 Energy Efficiency

The overall still efficiency is an energy consideration; it is the fraction of incident radiation that leaves the solar still as rejected condensation heat (Bhardwaj, et al., 2015, p. 483; Ibrahim & Elshamarka, 2015, p. 403).

$$\eta = \frac{m_{cond}\Delta H_{vap@cond} + m_{sur}\Delta H_{vap@surf}}{(I_T A_{surf})t} \quad (2)$$

where $\Delta H_{vap@cond}$ and $\Delta H_{vap@surf}$ is the latent heat of vapourisation at the temperature of the condenser and cover surface, respectively, and I_T is the total radiated energy incident on the solar still during the working time of the solar still.

2.5.3 Energy Balance Analysis

The energy balance analysis is another tool used to evaluate the performance adjustments made to the active solar still. The energy balance analysis reduces to

$$(\Delta\dot{U})_{cv} = \dot{Q}_{in} - \dot{Q}_{out} - \dot{Q}_{condensate} - \dot{Q}_{condenser} - \dot{Q}_{un} \quad (3)$$

where Q_{in} is the incident solar radiation, Q_{out} consists of the energy losses from the solar still, $Q_{condensate}$ is the rejected latent energy to form condensate, and Q_{un} is the unaccounted energy of the still excluded from the initial energy balance analysis; radiative side wall losses, inaccurate state-point evaluations, and or uniform temperature assumptions are all possible sources of unaccounted energy. $(\Delta U)_{cv}$ is decomposed to give

$$(\Delta\dot{U})_{cv} = (\Delta\dot{U})_{water} + (\Delta\dot{U})_{isoboard} + (\Delta\dot{U})_{cover} + (\Delta\dot{U})_{air} \quad (4)$$

Equation (5) represents the change in internal energy for the water, extruded polystyrene, and cover surface whereas Equation (6) represents the internal energy change for the humid air.

$$(\Delta\dot{U})_i = m_i C_{p,i}(T_{i-final} - T_{i-initial}) \quad (5)$$

$$(\Delta\dot{U})_{air} = m_{air}C_{v,air}(T_{air-f} - T_{air-i}) + m_{air}(X_f h_{water-f} - X_i h_{water-i}) \quad (6)$$

where *X* is the quality of the humid air, *h* is the enthalpy of the vapourised water in the air, and the subscripts *f* and *i* represent the final and initial conditions of the experiment. The internal energy change of the external condenser was not considered; it was assumed to be negligible compared to the internal energy change of the active solar still.

The remaining energy terms from Equation (3) are expressed below.

$$\dot{Q}_{in} = (I_T A_{surf}) \tag{7}$$

$$\dot{Q}_{out} = \dot{Q}_{conv-surf} + \dot{Q}_{rad-surf} + \dot{Q}_{refl-surf} + \dot{Q}_{rad-base} + \dot{Q}_{cond-body} \tag{8}$$

$$\dot{Q}_{conv-surf} = h_e A_{surf}(T_{surf} - T_{amb}) \tag{9}$$

$$\dot{Q}_{rad-surf} = \sigma \epsilon A_{surf}({T^4}_{surf} - {T^4}_{sky});\ where\ T_{sky} = 273 + (T_{amb} - 6°C) \tag{10}$$

$$\dot{Q}_{condensate} = m_{cond} \Delta H_{vap@cond} + m_{sur} \Delta H_{vap@surf} \tag{11}$$

$$\dot{Q}_{condenser} = UA\Delta T \tag{12}$$

The reflective cover losses, radiative base losses, and conductive body losses are shown below, respectively.

$$\dot{Q}_{refl-surf} = \sigma \epsilon A_{surf} {T^4}_{surf} \tag{13}$$

$$\dot{Q}_{rad-base} = \sigma \epsilon A_{surf}({T^4}_{base} - {T^4}_{surf}) \tag{14}$$

$$\dot{Q}_{cond-body} = \frac{kA_i(T_{i-in} - T_{i-out})}{\Delta x_i};\ where\ i = base, backwall, and\ 2\ sides \tag{15}$$

To accurately account for the effects of orientation on radiation and reflection heat transfer between two surfaces (currently shown Equations (13) and (14)), the view factor is used (Çengel & Ghajar, 2015, p. 710). For the active solar stills, this level of complexity is omitted and simplified by finding the effect of radiative and reflective losses from the cover surface to ambient, expressed by Equations (10) and (13).

The analysis then comes in expressing each energy loss term as a fraction of the total energy available (Q_{in}) (Bhardwaj, et al., 2015, pp. 482-483; Marais, 2018, pp. 45-50). The radiative losses, reflective losses, and other measurement errors were grouped together to form Q_{un}.

$$\dot{Q}_{un} = \dot{Q}_{in} - \dot{Q}_{condensate} - \dot{Q}_{cond-body} - \dot{Q}_{condenser} \tag{16}$$

2.5.4 Energy Profiles

The energy profiles go beyond the temperature profiles to visualise the energy movement across a specific still component or fluid body, for example back wall, humid air, or water temperature.

Depending on the still component or fluid body being examined, the energy equations used for the energy profile will change. For example, visualising the energy profile of the humid air will use the latent equation of Equation (11) as the humid air is saturated. For humid air that passes through the heat exchanger, the energy profile will be described by Equation (6). For the energy profiles of the condensate, Equation (11) will be used to quantify the energy removed where the mass profile of the condensate and temperature profile of the tube surface will be used as inputs.

2.6 Life Cycle Cost Analysis

In addition to the annualised cost per litre value used as a quick analysis of cost attractiveness, the annual cost, salvage cost, and maintenance cost are also included for a thorough cost analysis of the solar still. The comparison of financial positions allows the cost viability of solar stills to be compared, indicating the most favourable financial terms and operating conditions.

The annual cost of a solar still is estimated by the following equations (Srivastava & Agrawal, 2014; Kumar, et al., 2014):

The first annual cost (FAC) is

$$FAC = CRF * P \tag{17}$$

where CRF is the capital recovery factor calculated as

$$CRF = \frac{r(1+r)^n}{(1+r)^n - 1} \tag{18}$$

and *P* is the initial cost of manufacturing of a solar still, including labour. *r* is the annual interest rate which was 11.75 % (as of 21 December 2023) and *n* is the useful lifecycle of the still.

The annual salvage value (ASV) is given by

$$ASV = SSF * S \tag{19}$$

where the sinking fund factor (SFF) is

$$SSF = \frac{r}{(1+r)^n - 1} \tag{20}$$

and the salvage value (S) is assumed as 50 % of the first annual cost.

The annual maintenance cost (AMC) is assumed 15 % of the first annual cost. The annual cost (AC) is

$$AC = FAC + AMC - ASV \tag{21}$$

The water production cost (WC) is calculated as

$$WC = AC/m \tag{22}$$

where *m* is the average annual productivity. The annual cashflow (ACF) becomes

$$ACF = Sp * m \tag{23}$$

where *Sp* is the selling price of distilled water, usually taken as 10 times the water production cost. For a market value of *Sp*, the net profit (N) is

$$N = ACF - AC \tag{24}$$

Equations (18) and (24) show that the cost analysis of a solar still depends on the performance of the solar still in the form of the average annual productivity, *m*, and the lifecycle of the still, *n*. To produce a cost-effective solar still, *m* and *n* must be as high as possible. But as mentioned in Section 2.3.3, keeping *n* within the five-to-ten-year mark could be more beneficial by using cheap components and simple still designs, reducing the capital investment required, and creating low skills jobs to build the simple solar stills.

3. Experimental

The project aims to cover three interconnected investigations; the cover surface performance, characterisation of the external condensers in a controlled environment using a heated water bath, and active solar still performance characterisation based on the findings of the aforementioned investigations. The purpose of the cover surface experiments is to find a cover surface material that reduces heat losses from the cover surface and increases the total irradiance on the absorber surface. Although this wasn't part of the original scope, reducing cover losses became imperative considering Marais' (2018) results as summarised in Section 2.2.2.

The experimental design and apparatus used during the heated water bath and active solar still experiments were built using the design of still variation 3 due to this variant being the best performing still design from Marais' (2018) experimental optimisation. The heated water baths were used to isolate the heat transfer performance of the external condenser and to characterise the overall heat transfer coefficient of the heat exchanger. Running the external condenser directly on the active solar still would have made it difficult to isolate the effect of the external condenser. Instead, running the external condensers in a controlled environment will isolate and indicate the direct effect of the condensers in terms of its heat transfer performance. The effect of natural and forced convection cooling on the external condenser were also investigated.

Once the cover surface and heated water bath experiments were concluded, the best performing cover surface material and external condenser, with a specific convection cooling mode, was implemented on the active solar still. The main purpose of the active solar still is to determine if fluid flow in a passive solar still affects the performance of a simple basin solar still. Fluid flow will be implemented through air fluid flow and basin water fluid flow. The external condenser, coupled with the air fluid flow, will be rated on how well it can direct condensation away from the cover surface.

3.1 Apparatus

3.1.1 Fluid Flow Configuration

Figure 12 shows the fluid flow configuration design, indicating positions of the fluid flow equipment. The water extracted from the base of the solar still is returned to the still at the top of the back wall, while hot humid air leaves the solar still from the top of the back wall and is returned closer to the base of the back wall slightly above the water level. The air/water crossflow allows the hot water to be sprayed over the back wall, simultaneously allowing the cooler air to increase in temperature as it flows upward along the back wall.

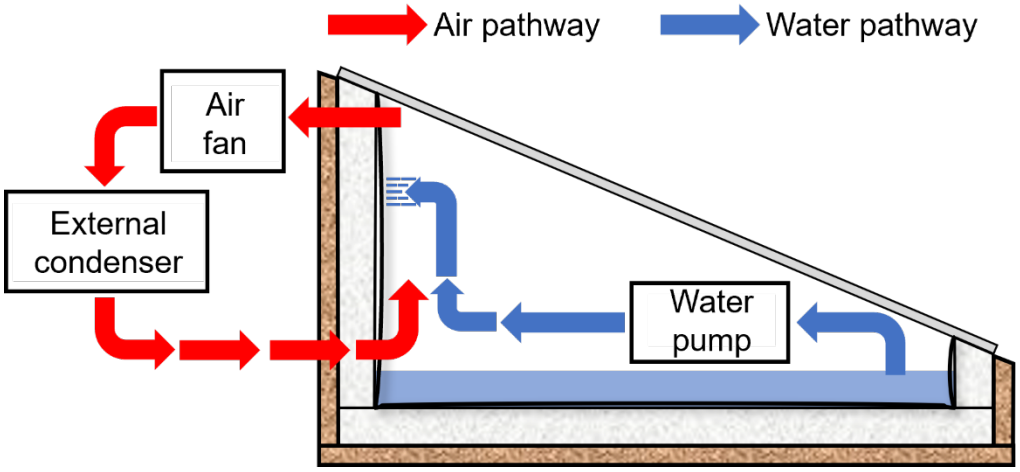

Figure 12: Modified basin solar still enabling fluid flow modifications

The air pathway used an air fan (computer fan) as a fluid mover to induce air flow from the solar still to the external condenser, and an external condenser to condense water from the humid air. The air fan was placed in the delivery line to the external condenser. The fan used was an 80 mm diameter axial air fan with a plastic casing, rated at 12 VDC and 2.4 W, with a specified airflow of 20 $m^3.hr^{-1}$.

The water pathway used an off-the-shelf water pump to circulate water over the back wall of the still. The water pump operated at 12 VDC and 8.4 W rating with a specified maximum flowrate of 8 $L.min^{-1}$.

3.1.2 Cover Surface Experimental Equipment

The cover surface experiments were run in polystyrene cooler boxes which were altered to suite the design of simple basin solar stills. As seen in Figure 13, the polystyrene still dimensions were 300 x 620 x 220 mm and a cover angle of 25°; the cover surface options were a 5 mm PMMA, 4 mm single pane glass (SPG) and a 4 mm double pane glass (DPG) cover (with a 2 mm sealed air gap) with an overall thickness of 8 mm. The cover surface area of all variants was approximately 0.2 m^2.

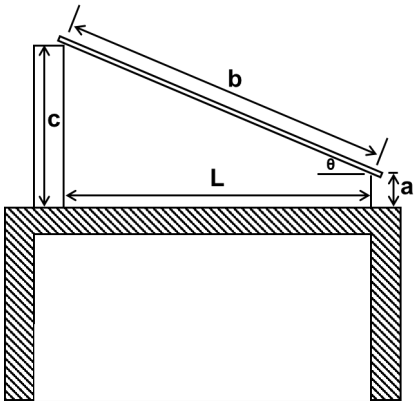

a – 74 mm
b – 334 mm
c – 220 mm
L – 300 mm
θ – 25°
width of still – 620 mm

Figure 13: Dimensions of the polystyrene solar still

The optical properties of PMMA, single pane glass, and double pane glass are shown in Table 8 Table 8: Thermal and Optical properties of experimental cover surface materials (Çengel & Ghajar, 2015, p. 853). The optical properties of double pane glass were approximated solely for comparison and not for thermal analysis. Table 8 shows PMMA's superior optical properties over single pane glass and double pane glass; a lower emissivity means less energy is emitted as radiation, a higher transmissivity means more radiation is transmitted through the cover surface, and a lower absorptivity means less radiation is absorbed by the cover surface. Contrasting this with literature which shows a 27 % daily yield increase from a glass cover surface compared with a PET cover surface; Table 1 (Bhardwaj, ten Kortenaar & Mudde, 2013), the cover surface experiments will confirm which cover surface gives the best performance.

Table 8: Thermal and Optical properties of experimental cover surface materials (Çengel & Ghajar, 2015, p. 853)

Material	k ($W.m^{-1}K^{-1}$)	R (K/W)†	ε	τ_s	α_s	Ref‡	Cost price ($R.m^{-2}$)
SPG*	0.70	476.2	0.9 – 0.95	0.79	0.14	13%	259 (3 mm)
DPG*	–	17.87	0.9 – 0.95	>0.79	>0.14	11%	518 (8 mm)
PMMA	0.19	1,053	0.86	0.92	<0.005	8%	974 (5 mm)

* SPG/DPG – single/double pane glass

† Resistance of material

‡ Reflectance of material

The cover surface was modified with 25 mm aluminium equal angle channels to collect run-off droplets. The polystyrene stills allowed quick alterations and easy operation compared to a larger, well-insulated still. The bottom of the polystyrene still was covered with black PVC tarpaulin to act as a solar absorber surface. The polystyrene stills were fitted with a hole on the back wall. The cover surface was sealed onto the still with water added through a hole at the back. The hole is plugged and taped shut after filling the still.

3.1.3 Heated Water Bath Experimental Equipment

Table 9 shows the different external condenser parameters used for the heated water bath experiments; all external condensers used a 20 $m^3.hr^{-1}$ axial fan as fluid mover – this equated to a linear velocity of 1.1 $m.s^{-1}$. With the Reynolds number being below ~2,000, flow is indicated to be laminar through the tubes. Flow is most likely turbulent due to the tube entrances and exits, bends, and fluid mover encountered in the flow path, as well as flow not being fully developed due to the compact design of the heat exchange system. The external heat transfer surfaces were made of aluminium; the high thermal conductivity of aluminium made it suitable as a heat rejection medium. Compared to other thermal conductors, aluminium is cost effective, corrosion resistant, lightweight, and malleable (Çengel & Ghajar, 2015, p. 844).

Table 9: Physical flow characteristics of external condensers

External condenser	No of tubes	Exposed tube length (mm)	Surface area (m^2)	Total CRA† for flow (m^2)	Reynolds number‡
Heat sink	–	–	1.71e-1	3.99e-3	6,366
9.5 mm tube bank	15	136	4.81e-2	6.63e-4	3,512
12.7 mm tube bank	15	136	6.41e-2	1.23e-3	2,582
9.5 mm tube bank(m*)	13	92	3.58e-2	5.74e-4	4,052
9.5 mm tube bank(m*)	9	100	3.59e-2	7.35e-4	4,304

* m – modified

† CRA – cross-sectional area

‡ Evaluated at an average temperature of 50 °C

The heat sink heat exchanger used two heat sinks placed back-to-back. One of the heat sinks was enclosed and used as an enclosed path for humid air fluid (internal heat sink) while the adjacent heat sink was left open to reject heat to the surrounding environment (external heat sink). As humid air circulates through the internal heat sink, heat rejection at the external heat sink will cause condensate to form and collect into the condensate collector. Each heat sink was 150 mm long and 200 mm wide, with full dimensions shown in Figure 14.

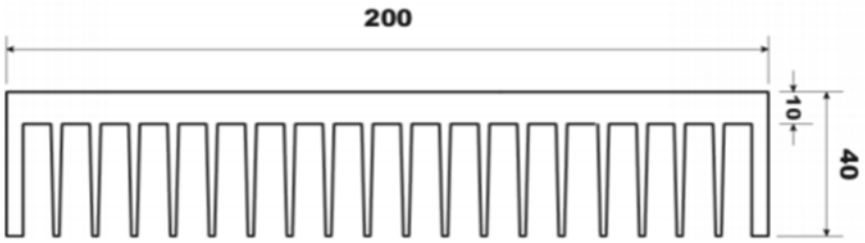

Figure 14: Heat sink profile and dimensions in mm

The tube bank comes in two configurations: (1) 9.5 mm outer diameter with 1 mm wall thickness, and (2) 12.7 mm outer diameter with 1.25 mm wall thickness; the tube bank runs vertically with a 0° inclination angle. The tubes are split across two rows in a staggered pattern. The tube banks occupy the same dimensions as the heat sink, i.e., the tube bank has a length of 150 mm and a depth of 40 mm, with the tubes spread evenly across the 200 mm heat exchanger width. The tube pitch and placement for the 9.5 mm and 12.7 mm heat exchangers are shown in Figure 15. The heat sink and tube bank external condensers are shown by Figure 16.

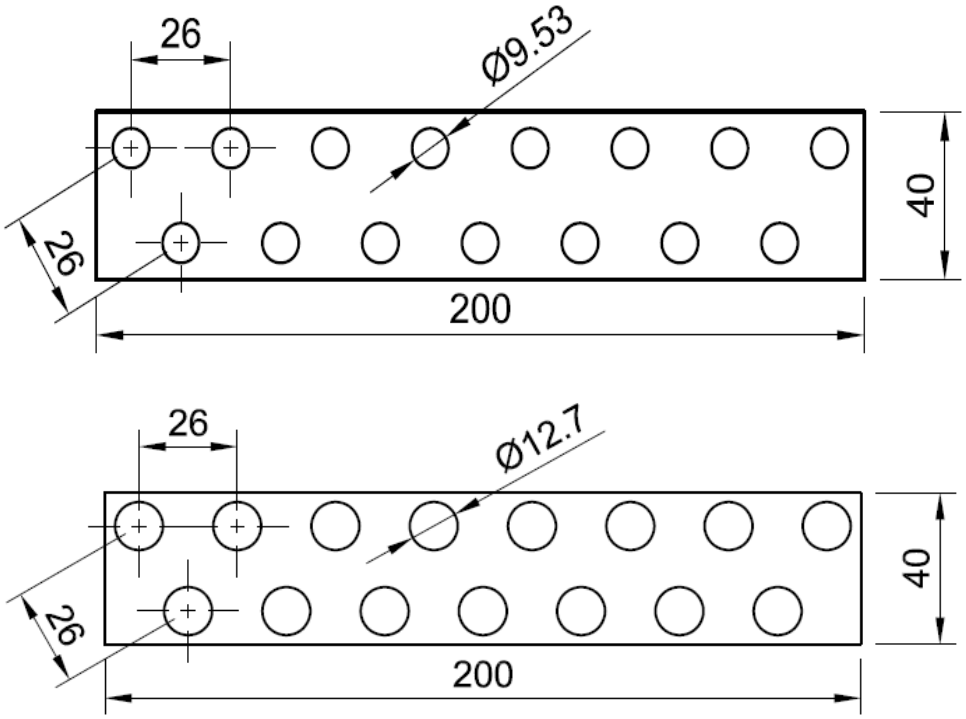

Figure 15: Tube bank tube layout (OD of 9.53 mm and 12.7 mm)

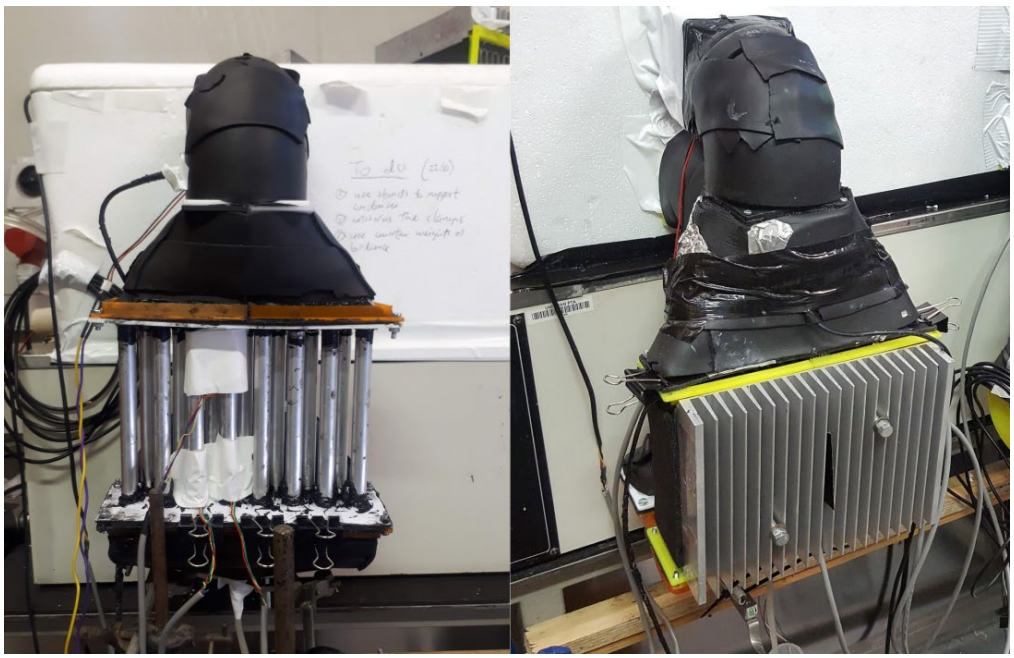

Figure 16: External condenser: (a) Heat sink and (b) Tube bank

Figure 17 shows the modified tube bank external condenser. The modifications include the number of tubes, the inclination angle of tubes, transverse and longitudinal pitch, and exposed length of tubes; the modified tube banks were also built for a diameter of 9.5 mm and 12.7 mm. Table 9 compared the dimensions of the modified tube banks against the existing heat sink and tube banks; the modified tube bank had an inclination angle of 25°.

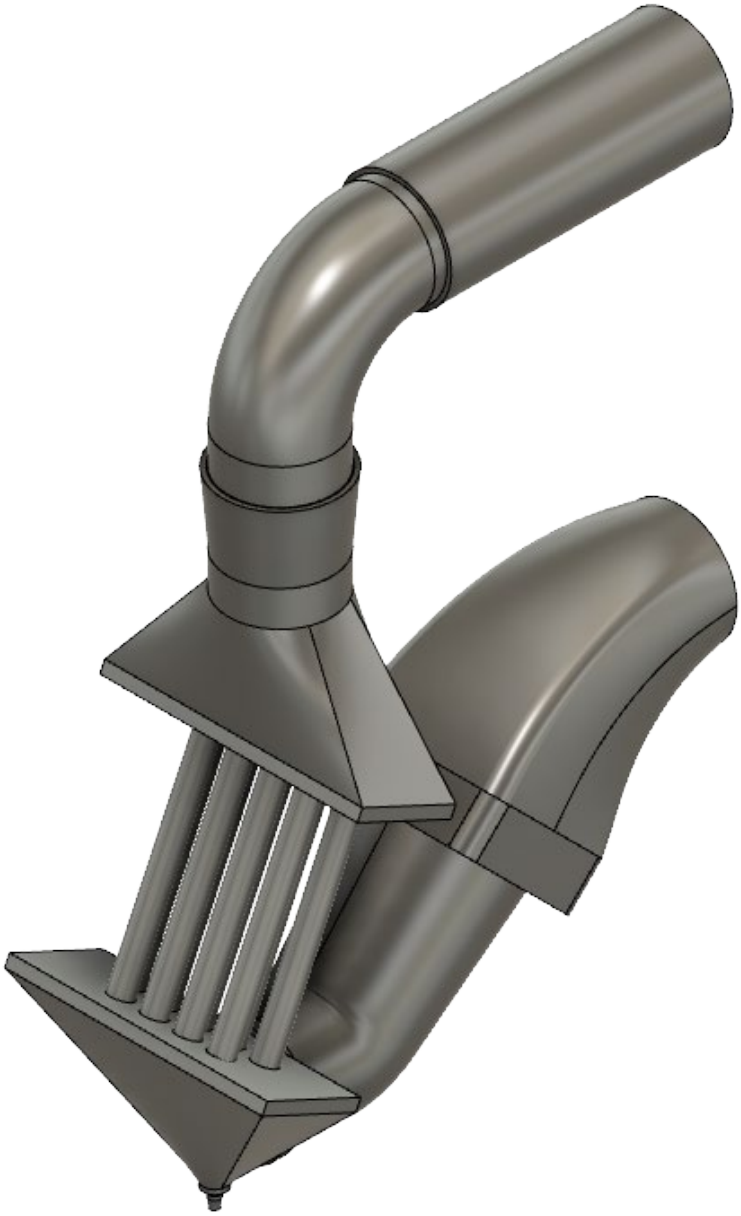

Figure 17: External condenser: Modified tube bank

The dimensions of modified tube banks were designed to ensure both tube banks have the same surface area. In this way, the difference in the diameter is the only variable. The modified tube banks can be used to determine if the external condenser and still performance favour a smaller or larger tube diameter, i.e., 9.5 mm or 12.7 mm.

The external condensers can be further adapted by using an air fan to provide forced air flow over the external condenser, creating a forced convection cooling scenario. The heat exchangers' performance was investigated under natural convection and forced convection cooling modes.

The heated water bath is illustrated in Figure 18 with the air flow pathway also shown. The heated water bath provides 3 kW of heating energy and ensures that the humid air remains within an acceptable temperature range. The heated water bath was partitioned to accommodate the simultaneous runs of the natural and forced convection cooling experiments.

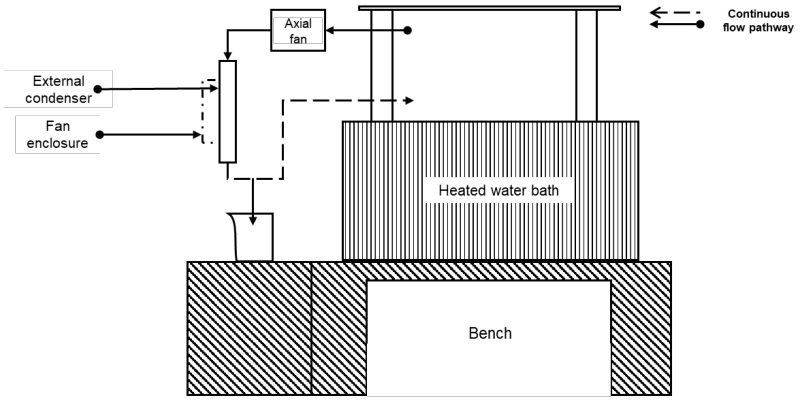

Figure 18: Experimental illustration of the heated water bath

3.1.4 Active Solar Still Experimental Equipment

As previously shown in Section 2.2.1, and shown by Figure 3 and Figure 4, the solar basin still dimensions used by Marais (2018) were geometrically optimised from literature by:

- Using a ratio of length to width of 2 (Feilizadeh, et al., 2017, p. 163).
- Using the minimum, practical still front height that allowed inclusion of a water collection system and a sufficient angle of inclination for the cover surface condensation to run down (Feilizadeh, et al., 2017, p. 163).
- Using the latitude location of Pretoria as the angle of inclination. This is the location where experiments were conducted (Singh & Tiwari, 2004).

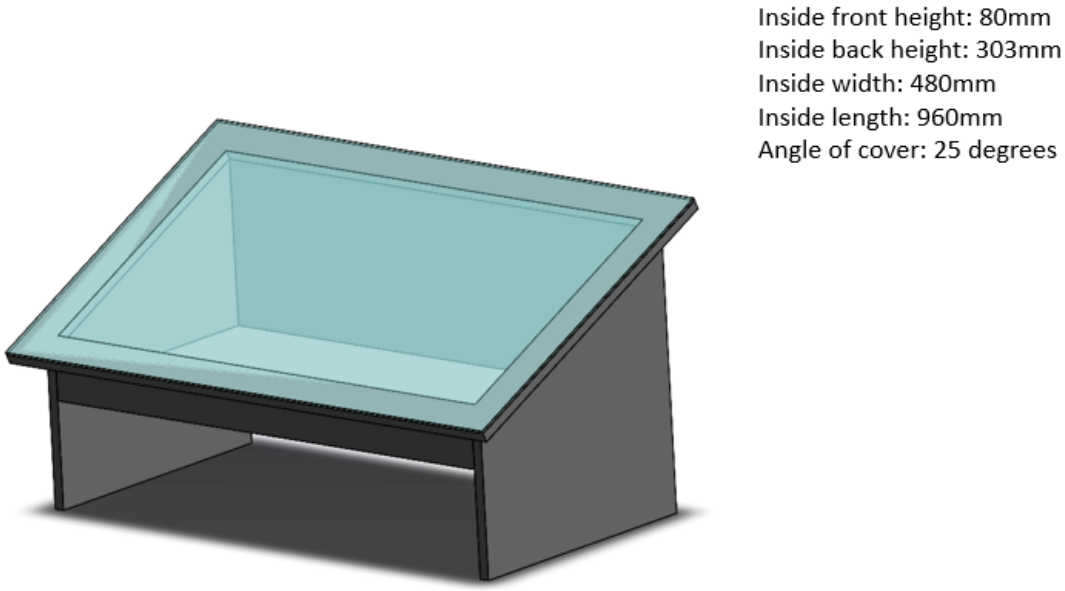

Figure 3: Geometry of Marais' (2018) passive basin solar still

The most superior still, still variation 3, shown in Figure 4 was only modified by adding the air and water circulation pathways as illustrated in Figure 12. The unmodified version of still variation 3 was used as the reference still for the active solar still baseline experiments. The best performing cover surface and external condenser were used for the active solar still.

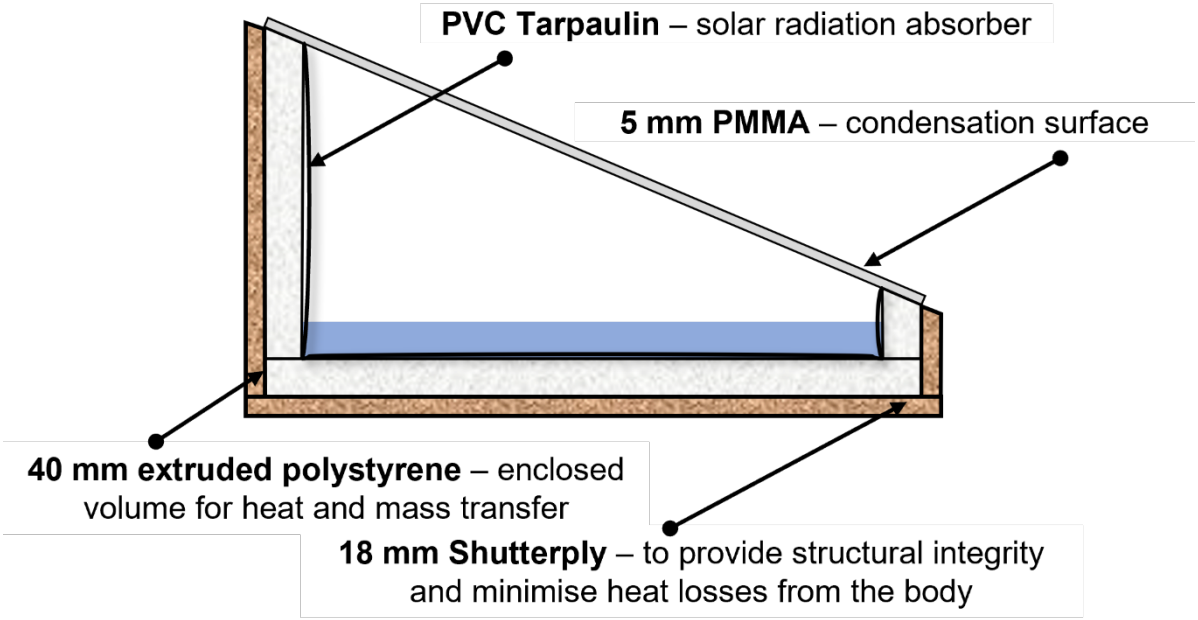

Figure 4: Base design of still variation 3 (Marais, 2018)

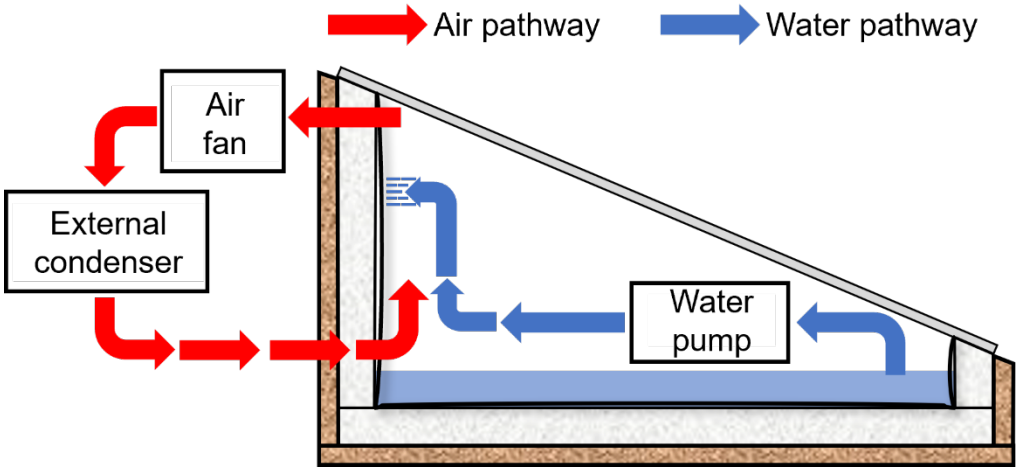

Figure 12: Modified basin solar still enabling fluid flow modifications

3.1.5 Instrumentation and Data Acquisition

The performance variables of the cover surface, heated water bath, and active solar still experiments were monitored and measured by an Arduino™ MEGA 2560 microcontroller with a data logging shield. The data captured was logged to the SD card every four seconds for the heated water bath experiments, and every 60 seconds for the cover surface and active solar still experiments. Table 10 summarises the different types of sensors used, the respective variable measured, and the range and accuracy of the sensor.

Table 10: Position, variable, and uncertainty error of the different types of sensors

Type of sensor	Variable	Range and Accuracy	% Error
DHT22	Temperature	-40:125 ± 0.5 °C	0.5
DS18B20	Temperature	-10:85 ± 0.5 °C	1.2
TAL220 load cell	Mass	0 – 1 kg ± 0.001 kg	–
TAL220 load cell	Mass	0 – 5 kg ± 0.005 kg	–

The DS18B20 temperature sensors came in two types: the chip sensors were used to measure surface temperatures while the waterproof version was used to measure the water temperature of a solar still. The condensation rates were recorded via a TAL220, 1 kg or 5 kg load cell, and a HX711 load cell amplifier. The specific load cell used was determined by the maximum total mass to be collected over 24 hours of operation. To

confirm the accuracy of the load cell, the condensation rates recorded from the load cell were verified against the condensate volumes collected. Solar radiation and ambient data from the Southern African Universities Radiometric Network (SAURAN) were used as reference for the ambient conditions (Brooks, et al., 2015).

Figure 19, Figure 20, and Figure 21 show the sensor positions and variables measured in each of the three experiment types.

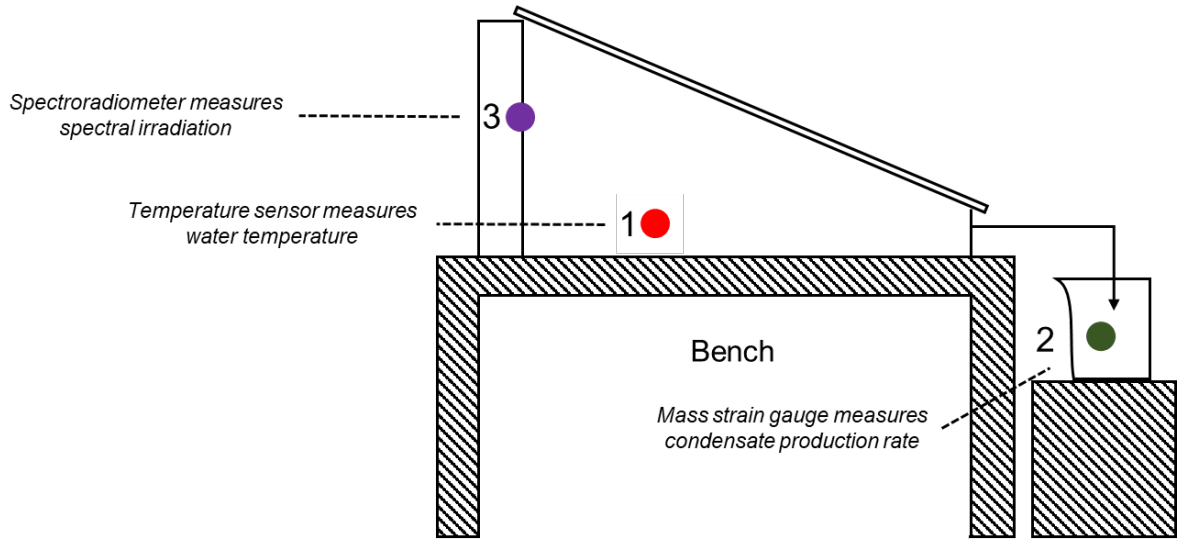

Figure 19: Sensor positions of the polystyrene solar still

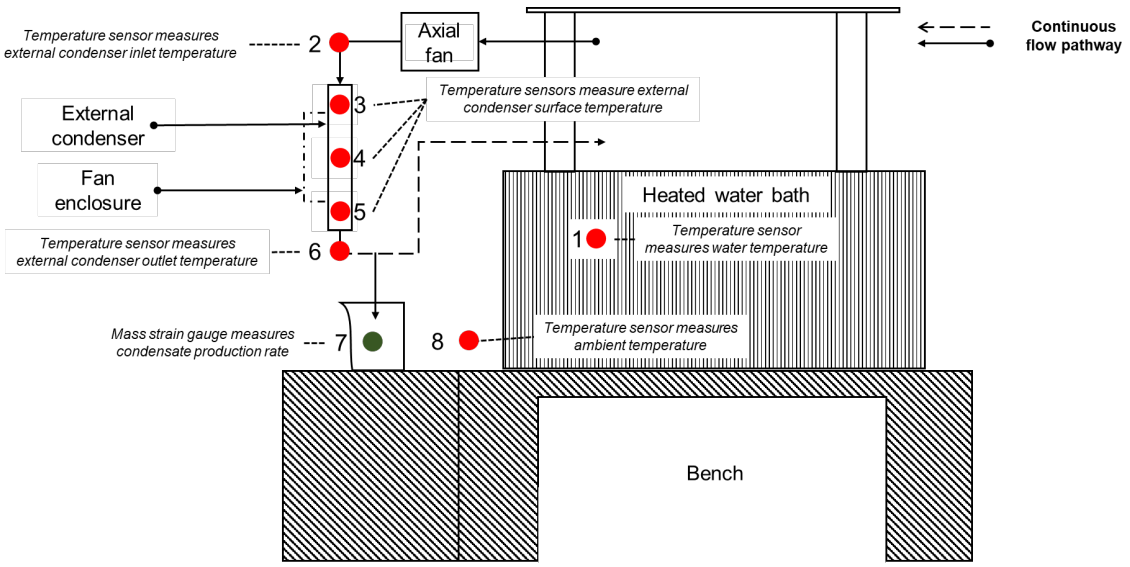

Figure 20: Sensor positions of the heated water bath

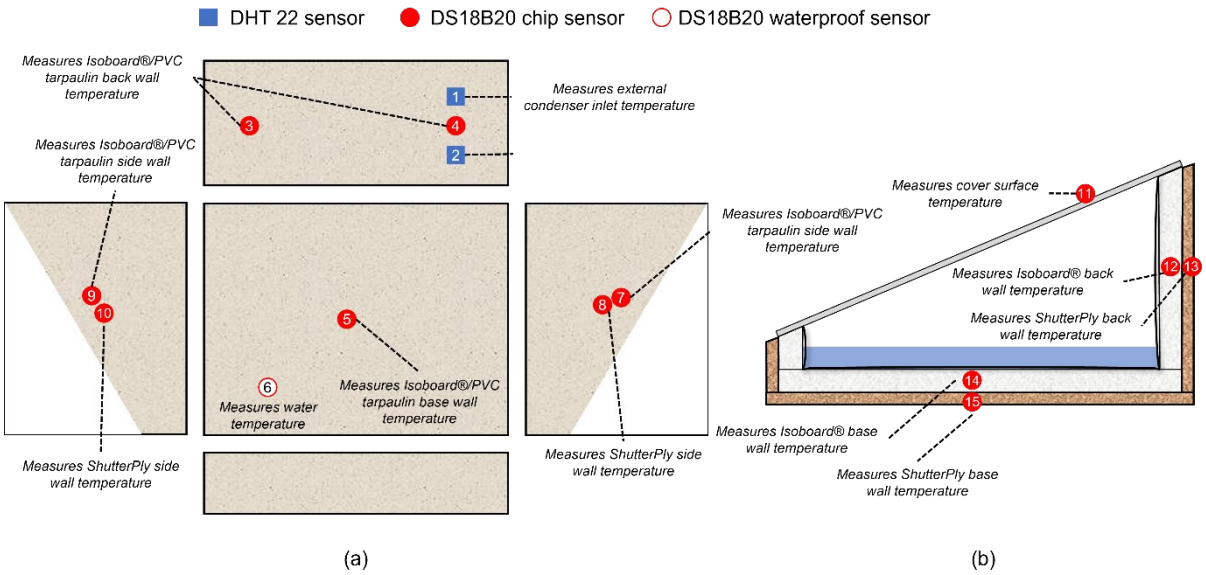

Figure 21: Sensor positions (a) inside and (b) outside of the active solar still

The load cell of the active solar still was omitted from Figure 21 as it was placed underneath the active solar still. Although the external condenser was not shown, the external condenser had its own set of sensors as indicated in Figure 20.

3.2 Experimental Design

3.2.1 Reporting of Solar Radiation

The global horizontal irradiation data from SAURAN was used as solar radiation data for the experiments. A baseline for winter 2021, summer 2021/22, and winter 2022 was generated using the average of between 5 – 10 clear and sunny days to determine the total solar irradiation for the specific season. As the current experiments will be run in the summer, the baseline days used the same period range across summer 2021.

The average solar radiation baseline will be reported as the 100 % level of radiation. All experimental days will report its respective solar radiation level as a percentage to the average solar radiation. The reported percentages acts as an initial test of the validity of comparing the experimental results across the different experimental days.

3.2.2 Cover Surface Experiments

The objective of the cover surface experiments was to find a cover surface that will reduce the energy losses of the current 5 mm PMMA cover surface. Three identical polystyrene stills were built to run the cover surface experiments simultaneously, i.e., one solar still with a 5 mm PMMA cover surface, one with a 4 mm single pane glass cover surface, and the other with a 10 mm double pane glass cover surface. The cover surface experiments were performed across two weeks between 25 August 2022 – 02 September 2022.

A StellerNet BLUE-Wave VIS-25 spectroradiometer was used to measure spectral irradiation through the cover surfaces, by means of a cosine-corrected detector, in the wavelength range of 350 – 1000 nm. The condensate yield, water temperature, and solar irradiance inside the still were used to compare the performance of the cover surface material. Measuring the water temperature and solar radiation allows us to compare the effect of the type of cover surface on the condensation collection profiles, water temperature profiles, and radiation losses through the cover surface. The cost benefit of the cover surfaces is considered in the performance analysis of the polystyrene solar stills; the condensate yield will be used to determine if the cost difference and performance difference of the cover surfaces is enough to justify the use of the selected cover surface material. The threshold performance required by the single-, and double pane glass is to produce more yield, retain more energy, and transmit more solar radiation than the PMMA.

3.2.3 Heated Water Bath Experiments

The objective of the heated water bath experiments was to find the best performing external condensation surface, under a specific convection cooling mode, that allows the right amount of heat loss without sacrificing overall still performance:

1. To characterise the performance of the external condensers in a controlled environment.
2. To improve the performance of the external condensers through physical modifications.

Between 5 – 10 heated water bath experiments were run in the laboratory, using an enclosed heated water bath to produce a humid environment similar to a solar still. This allowed the exact performance of the external condenser to be isolated without the effect of ambient conditions. The heated water baths also allowed quicker alterations to the experimental design compared to building full-size prototypes for testing.

The water temperature of the heated water bath was initially set to 60 °C. This was chosen from Marais' (2018) results which showed maximum temperatures of 60 °C during the day. However, to quantity the effect of water temperature on the performance of the external condenser, the heated water bath was also run at 50 °C and 55 °C.

The temperature of the saturated humid air in and out streams were used to determine the energy transferred by the heat exchanger and consequently determine the overall heat transfer coefficient by means of Equations (12). The change in humid air was also used to rate the cooling impact of the heat exchanger – the smaller the $\Delta T_{humid\ air}$, the better the heat exchanger performance as more energy was used for condensation and not subcooling. The change in surface temperature of the heat exchanger was monitored to rate the driving force potential of the heat exchange.

The distillate yield and energy efficiency given by the external condenser; calculated by Equation (3), were also used to rate the performance of the external condenser. The yield per area ratio completed the set of metrics used to rate the performance of the external condenser.

The air fan, rated at 20 $m^3.hr^{-1}$, simulated the forced convection cooling mode, and was used to determine the effect of natural or forced cooling mode on the external condenser. The water and ambient temperatures were measured to ensure the experimental results were comparable and no anomalous conditions were experienced.

3.2.4 Active Solar Still Experiments

The objective of the active solar still experiments was to use the best performing cover surface and external condenser, respectively, attached on the active solar still:

1. To field test the active solar stills with external condensers attached.
2. To use the active solar still to achieve a water production cost on par with current local municipal water rates of 0.67 c/l, or cheaper (City of uMhlathuze, 2021; Sol Plaatje Municipality, 2021). The water production rate will also be compared against the current distilled water market rate of R4.40/l (Checkers, 2021).
3. To reduce energy accumulation of the back wall.

Literature has shown that using an active solar still with an agitation effect can improve the yield productivity by up to 40 % and give an energy efficiency as high as 50 % (Fath & Elsherbiny, 1993). Because the active solar still was compared against Marais' (2018) still variation 3 which recorded a daily productivity of 2.4 $L.m^{-2}$, 3.4 $L.m^{-2}$ was used as the threshold for the active solar still – to reach the current local municipal water rates of 0.67 c/l, a daily productivity of 4.7 $L.m^{-2}$ is needed – representing a 96 % condensate increase. Similarly, Marais' (2018) still variation 3 recorded a still efficiency of 26 %. To reach 0.67 c/l, the still efficiency will almost have to double to reach a target of 51%. Literature (Ibrahim, et al., 2015) indicated a 30 % performance increase was realistic, giving an achievable energy efficiency target of 34 %. The production cost for Marais' (2018) still variation 3 was ~R1.25/l. Although when compared to the current target of 0.67 c/l, this represents a 46 % increase in active solar still water production cost – the active solar still cost investment is likely to increase by at least ~38 %. The cost investment increase, without the performance increase will mean the still does not reach the municipal water rate target (0.67 c/l).

To completely isolate the effect of the fluid flow, cover surface, and external condensation area modifications, the performance of the active solar still will be baselined against Marais' (2018) still variation 3 – used in this case as a reference still. The baseline experiments quantified the performance difference between the reference still and the active solar still, based on the inherent difference of the still – caused by the variability in materials and construction. To ensure the performance of

both stills was comparable, both stills were run simultaneously under the same meteorological conditions.

From Equations (4), (5), and (6), temperature profiles of the water, extruded polystyrene, cover surface, and humid air were used to determine the internal energy of the still control volume. The solar intensity was used to find the energy flow into the system through Equation (7). Equation (8) gave the outflow of energy out of the system by considering convection, radiation, reflection, and conduction across the solar still; described by Equations (9), (10), (13), (14), and (15). Recording the temperature profiles of the cover surface, ambient temperature, and still base, backwall, and sides are used to determine the various energy transfers described by Equations (9), (10), (13), (14), and (15).

The condensate energy of Equation (11) is dependent on the distillate yield and temperature of the cover surface and external condenser. The unaccounted energy can be determined by Equation (16). These set of equations form the energy balance equations – where increased condensate energy and reduced cover and body energy losses [compared to the baseline] indicate an optimal active solar still operation.

The distillate yield and energy efficiency are also used to rate the performance of the active solar still. Taking this further, the condensate recovered from the external condenser can be compared against any condensate recovered from the cover surface to determine how effective the external condenser is in directing condensation away from the cover surface. In addition to using the distillate yield and energy efficiency to rate the active solar still performance, the initial cost of the still and annualised water cost per litre were used to determine the economic feasibility of the active solar still.

Considering the humid air and the basin water fluid flow designs, the active solar still can experience three types of circulation:

- **Humid air circulation** where only the external condenser air fan is operational,
- **Water circulation** where only the water pump is operational, and
- A combination of **humid air and water circulation** where both devices are operational.

Once switched on, the water pump runs according to two scenarios:

- Run scenario 1 – the water pump runs unless the temperature difference between the back of the still and basin water is zero, and
- Run scenario 2 – the water pump runs between 09h00 and 17h00, while the sun is up.

A break in either run scenario will lead to the pump being switched off.

Table 11 shows that the experiments performed in the active solar still will only be varied by the mode of circulation. The best performing external condenser will be tested on the active solar still, where the more effective convection cooling mode will also be applied.

Table 11: Experimental cases for the active solar still

Case	Mode of circulation
1	Water
2*	Humid air
3†	Humid air and water

* if tube bank is best performing condenser, both the 9.5 mm and 12.7 mm tube banks will be run on Case 2

† if tube bank is best performing condenser, the best performing tube bank from Case 2 will be run on Case 3

3.2.5 Equation Constants and Physical Properties

The constants and physical properties used in the energy balance equations are noted in Table 12 (Çengel & Ghajar, 2015, p. 860).

The properties of the single pane glass and PMMA cover surfaces, aluminium, and extruded polystyrene were evaluated at a room temperature of 23 °C. Humid air and water were both evaluated at an average temperature of 50 °C. It is assumed that the effect of the variation of the properties of air and water due to temperature variations will be insignificant to the outcome of the results. Stefan-Boltzmann's constant was included as 5.67×10^{-8} $J.s^{-1}.m^{-2}.K^{-4}$.

Table 12: Equation constants and physical properties

Material	k ($W.m^{-1}.K^{-1}$)	R (K/W) †	ε	ρ ($kg.m^{-3}$)	C_p/C_v ($J.kg^{-1}.K^{-1}$)	μ ($kg.m^{-1}.s^{-1}$)	Pr
SPG	0.7	476	0.925	2,500	815	–	–
DPG	–	17.87	0.925	–	–	–	–
PMMA	0.19	1,053	0.86	1,180	1,270	–	–
Aluminium	222	4.51×10^{-3}	–	2,770	875	–	–
Extruded polystyrene	0.035	1,143	–	32	1,400	–	–
Water	0.673	–	–	1,000	4,200	0.33×10^{-3}	2.08
Air*	0.027	–	–	1.10	720	1.96×10^{-5}	0.72

* Evaluated at an average temperature of 50 °C

† Resistance of material

3.2.6 Cost Analysis

The cost objective of the active solar still is to achieve a water production cost on par with the current local municipal water rates of 0.67 c/l, or cheaper (City of uMhlathuze, 2021; Sol Plaatje Municipality, 2021).

The life cycle cost analysis is used to determine the annualised unit cost per litre of distilled water. Literature shows that simple basin stills have a cost range of R 0.2/l – R 0.5/l while complex solar stills are in the R 0.9/l – R 1/l range (Table 5). However, literature suggests using market costs as a benchmark to rate the annualised unit cost per litre of the active solar still. Using local rates gives a better indication of how well the solar still performs. The annualised cost of the active solar still is also compared to the reference still. This comparison will indicate the annualised cost implication of the fluid flow, cover surface, and external condensation area modifications.

The life cycle cost analysis uses the initial capital cost of the active and reference solar stills to determine the annualised cost. Using the prime lending interest rate and the respective solar still performance metrics of condensation area, daily productivity,

annual runtime, and lifecycle years, the annualised cost for each still can be calculated.

Additionally, the effect of extending the lifecycle years on the annualised cost is determined to understand whether it's better to create a robust still that lasts between 10 and 15 years, or to create a cheap still that lasts 5 years on average. The trade-off here compares the economic value generated from frequently producing solar stills against creating robust stills that can be used for an extended period without the need for major repairs.

3.3 Method

The cover surface and active solar still experiments were run at the University of Pretoria Hillcrest Campus, Experimental Farm site located in Pretoria, South Africa, at the coordinates of 25.74° S, 28.23° E. The Experimental Farm provided an open field with no obstructions to natural air flow and sunlight. The solar stills were north facing for maximum exposure to solar radiation.

3.3.1 Cover Surface Experiments

All three polystyrene stills were run simultaneously. The experiments were run early morning to the following morning. The collected data was filtered to only include the period between 09h00 and 17h00. All three stills were charged with the same amount of water (approximately 4 L) to ensure that the bottom surface is completely covered and does not run dry during the experiment.

The internal water temperature, ambient temperature, and condensate collected were recorded as discussed in Section 3.1.5. Solar irradiance data was collected outside the stills and thereafter inside the stills to determine the difference in the solar irradiance caused by the still cover material. These measurements were taken on a clear day and were repeated for early morning exposure, noon exposure, and in the afternoon.

3.3.2 Heated Water Bath Experiments

The heated water baths were run indoors, in a temperature-controlled laboratory. The heated water bath was sealed with a polystyrene cover after being filled with tap water to an appreciable height. The depth of water was enough to ensure a sufficient and continuous supply of water vapour to the heat exchanger.

After the heat exchanger was connected to the condensate collector, the air fan was switched on. The integrity of the setup was checked for any leaks or airgaps. If there were no leakages, the heated water bath was switched on. The water temperature of the heated water bath was set to a pre-determined temperature, for example 60 °C. The experimental runs were performed on an hourly basis. At the end of the run, the air fan was switched off while the water heater remained on. The condensate collector was weighed, and the condensate mass was recorded. After reconnecting the condensate collector, the still was ready for the next experimental run.

3.3.3 Active Solar Still Experiments

The solar stills were started early morning between 06h00 and 08h00 with the start-up procedure as follows:

1. Clean the inside and outside of the cover surface.
2. Fill each still with the required 9.2 kg of water.
3. Choose mode of circulation for the active solar still.
4. If either “Water” or “Humid air and Water” circulation mode is chosen, switch on pump.
5. Close the still cover, ensuring it is properly sealed.
6. Calibrate the load cells on each still with a four kg calibration mass and the respective zero weights.
7. Begin logging data for the stills.
8. Add 0.2 kg of water to each collection container to act as a baseline measurement.
9. Still runs in the day, through the night, and into the next morning, ready for re-run.
10. Transfer still data from SD card and verify final condensate volumes.

The procedure is identical for the reference and active solar stills, except for steps three and four which only applies to the active solar still. Before the still is started for the next run, the water level needs to be topped up to the 20 mm depth, which is the minimum practical depth to ensure no possibility of a dry-run scenario (Feilizadeh, et al., 2017, p. 163). This is accounted for in step two. Once the water mark is confirmed, steps 3 – 10 are repeated for the next experiment.

3.3.4 Data Analysis

The measured and recorded solar still data was processed using Excel. The analysis was based on a steady state model of time discretisation; assuming the change in time intervals were small enough to cover over 95 % of the graph areas analysed. The steady state model was confirmed by repeatedly running experiments under the same operating conditions, making it easier to highlight patterns of normal, steady state operation. Some of the assumptions stated for the different experiments might contribute to any deviations from the steady state assumption.

Because the condensate yields in the solar still experiments were dependent on the incident solar radiation received on a particular day, each day was calculated as a percentage of the average solar radiation recorded during the previous season. The fraction of solar radiation received was considered when comparing condensate yields across different days.

The main assumptions made to simplify calculations and analysis of the different experiment datasets were shown.

All Experiments

- Assume ideal gas law holds.
- Fluid flow is assumed to follow bulk behaviour, ignoring point-to-point variations in physical properties (Çengel & Ghajar, 2015).
- Assume the no-slip condition applies, the layer of fluid adjacent to the boundary has zero velocity relative to the boundary (Welty, et al., 2015, p. 83).
- PVC tarpaulin is considered to not significantly be a resistance to heat transfer.

Cover Surface Experiments

- Ambient effects (wind speed, ambient temperature; except solar radiation) were noted as natural disturbance variables and assumed to cause insignificant differences between the three identical stills that were run co-currently.

Heated Water Bath Experiments

- The fluid properties of air and water will have negligible variations over the planned range of temperatures.
- Furthermore, analysis of the humid air energy balance metrics was assumed to remain in a range between 15 and 85 °C, leading to an average temperature of 50 °C used to evaluate the humid air properties. The % error between the temperature range and the average temperature was 0.02 %, with a final impact of 2.20 % on the humid air energy accumulation, indicating minimal deviation with the average temperature assumption. The density and specific heat capacity in the 20 to 80 °C range varied at a rate of 0.27 % and 0.01 % per degree Celsius change in temperature. The impact of temperature change is minimal when kept within a few degrees Celsius.

The energy analysis of the heated water bath was used to determine to $Q_{air\ dif}$ – energy available for condensation losses, UA – overall heat transfer coefficient of the external condenser, and the combined energy efficiency of the cover surface and external condenser. The control volume of the heated water bath, cutting the humid air flow streams, was used for the analysis.

Active Solar Still Experiments

- No seasonal variation on the performance of the active solar still.
- Humid air remains saturated across the external condenser and active solar still and the absence of a significant process pressure change meant subcooling of the humid air was not considered.
- Assume the configuration differences between the 9.5 mm and 12.7 mm tube banks are negligible.

Still variation 3 was benchmarked against the active solar stills experiments without any circulation, with the performance difference of the active solar still attributed to the circulation mode of the active solar still. The energy balance used the still body as the control volume, considering the sides, backwall, and base of the still. The energy lost as condensate over the cover surface and external condenser was the energy efficiency of the active solar still when compared to the total radiation energy received.

The annualised unit cost of distilled water used solar still condensate productivity and still dimensions to calculate the life cycle cost comparison of the reference solar still and active solar still.

4. Results and Analysis

4.1 Solar Radiation Baseline

The average solar radiation baseline on a clear, sunny day for summer, and winter is shown by Figure 22. The average solar radiation baseline is compared against the solar radiation recorded during experimental runs to determine similarity of the solar radiation. This was possible due to the incremental deviation seen within each dataset; 18,020 ± 540 kJ.m^{-2} for winter 2021 (3 % deviation), 30,890 ± 1,140 kJ.m^{-2} for summer 2021/22 (4 % deviation), and 15,850 ± 110 kJ.m^{-2} for winter 2022 (1 % deviation). The incremental deviation validated the use of the average solar radiation baseline for comparison with solar radiation recorded during experimental runs performed between 25 August 2022 – 02 September 2022. The average solar radiation for summer 2021/22 was reported as the 100 % radiation level, with all radiation values reported as a percentage to the average solar radiation. The cover surface experiments saw an average of 20,940 ± 380 kJ.m^{-2} (2 % deviation) of solar radiation, which is 68 % of the summer 2021/22 average.

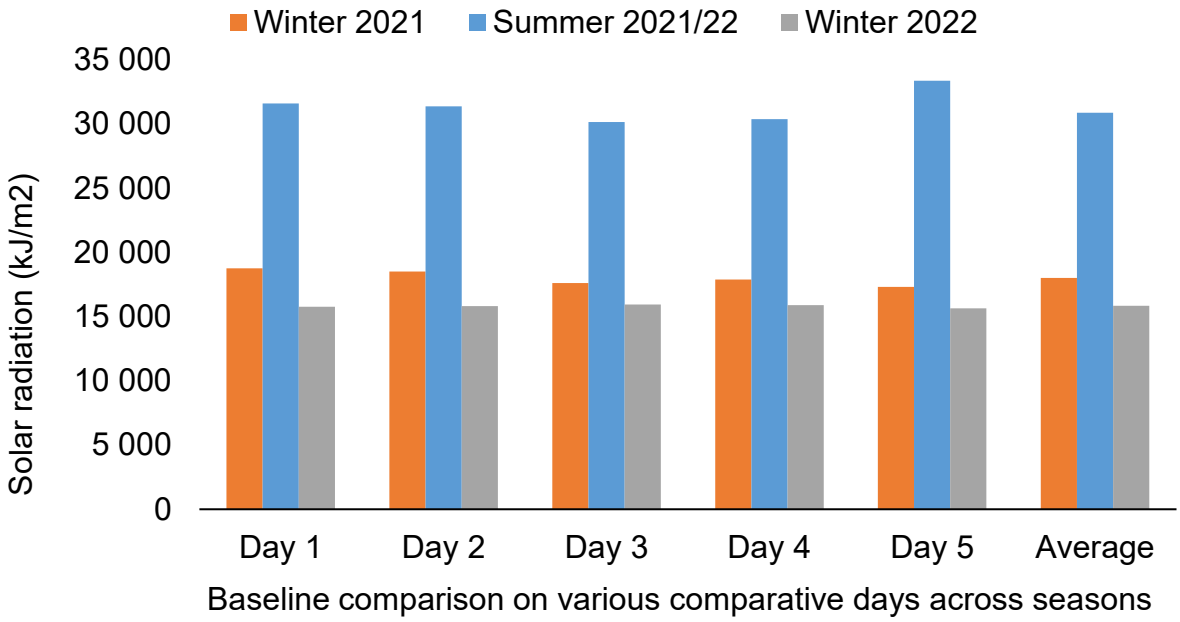

Figure 22: Average solar radiation baseline on a clear, sunny day (Brooks, et al., 2015)

4.2 Cover Surface Experiments

The cover surface experiments were used to confirm which cover surface – PMMA or single pane glass – gave the best performance.

4.2.1 Effects of Disturbance Variables

Although ambient effects – except solar radiation – were assumed to be insignificant, wind speed and ambient temperature can have a significant effect on the output of the polystyrene solar still in two ways; 1) by causing vibrations to the cover surface that could increase the condensate runoff which would allow more condensation to form on the cover surface and give less reflective losses from the cover surface, and 2) by influencing the overall heat transfer coefficient across the cover surface and external condenser; a light moving wind will improve the heat transfer coefficient, however if the wind is at a low temperature, the driving force to ambient will increase the heat lost through the cover surface. However, no correlations were investigated as ambient conditions are constantly changing and were noted as natural disturbance variables. Prioritising datasets that were run under clear, ambient weather conditions meant that any variation in solar still performance was influenced by the cover surface used.

4.2.2 Cover Surface Performance

4.2.2.1 Temperature Profiles

Figure 23 showed that water temperature in both stills started increasing around 09h00, reaching a peak of 70 °C, 67 °C, and 62 °C at 13h00, for the double pane glass, single pane glass, and PMMA, respectively. Towards sunset (18h00), the water temperature decreased rapidly due to the loss of solar radiation into the stills while condensate was still being generated. The water temperature of glass surfaces heated up more quickly than the PMMA during daylight hours; although the water temperature of the single pane glass still cooled down much quicker than the water temperature of the PMMA still during night hours (shown by the temperature dip at sunset), the double pane glass was able to retain heat energy better than the PMMA or the single pane glass; this was due to the overall resistance to heat transfer of the single pane glass and the insulation effect of the double pane glass. After sunset, the water temperatures remained constant at around the ambient temperature.

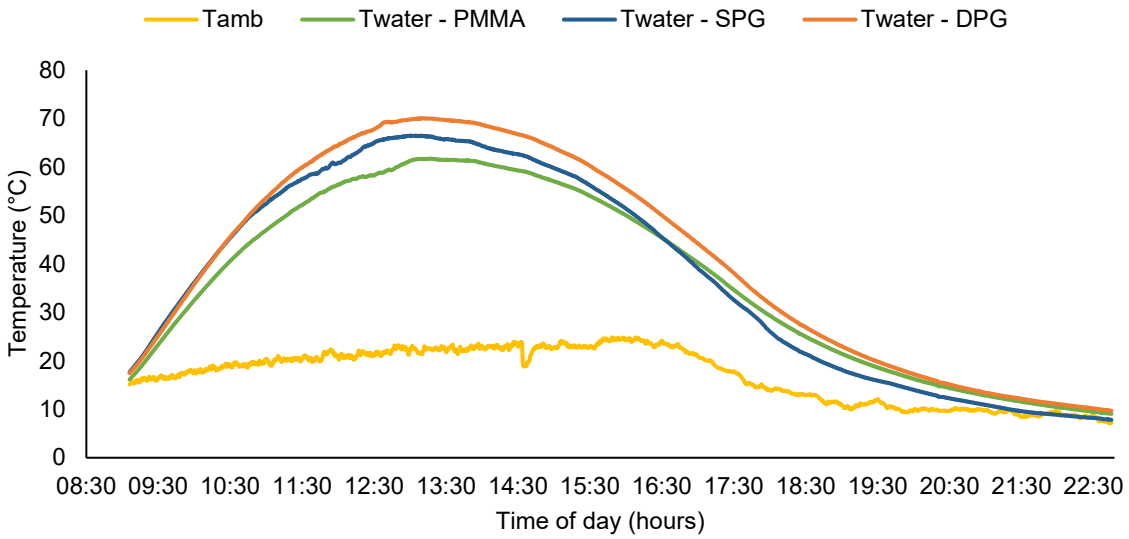

Figure 23: Daily relationship of water temperatures for PMMA, single pane glass, and double pane glass. Sensor 1 referenced from Figure 19

4.2.2.2 Condensate Collection Rate

Figure 24 showed that condensate collection started a few hours after solar radiation was first recorded, eventually peaking after midday at a value of 2.74 $L.day^{-1}.m^{-2}$, 4.27 $L.day^{-1}.m^{-2}$, and 1.08 $L.day^{-1}.m^{-2}$ for the double pane glass, single plane glass, and PMMA, respectively. On average, water collection between 12h00 and 17h00 accounted for between 66 % and 75 % of the total yield; the maximum water temperature was recorded during this period.

The condensate collection rate approached zero as sunset approached, with no additional condensate recovered after sunset; the water production profiles were similar for all cover surfaces – with the only difference being the condensate yields collected. A higher internal water temperature correlated to higher cumulative yields; the single pane glass with a maximum internal water temperature of 67 °C gave a total yield of 0.442 kg compared to the PMMA which had a maximum internal water temperature of 62 °C and gave a total yield of 0.112 kg; a recovery increase of 296 % for a 4 °C change.

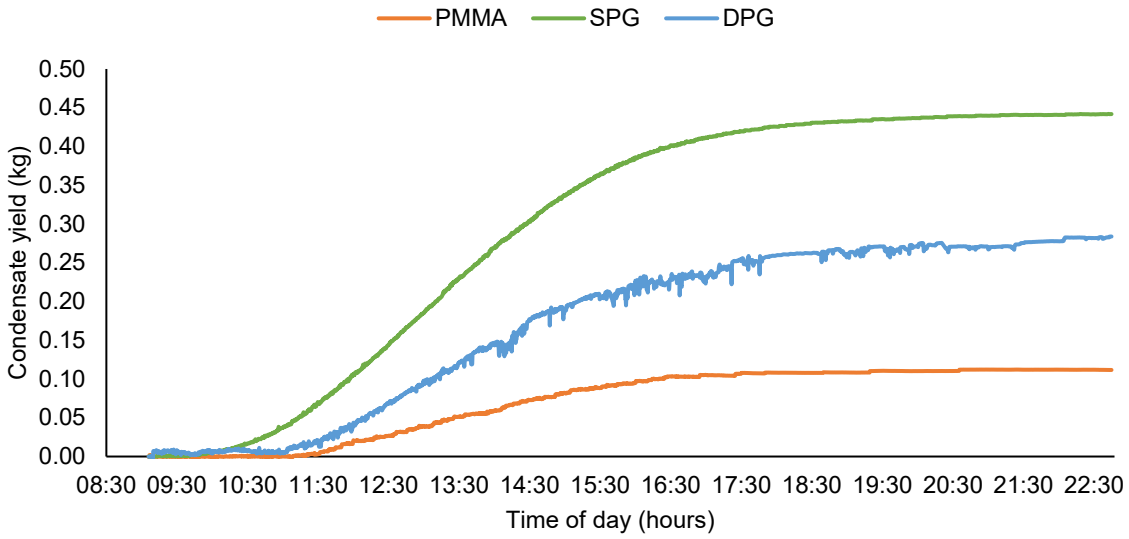

Figure 24: Daily relationship of condensate yield for PMMA, single pane glass, and double pane glass. Sensor 2 referenced from Figure 19

Although to a lesser extent, the double pane glass gave a total yield of 0.284 kg for a larger 8 °C change. The presence of high temperatures results in more condensate collected for the glass surfaces than PMMA (this is also due to other factors such as cover surface runoff mechanism – discussed in more detail in later paragraphs). PMMA deforms at high temperatures, resulting in a convex surface on the inside of the still – this results in water droplets losing speed as they run down the PMMA surface, stagnating, and dripping back into the still. The condensate yield recovered was for a cover surface area of 0.21 m^2.

The distillate yield and changes in yield performance of the cover surfaces are shown in Table 13.

All the test days were comparable since ambient weather conditions were similar compared to the average solar radiation of summer 2021/22 baseline. Table 13 showed that the single pane glass polystyrene solar still had a higher condensate recovery than the double pane glass and PMMA polystyrene stills, recovering condensate at an average of 0.446 kg compared to 0.232 kg and 0.119 kg, respectively; the single pane glass polystyrene still showed 275 % better recovery than the PMMA polystyrene still, while the double pane glass also showed a better recovery performance of 95 %; the single pane glass performance was almost twice of the

double pane glass. This confirmed that the process of losing energy through the cover surface is critical to improve condensate recovery of a solar still.

Table 13: Cover surface yield performance

Day	Solar radiation (%)*	PMMA yield (kg)	SPG yield (kg)	Increase in yield (%)†	DPG yield (kg)	Increase in yield (%)†
1	69	0.123	0.450	264	0.164	32
2	68	0.135	0.477	253	0.153	13
3	67	0.125	0.459	268	0.263	111
4	67	0.109	0.464	326	0.259	138
5	66	0.111	0.450	306	0.216	95
6	68	0.112	0.442	296	0.284	154
7	69	0.117	0.381	224	0.283	140
Average	68	0.119	0.446	275	0.232	95

* 30,890 $kJ.m^{-2}$ of solar radiation reported as 100 % level

† Increase in yield based on PMMA yield

The superior single pane glass performance was due to the condensate forming mechanism inherent to each cover surface. Condensate on the hydrophilic single pane glass surface formed thin films and ran down as a continuous stream compared to the dropwise condensation of the hydrophobic PMMA surface (Klöckner & Büchs, 2011; Ko, et al., 2017). Droplets that reached critical mass dropped back into the basin if not close enough to the collection point. Film condensation reduced this type of losses while allowing more solar radiation to reach the base of the polystyrene still; this also explained why the single pane glass surface had higher distillate yields. Dropwise condensation also posed a stronger resistance to heat transfer; the heat transfer coefficients for condensation are in the range of 10,000 $W.m^{-2}.K^{-1}$ for film condensation and 200,000 $W.m^{-2}.K^{-1}$ for dropwise condensation. For the same heat loss, film condensation will give faster rates of condensation (Çengel & Ghajar, 2015, pp. 205, 618-627).

Film condensation left the glass surface clear and transparent while dropwise condensation left the PMMA surface partially opaque. This is shown in Figure 25. A clear glass surface resulted in more solar radiation reaching the solar still base; as more solar radiation reached the base, less reflection, radiation, and scattering was experienced at the cover surface.

(a) (b)

Figure 25: Comparison of condensation mechanisms for (a) PMMA and (b) Single pane glass

The StellerNet BLUE-Wave VIS-25 spectroradiometer sensor of a solar concentrator was used to measure spectral irradiation through the cover surfaces. When placed normal facing the sun, solar radiation was ~1,140 $W.m^{-2}$ compared to ~271 $W.m^{-2}$ (24% of direct, normal radiation) when placed away from the sun, without any cover surface interference; this is shown in Table 14, along with the average solar radiation interference of the glass cover surfaces.

Table 14: Radiation transmittance of cover surfaces

Cover surface	Irradiation ($W.m^{-2}$)*	Radiation transmittance of cover surface (%)	Dominant wavelength absorbed (nm)†
Direct	1,140	–	900 – 1,100 (77 %)
Ambient	271 (24 %)	100	900 – 1,100 (26 %)
PMMA	217 (19 %)	80	400 – 500 (23 %)
SPG	208 (18 %)	77	400 – 500 (24 %)
DPG	196 (17 %)	72	400 – 500 (26 %)

* Irradiation of cover surfaces compared to direct normal radiation of ~1,140 $W.m^{-2}$

† % of dominant wavelength shown in parentheses

The different cover surfaces changed the amount of radiation refracted through the cover surface; PMMA was the best performing, allowing 80 % of refracted radiation through – compared to 77 % and 72 % for SPG and DPG. Although dropwise condensation of PMMA allowed more heat energy through into the cover surface still, the convex deformation of PMMA and drop back of dropwise condensation reduced the collected condensation of PMMA (0.119 kg) when compared to SPG (0.446 kg) and DPG (0.232 kg).

Additionally, the different cover surfaces absorbed heat at the same wavelength of 400 – 500 nm, although the dominant wavelength for direct, normal radiation was 900 – 1,100 nm. The absorption of lower wavelengths through the cover surfaces showed that the 400 – 500 nm wavelength retained more heat when compared to the 900 – 1,100 nm range.

Although PMMA has better optical properties over the glass surfaces, the convex deformation and condensate drop back experienced by PMMA stills introduced a disadvantage that allowed the glass surfaces to produce better distillate yields over the PMMA. The film condensation mechanism was less pronounced on the double pane glass; due to the insulation effect of the double pane glass, more energy was retained by the double pane glass rather than let through to the base of the still.

4.2.3 Cover Surface Comparison

The results of the cover surface experiments are summarised in Table 15 where the performance of the PMMA cover surface was used as baseline; the average dataset was used for the final analyses.

Table 15: Comparison of the polystyrene solar still data analyses

Dataset	Cover surface*	$T_{ambient}$ (°C)	Solar radiation ($kJ.m^{-2}$)	T_{water} (°C)†	Total yield rate ($L.day^{-1}.m^{-2}$)
Minimum	PMMA	12.0	20,340 (66 %)	16.1	1.05
	SPG			17.6	3.40
	DPG			17.4	1.48
Maximum	PMMA	25.2	21,430 (69 %)	65.6	1.22
	SPG			69.7	5.79
	DPG			74.9	3.05
Average	PMMA	18.7	20,940 (68 %)	41.8	1.22
	SPG			43.5	4.58
	DPG			45.3	2.38

* SPG/DPG – single/double pane glass

† Water temperature at 9am used for the minimum dataset

The difference in cover surface performance was independent of solar radiation due to the experimental runs showing similar levels of solar radiation across the test days. Although the single pane glass achieved higher peak water temperatures compared to the PMMA, the order of difference was always within 4 %. The double pane glass produced water temperatures 4 % higher than the single pane glass; the improved performance on water temperature was due to the insulation effect of the double pane glass reducing the energy losses through the cover surface.

Total condensate collected showed a major difference in performance. Single pane glass achieved 275 % condensate recovery ahead of the baseline PMMA cover surface while the double pane glass recovered 95 % more than the baseline. The performance difference was attributed to the different modes of condensation inherent to each cover surface; PMMA experienced dropwise condensation – where the

resistance to heat transfer was 200,000 $W.m^{-2}.K^{-1}$, while the glass cover surfaces experienced film condensation – where the resistance to heat transfer was 10,000 $W.m^{-2}.K^{-1}$.

Comparing the PMMA, single pane glass, and double pane glass, the higher heat retention of the double pane glass coupled with being the second highest condensate collected indicated a significant reduction in energy losses even as the film condensation of the double pane glass had a lower resistance to heat transfer [compared to the PMMA surface]. This was mainly due to the insulation effect of the double pane glass which showed a resistance to heat transfer of 1.43 $W.m^{-1}.K^{-1}$ compared to 0.19 and 0.7 $W.m^{-1}.K^{-1}$ of the PMMA and single pane glass, respectively. The single pane glass showed reduced energy losses when compared to the PMMA, but to a lesser extent [when compared to the double pane glass] as the single pane glass produced the most condensate of the three cover surfaces.

The final layer of analysis was the cost comparison; a 5 mm thick PMMA cost R 974 per m^2 while a 4 mm thick single pane glass and a 10 mm thick double pane glass cost R 259 per m^2 and R 518 per m^2, respectively. There was a 73 % cost savings from using single pane glass. The only caution was the fragility of single pane glass which can quickly turn into a cost burden by increasing the maintenance cost of the solar still. Accounting for a spare single pane glass cover, the final cost savings was 47 % (same as the double pane glass); either of the single or double pane glass cover surfaces will positively impact Objective 4 – achieve a water production cost of 0.67 c/l or cheaper.

The double pane glass presented as the most balanced option between reducing energy losses and producing condensate at the fastest rate. The double pane glass cover surface met Objective 5(a) (reduce energy losses of the PMMA cover surface) and is recommended for the active solar still experiments. How the active solar still performs when attached with a double pane glass is investigated in Section 4.4.

4.3 Heated Water Bath Experiments

The heated water bath experiments characterised the heat transfer ability of the heat exchangers (UA as a function of flow and temperature). The UA values were then used to determine the best performing heat exchanger in the field.

The heated water bath works by maintaining the temperature of the water bath at a set temperature, by turning the heating element on and off according to the temperature deviation from the set temperature – resulting in a temperature range of 45 ± 1.2 °C with a wave period of five minutes. Figure 26 and Figure 27 show the different temperature profiles of the heat sink. The data generated during the transient, start-up phase is not used and only the data obtained during steady operation, albeit varying periodically, is used for analysis.

4.3.1 Heat Sink Heat Exchanger Performance

The heat sink heat exchanger has an area for condensation of 0.171 m^2, while using an air fan with a measured airflow of 20 $m^3.hr^{-1}$. As the natural cooling and forced cooling experiments were run simultaneously, any difference in performance was due to the difference in cooling modes experienced and not due to changes in external variables.

4.3.1.1 Temperature Profiles

Figure 26 and Figure 27 show the internal heat sink surface temperature profiles for natural and forced convection cooling modes, respectively (NB: internal heat sink is the enclosed heat sink used in the circulation path of the humid air fluid). Figure 26 shows a temperature driving force of 0.2 ± 0.1 °C across the inlet and outlet of the heat sink while Figure 27 indicates a marginally better temperature driving force of 0.5 ± 0.1 °C across the inlet and outlet of the heat sink.

The temperature driving force between the two heat sinks was 1.3 ± 0.1 °C during natural cooling and -2.4 ± 0.2 °C during forced cooling. The heat transfer across the natural cooled setup was so poor that all temperature profiles shown on Figure 26 are

very close to one another; i.e. a uniform heating surface was created across the heat sink.

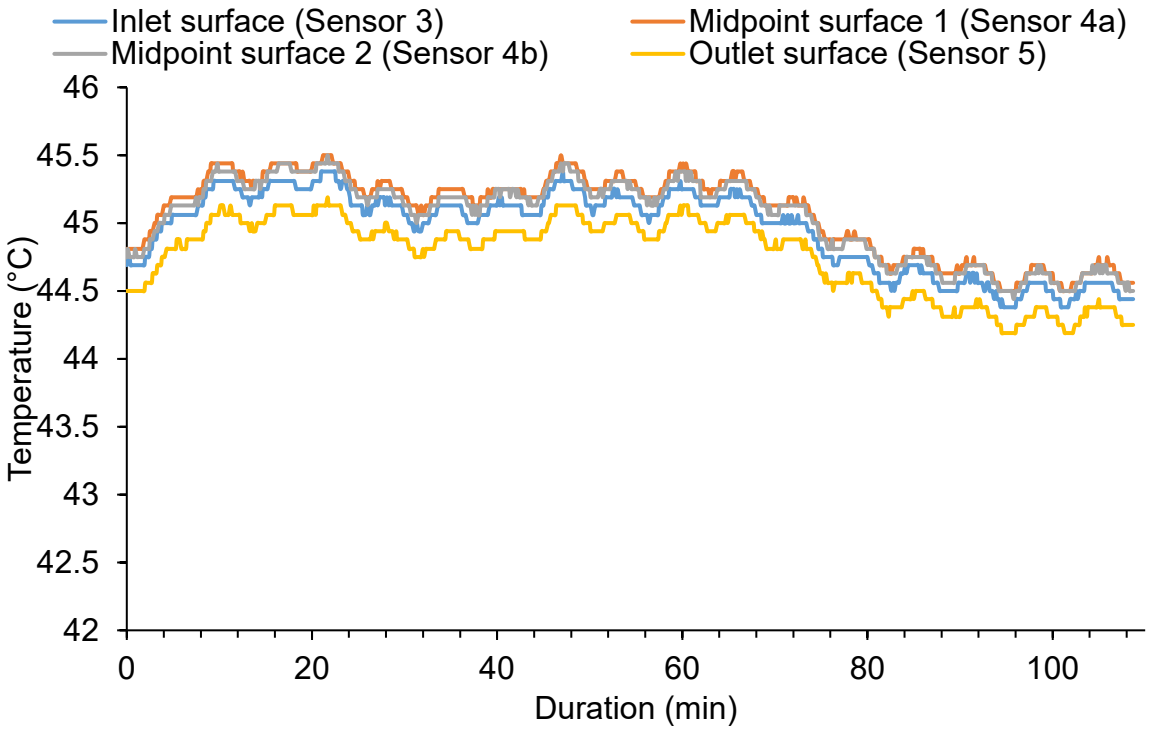

Figure 26: Surface temperature profiles of internal side heat sink in natural cooling mode; sensors referenced from Figure 20

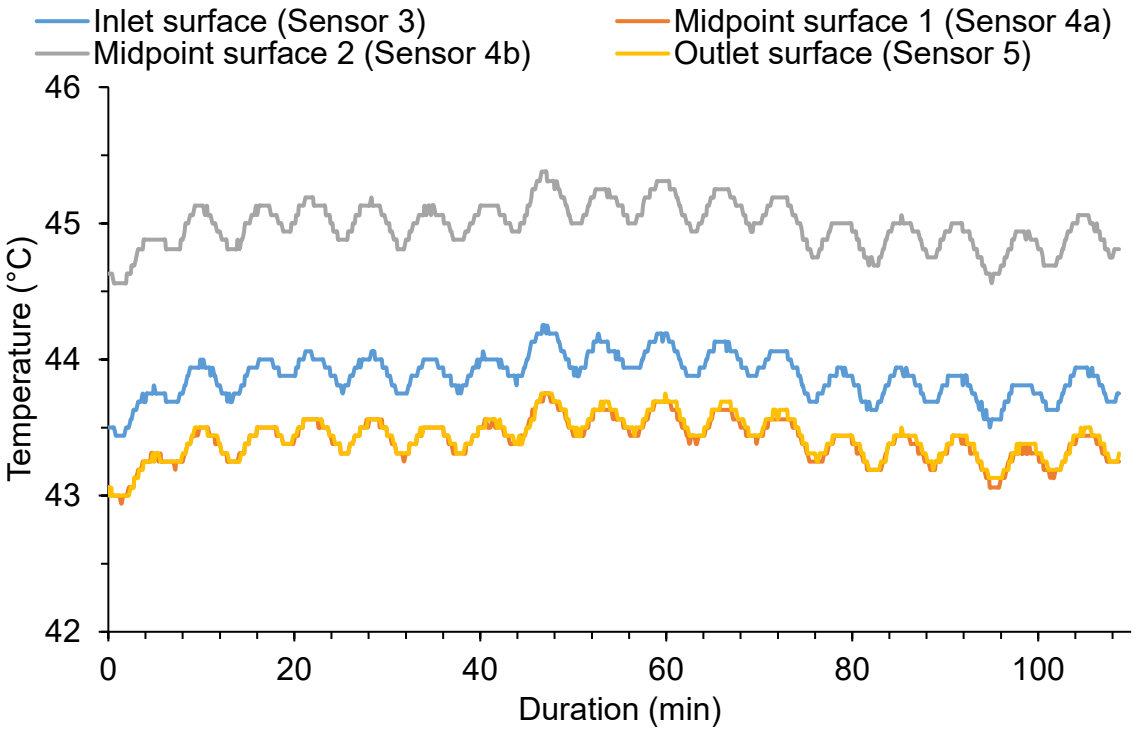

Figure 27: Surface temperature profiles of internal side heat sink in forced cooling mode; sensors referenced from Figure 20

Figure 28 shows that the forced cooling mode has better steady state heat transfer than the natural cooling mode. The temperature change of the humid air during the natural cooling mode is 1.4 ± 0.1 °C, significantly smaller than the air temperature change of 13.2 ± 0.7 °C achieved with the forced cooling mode.

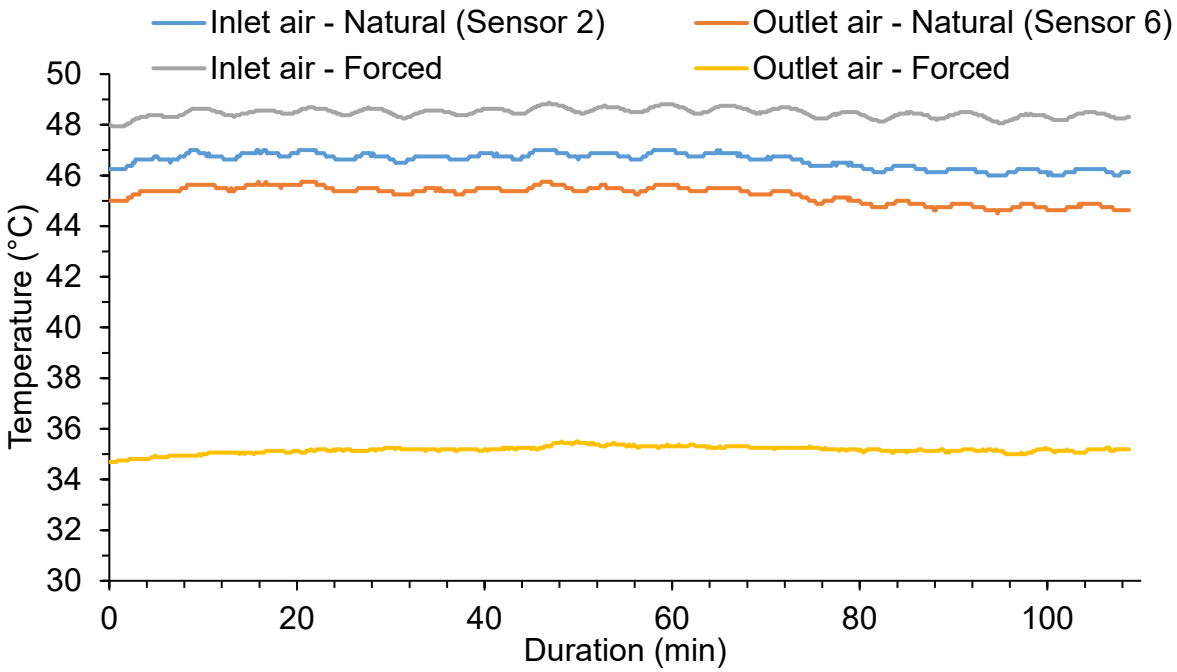

Figure 28: Comparison of the inlet and outlet air temperature of the heat sink; sensors referenced from Figure 20

It is important to note that the inlet humid air from the water bath during forced cooling was 1.8 ± 0.3 °C higher than inlet humid air during natural cooling. This should not be the case as the experiments are run in the same heated water bath. This discrepancy was due to the absence of water circulation in the still; a water pump was used to circulate the water, resulting in a more even heat and water flow distribution.

Figure 29 gives an in-depth temperature profile of the external heat sink for both cooling modes (NB: external heat sink is the heat sink left open to the atmosphere). The forced cooling heat sink is 2.8 ± 0.5 °C warmer than the natural cooling heat sink. Although a higher temperature external heat sink reduces the temperature driving force between the external heat sink and internal heat sink, the external heat sink had a larger temperature driving force to ambient.

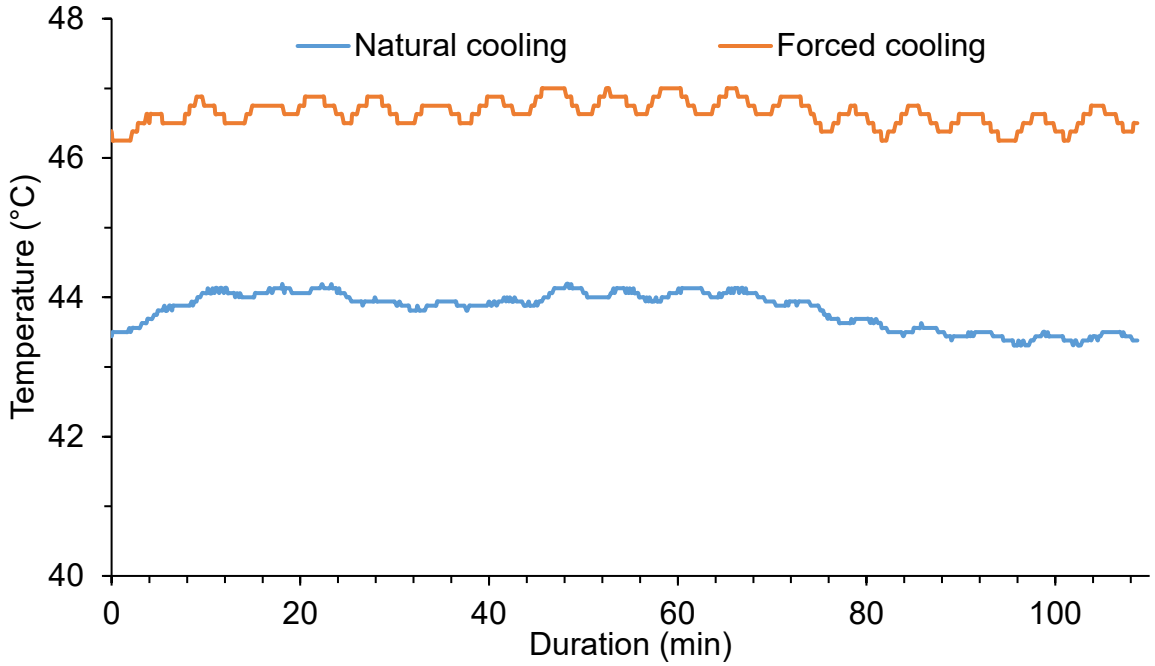

Figure 29: Temperature profiles of external heat sink; sensor 4 referenced from Figure 20

All other experimental datasets and thermal imaging followed the temperature and heat profiles described above. The datasets are summarised along key metrics in Table 16. The forced convection experiments gave better heat transfer dynamics across the heat sink, gave larger temperature drops across the condenser, and resulted in higher condensate yields.

Table 16: Summary of heat sink temperature metrics

$T_{heated\ water\ bath}/(T_{humid\ air\ in})$	Cooling mode	$\Delta T_{heat\ sink\ surface}$		$\Delta T_{humid\ air}$		$T_{internal\ heat\ sink}$		Mass yield (g/h)	
		Max	Avg	Max	Avg	Max	Avg	Max	Avg
60 °C/(46 °C)	Natural	0.2	0.2	**1.5***	1.4	43.4	41.4	50.0	36.0
60 °C/(48 °C)	Forced	**0.5***	0.4	13.2	12.0	**46.0***	43.9	97.0	77.3
65 °C/(42 °C)	Natural	0.2	0.2	**1.5***	1.4	40.0	39.8	44.0	39.4
65 °C/(47 °C)	Forced	**0.5***	0.5	13.7	13.3	45.0	44.3	**97.5***	81.6

*best performing experiment for each metric

4.3.1.2 Energy and Efficiency Profiles

Figure 30 showed a representative, steady state energy profile of the heat sink experiments under natural cooling while Figure 31 showed the forced cooling scenario. For the natural cooling scenario, 65 % of the humid air energy content, 231 kJ, was lost as condensate energy over two hours, while less than 1 % of energy was lost through the heat sink. The heat sink made a substantial amount of energy available for condensation. For the forced cooling scenario, 18 % of the humid air energy content, 465 kJ, was lost as condensate energy. Although a lesser portion of the humid air energy content was converted, the forced cooling scenario still lost 2 times more energy through condensation. The humid air outlet temperature of the forced cooling case was 10 °C lower than the natural cooling case; 35 °C for the forced cooling case and 45 °C for the natural cooling case.

The humid air energy profiles for both convection cooling modes did not experience a large sudden drop in energy content which would have indicated the presence of subcooling. The absence of a subcooling dip in the humid air energy profile justifies the subcooling assumption made in Section 3.3.4.

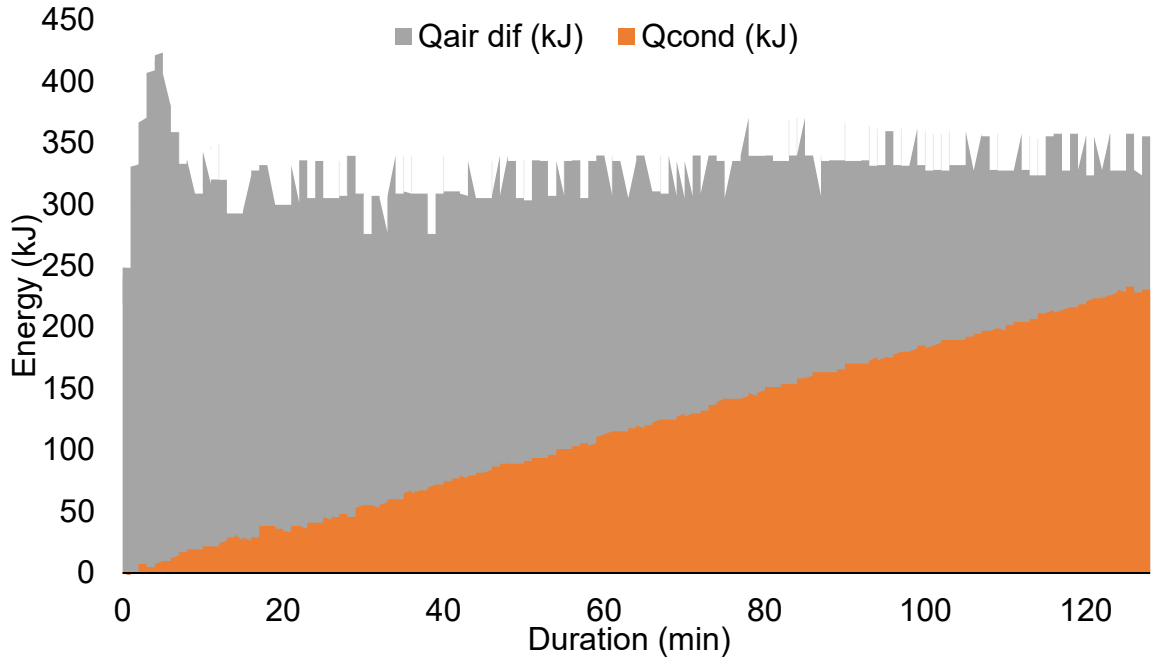

Figure 30: Energy profile of the heat sink heat exchanger under natural cooling

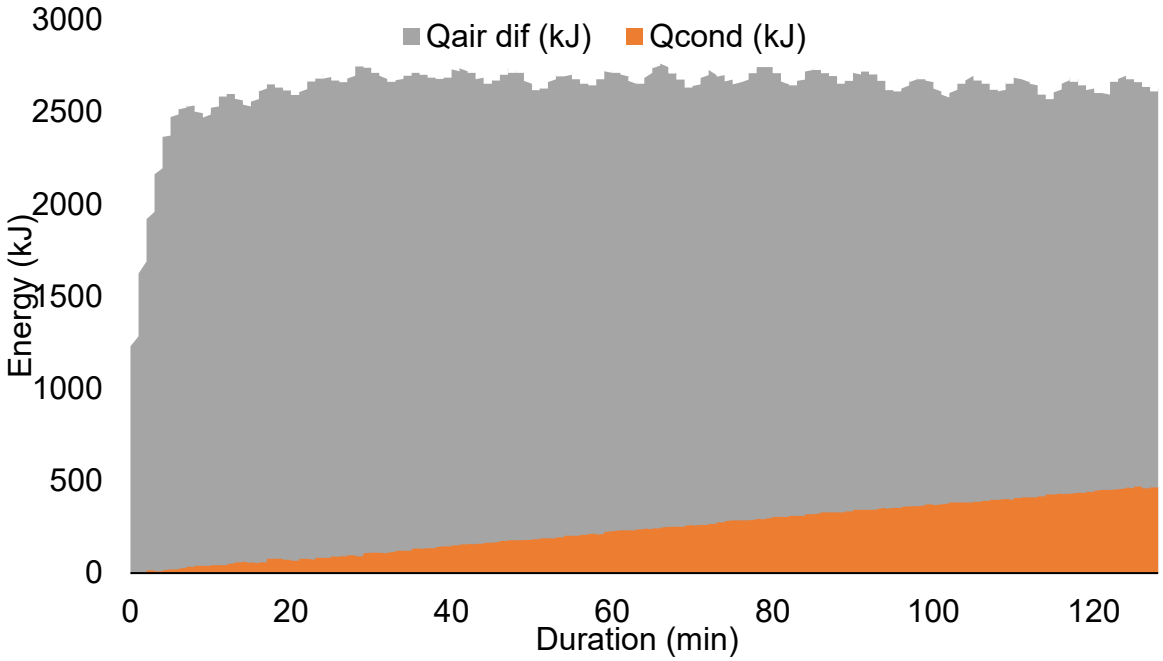

Figure 31: Energy profile of the heat sink heat exchanger under forced cooling

Table 17 summarised the energy profile metrics of the heat sink experiments. Although a lot of energy was available for condensation, on a mass basis the heat sink only had a 38 % conversion ratio with an energy efficiency of 5 % for the natural cooling case. For the forced cooling case, the heat sink managed an 11 % conversion ratio with a 12 % energy efficiency.

Irrespective of temperature, the forced convection cooling mode gave a superior performance compared to the natural cooling case; more energy was lost as condensate (499 vs 226 kJ) and higher yields were achieved (0.1 vs 0.05 kg). The only exception was the mass conversion efficiency where the natural cooling case gave better results; the natural cooling case had substantially lower ideal mass thresholds (11 % vs 37 %).

The overall heat transfer coefficient, UA, of the different heat sink experiments were also included in Table 17. Finding the UA for each condenser under a specific cooling mode allows the heat loss of the external condenser to be modelled during field testing of the active solar. Running the experiments under forced cooling significantly increased the overall heat transfer by ~21 times while running at a higher temperature had no effect.

Table 17: Summary of heat sink energy metrics

Variable		60 °C		65 °C	
		Natural cooling	Forced cooling	Natural cooling	Forced cooling
Q_{cond} (kJ)	Max	276	**604***	260	523
	Avg	226	499	236	496
Q_{in} (kJ)	Max	5,100	**5,537***	4,234	5,173
	Avg	4,649	5,233	4,226	5,136
Q_{eff}	Max	6 %	**14 %***	6 %	13 %
	Avg	5 %	12 %	6 %	13 %
M_{actual} (kg)	Max	0.05	**0.10***	0.04	**0.10***
	Avg	0.04	0.08	0.04	0.09
M_{ideal} (kg)	Max	0.12	**0.89***	0.10	0.82
	Avg	0.10	0.79	0.10	0.81
M_{eff}	Max	43 %	11 %	**44 %***	12 %
	Avg	37 %	11 %	40 %	10 %
UA ($W.K^{-1}$)	Max	0.60	11.95	0.61	11.45
	Avg	0.43	9.04	0.39	9.27

*best performing experiment for each metric

Figure 32 and Figure 33 show the energy efficiency and mass efficiency of the heat sink experiments. Figure 32 showed that the forced cooling mode resulted in better energy efficiencies in the heat sink while Figure 33 showed that forced cooling gave poor mass conversion results; forced cooling resulted in cooler air temperatures increasing the cooling potential while the actual condensate collected did not match the cooling potential available.

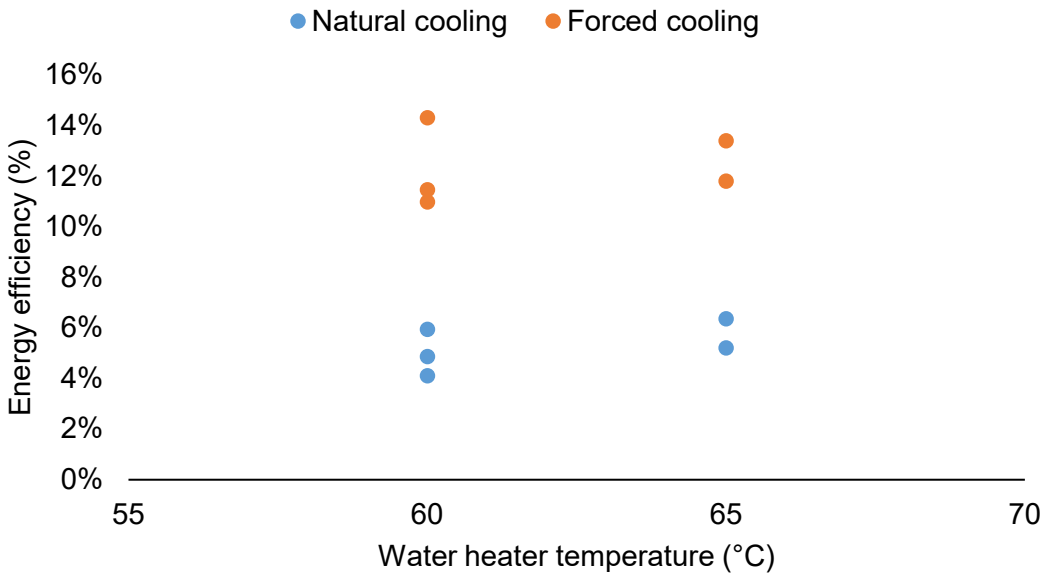

Figure 32: Energy efficiency graph of the heat sink experiments

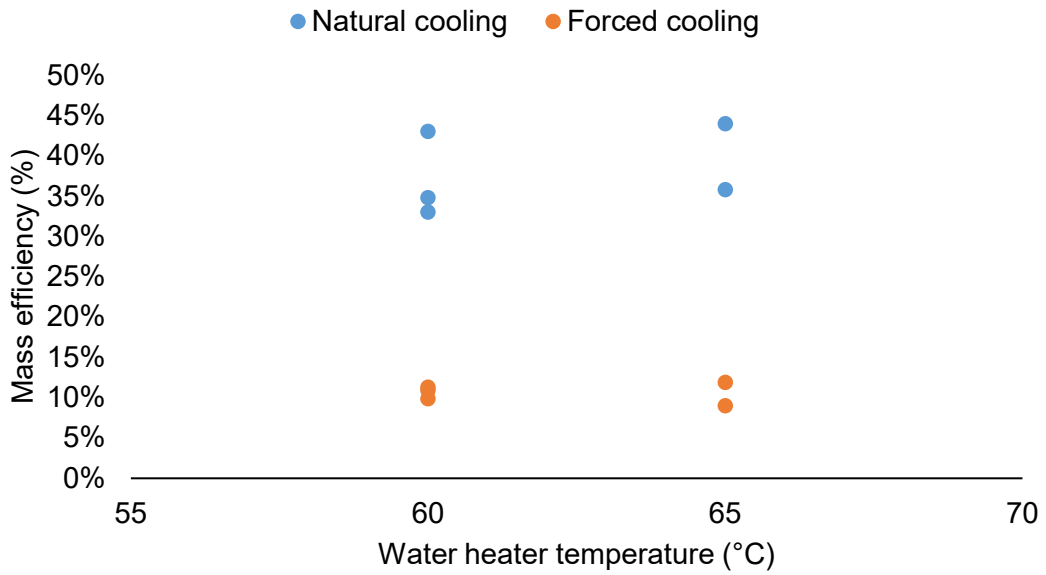

Figure 33: Mass efficiency graph of the heat sink experiments

One unexpected observation was that the increase in temperature from 60 °C to 65 °C did not affect the efficiency performance of the heat sink. Marais (2018) showed that higher water temperatures resulted in a performance improvement of the solar still; the absence of this effect might be due to the constant maintenance of the heated water bath at a specified temperature. This might have hidden the performance effect as naturally, the water temperature would have fluctuated more in a basin solar still.

Table 18 showed the rate of energy loss of the heat sink and tube bank at the three different heated water bath set temperatures of 50, 55, and 60 °C; the heat sink was not run at 55 and 60 °C. The highest energy loss rate of 3.70 kJ.min^{-1} was achieved with the heat sink at 60 °C, under forced cooling mode. The highest energy loss rate for the 12.7 mm tube bank was 2.62 kJ.min^{-1} and was also achieved at 60 °C under forced cooling mode. The energy rate loss was proportional to the set temperature of the heated water bath – this showed the reason why a high water temperature is favourable for an active solar still.

The heat sink showed a faster energy loss rate compared to the 12.7 mm tube bank due to the heat sink having more energy carrying mass, i.e. more mass to absorb energy means more energy available to lose through conduction and convection.

Table 18: Summary of energy loss rate (kJ.min^{-1}) at different heated water bath temperatures

External condenser	Cooling mode	50 °C	55 °C	60 °C
Heat sink	Natural	–	–	1.84
	Forced	–	–	3.70
12.7 mm tube bank	Natural	0.91	1.49	1.98
	Forced	1.14	1.92	2.62

4.3.1.3 Condensation Profiles

Table 19 showed the relationship between the condensate yield and the type of cooling mode used. Table 19 confirmed that forced cooling led to higher condensate yield; for all datasets the forced cooling condensate yields are higher than the natural cooling case. The forced cooling mode produced condensate on average twice as much as the natural cooling mode; for the 60 °C experiments, forced cooling gave an average condensate yield of 77 g/h compared to 36 g/h for natural cooling, while for the 65 °C experiments, forced cooling gave a condensate yield of 82 g/h compared to a condensate yield of 39 g/h for natural cooling. The maximum condensation rates for the natural and forced cooling modes were 50 g/h and 97.5 g/h respectively.

Table 19: Condensate yield comparison between natural and forced cooling modes

$T_{heated\ water\ bath}$	Experiment run	Natural cooling (g/h)	Forced cooling (g/h)
60 °C	10	26.8	71.2
	12	50.0	97.0
	13	38.3	84.0
	Average	36.0	77.3
65 °C	15	44.0	97.5
	18	36.0	72.7
	Average	39.4	81.6

Higher temperatures in the still led to higher condensation rates; more heat energy was made available which was used to evaporate more water into the circulating humid air.

Figure 34 shows the dynamic mass profiles for a two-hour run at 65 °C. Although both runs start to form condensate at approximately the same time, the forced cooling mode produced condensate at a faster rate, reaching a higher yield at the end of the run; 159 grams compared to 78 grams for the forced and natural cooling modes, respectively. Both mass profiles showed a constant rate of increase due to the constant nature of the heated water bath; the heated water bath was maintained at a specified temperature and so did not show any fluctuations, but rather a constant addition of heat energy lost as condensate yield.

Figure 34 also confirmed the faster heat transfer of the forced cooling mode; faster condensation rates are achieved under forced cooling. All experimental datasets followed the mass profiles shown by Figure 34.

Coupling a highly conductive, aluminium heat sink with a strong fluid mover and a cooling fan produced faster heat transfer dynamics. Faster heat transfer led to higher condensation rates. Experiments with forced cooling mode reached steady state faster as well.

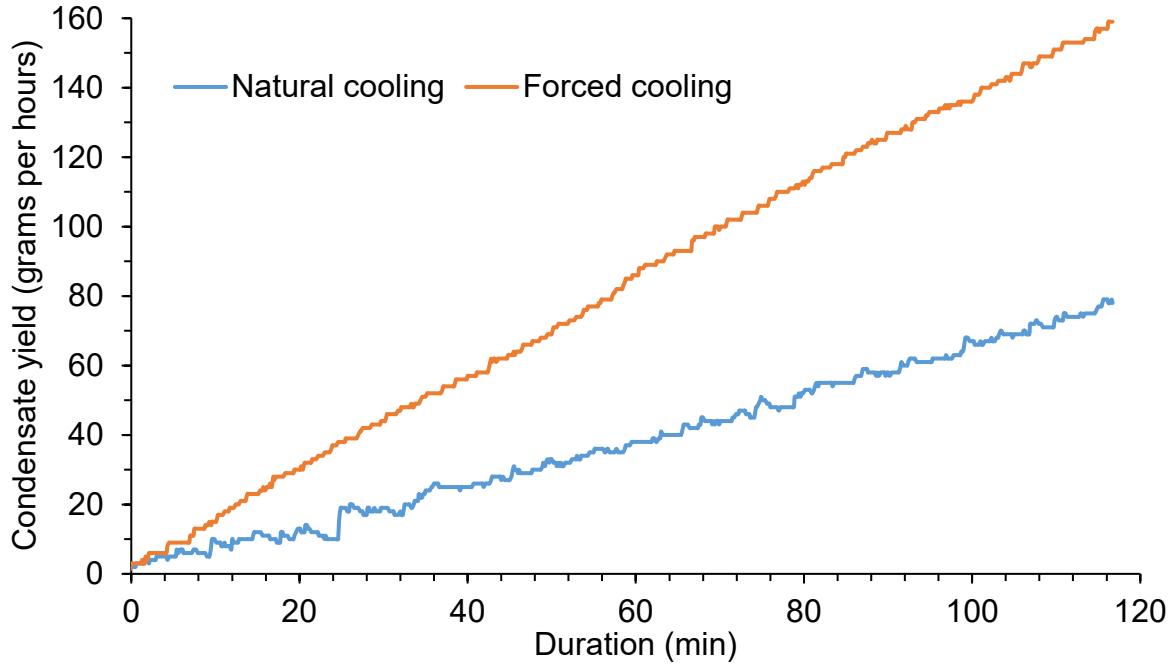

Figure 34: Dynamic mass profiles of the natural and forced cooling modes; sensor 7 referenced from Figure 20

4.3.2 Tube bank Heat Exchanger Performance

Although the tube banks are similar in configuration, they cannot be analysed based on condensation area alone. This is because different diameters result in differing spacing and different flow patterns between the tubes. However, for the purpose of analysing the tube bank datasets, it was assumed that the difference in configuration was negligible, and the tube bank comparison was based solely on condensation area.

The heat sink heat exchanger results indicated that forced cooling performed better than natural cooling. This trend was also expected for the tube bank heat exchanger. The more crucial piece of information was which tube bank performed better; the 9.5 mm tube bank or 12.7 mm tube bank.

The tube bank experiments were run at 50 °C, 55 °C, and 60 °C. Only experiments run at 60 °C were analysed and presented in Section 4.3.2 as the temperature effects noted from Section 4.3.1 still held.

4.3.2.1 Temperature Profiles

Figure 35 and Figure 36 showed a set of representative, steady state humid air temperature profiles of the tube bank experiments.

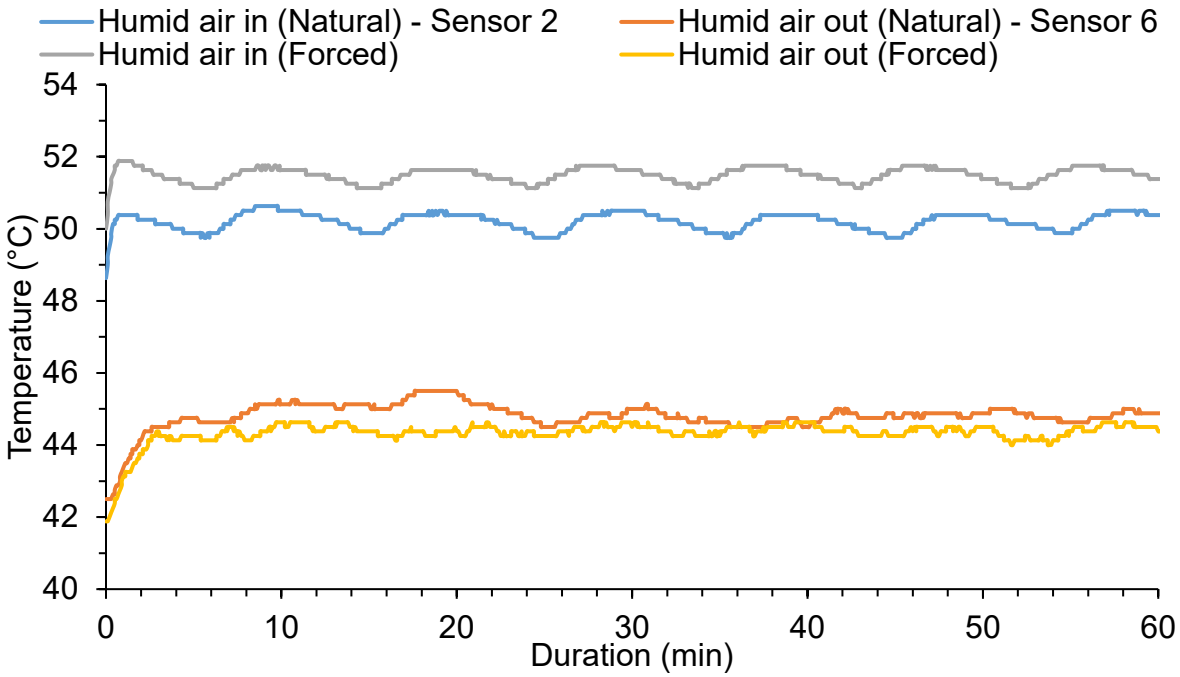

Figure 35: Temperature profiles of humid air for the 9.5 mm tube bank; sensors referenced from Figure 20

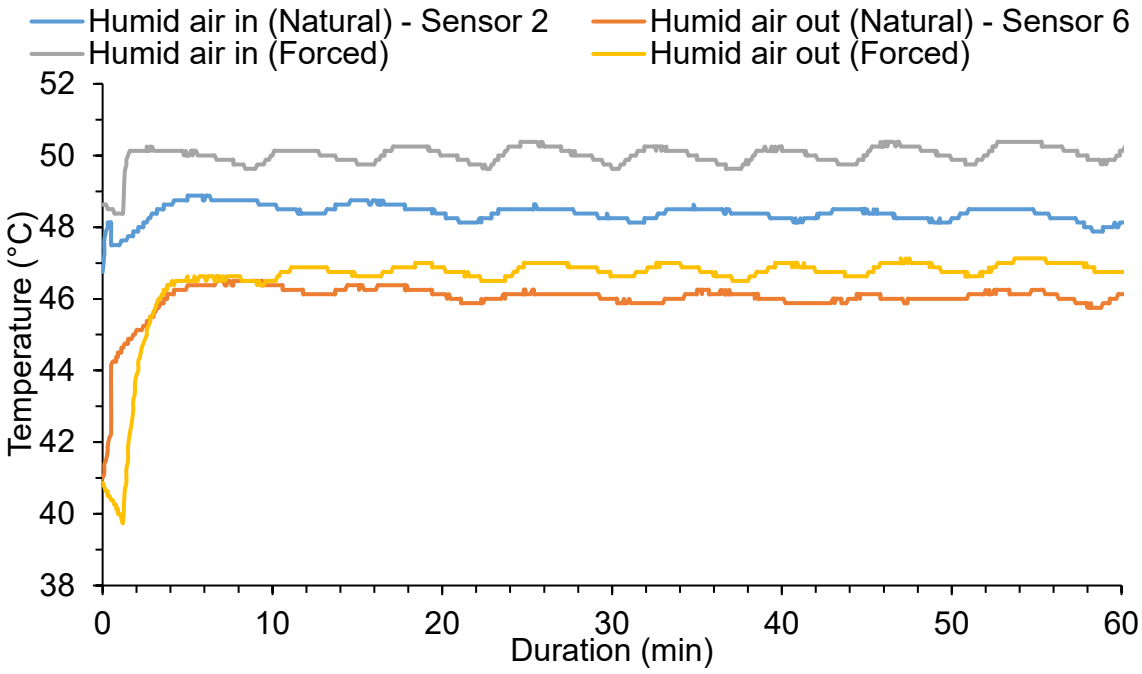

Figure 36: Temperature profiles of humid air for the 12.7 mm tube bank; sensors referenced from Figure 20

Forced cooling provided a humid air inlet and outlet temperature change of 7.2 ± 0.4 °C and 3.4 ± 0.9 °C over the 9.5 mm and 12.7 mm tube banks, respectively. This compared with the natural cooling case of 5.4 ± 0.4 °C and 2.4 ± 0.4 °C over the 9.5 mm and 12.7 mm tube banks, respectively.

The temperature driving force between the tube banks are shown in Table 20. The 12.7 mm tube bank under forced cooling showed the largest temperature driving force while the 9.5 mm tube bank under natural cooling showed the smallest.

Table 20: Summary of temperature driving force over tube banks

Tube bank	Natural cooling mode*	Forced cooling mode
9.5 mm	10.4 ± 0.5 °C (36 g/h)	11.6 ± 0.1 °C (52 g/h)
12.7 mm	13.0 ± 0.5 °C (49 g/h)	14.5 ± 0.8 °C (67 g/h)

* Corresponding condensation rates for analysed datasets

Table 21 also showed the corresponding condensation rates; the 9.5 mm tube bank produced condensate at 41.5 g/h and 62.5 g/h under natural and forced cooling respectively, while the 12.7 mm tube bank produced condensate at 49.2 g/h and 67.5 g/h, respectively. The 12.7 mm tube bank under forced cooling showed the highest condensate rate and largest temperature driving force.

The 9.5 mm tube bank under forced cooling provided better heat transfer. Forced cooling mode resulted in a performance improvement in heat transfer compared to the natural cooling mode. In addition, forced cooling mode resulted in higher humid air temperature profiles. The humid air-in profiles decreased from the 9.5 mm tube bank to the 12.7 mm tube bank while the air-out profiles increased. Figure 35 and Figure 36 began to hint at the superior heat transfer of the 9.5 mm tube bank.

Initially, the substantial temperature drop in humid air was assumed to be an effect in subcooling. However, subcooling was not considered due to the assumptions made in Section 3.3.4 and the absence of a subcooling dip in Figure 30 and Figure 31. The substantial temperature drop was either caused by the surface temperature of the external condenser flow pathway or the result of erroneous temperature sensor

readings; the possibility of erroneous readings could not be ruled out as subcooling was considered possible previously.

Figure 37 showed the temperature difference over the tube surfaces. The tube surfaces for two different tubes from the same tube bank were recorded and analysed; the tube surface with the larger temperature difference was used in Figure 37. The order of magnitude between the tubes was in the region of two; using the maximum temperature difference was a reasonable assumption. The natural cooling cases performed in the same range with no distinct performance advantage; the 9.5 mm tube bank gave a temperature drop of 6.5 ± 0.5 °C while the 12.7 mm tube bank compared with a temperature drop of 5.6 ± 0.4 °C. Counter to that, forced cooling mode showed a performance advantage between the 9.5 mm tube bank and the 12.7 mm tube bank; the 9.5 mm tube bank gave a temperature drop of 3.6 ± 0.2 °C while the 12.7 mm tube bank gave a temperature drop of 7.4 ± 0.6 °C. The 12.7 mm tube bank also experienced higher tube surface temperatures.

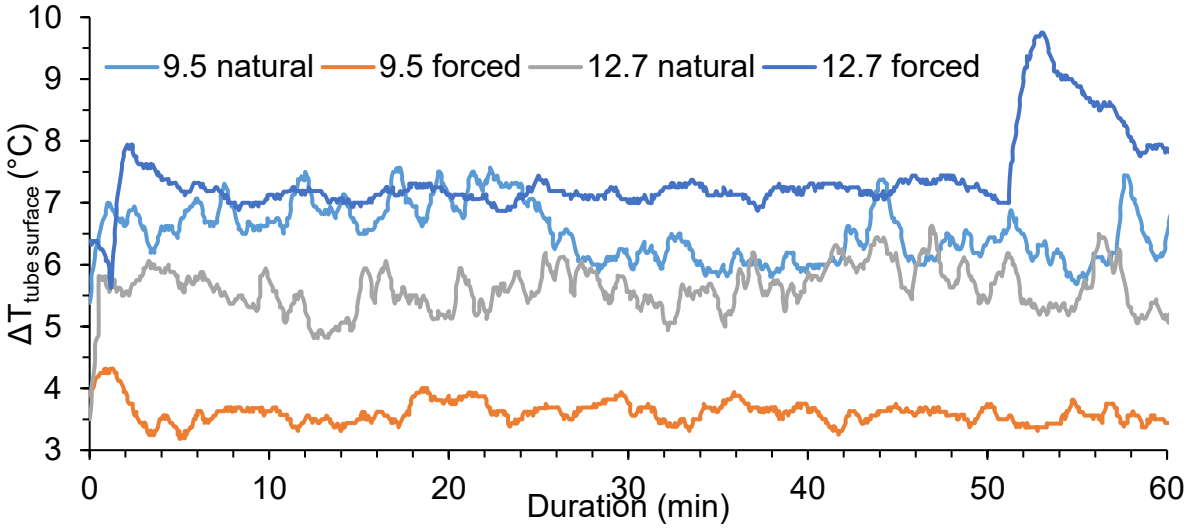

Figure 37: Tube surface temperature difference profiles of the tube banks; sensors 3 and 5 referenced from Figure 20

The $\Delta T_{tube\ surface}$ metrics are also shown in Table 21 along with the $\Delta T_{humid\ air}$ and condensate yield metrics. A substantial $\Delta T_{tube\ surface}$ suggested more energy was removed as latent energy while a small $\Delta T_{humid\ air}$ suggested the humid air did not experience any cooling; a tube bank that showed this trend had an optimised performance. Overall, the 12.7 mm tube bank gave better tube surface and humid air heat transfer.

Table 21: Summary of tube bank experiments at $T_{heated\ water\ bath}$ of 60 °C

Tube bank	Cooling mode	$T_{humid\ air\ in}$	$\Delta T_{tube\ surface}$		$\Delta T_{humid\ air}$		Mass yield (g/h)	
			Max	Avg	Max	Avg	Max	Avg
9.5 mm	Natural	50 °C	6.8	6.6	5.5	5.2	42.5	41.5
	Forced	51 °C	3.6	3.5	7.1	7.0	65	62.5
12.7 mm	Natural	49 °C	5.8	5.4	**2.5***	**2.4***	51.5	49.2
	Forced	50 °C	**7.4***	**7.2***	3.3	3.2	**70***	**67.5***

*best performing experiment for each metric

4.3.2.2 Energy and Efficiency Profiles

The 12.7 mm tube bank under natural and forced cooling showed similar energy profiles to the heat sink heat exchanger in Figure 30 and Figure 31. For the natural cooling scenario, 9 % of the humid air energy content, 239 kJ, was lost as condensate energy over two hours while 11 % of the humid air energy content, 314 kJ, was lost as condensate energy for the forced cooling scenario. Similar to the heat sink scenario, the forced cooling scenario lost more energy through condensation; only a 30 % improvement compared to a 100 % improvement for the heat sink scenario.

The 12.7 mm tube bank gave a better performance than the 9.5 mm tube bank across $\Delta T_{tube\ surface}$, $\Delta T_{humid\ air}$, and mass yield rates (refer to Table 21). The 12.7 mm tube bank and 9.5 mm mm tube bank were 4 % and 3 % energy efficient, respectively.

The overall heat transfer coefficient of the tube bank under forced cooling – 10.7 $W.K^{-1}$ – gave better performance compared to natural cooling case of 5.01 $W.K^{-1}$; the 9.5 mm tube bank showed better overall heat transfer (~3 times better) which was surprising given that the 12.7 mm tube bank had showed more consistent and higher heat transfer rates throughout the tube banks experiments; refer to Table 21.

4.3.2.3 Condensation Profiles

Tube banks under forced cooling performed better than the natural cooling case. However, unlike the heat sink heat exchanger where the forced cooling effect was twofold, the forced cooling effect in the tube bank scenario resulted in a smaller performance improvement for the tube banks. Forced cooling produced condensate at a rate of 59 g/h while natural cooling produced condensate at 43 g/h; this was a 37 % improvement in performance. The complete dataset is shown in Table 22.

The difference in performance improvement between the tube banks and heat sink was due to the air flow across each external condenser. Air flow across the tube banks was omnidirectional while the heat sink was unidirectional and obscured in all other directions. The tube banks were effectively cooled even without forced cooling; this is the reason forced cooling did not have a performance improvement on par with the performance improvement seen with the heat sink.

Table 22: Condensate yield comparison between natural and forced cooling modes

Tube bank	Experiment run	Natural cooling (g/h)	Experiment run	Forced cooling (g/h)
9.5 mm	2	26.0	2	39.5
	3	31.5	3	38.5
	4	34.0	16	65.0
	5	39.0	17	60.0
	7	37.0	–	–
	8	40.0	–	–
	10	42.5	–	–
	11	40.0	–	–
	12	42.0	–	–
	Average	37.0	Average	52.0
12.7 mm	15	47.0	12	66.5
	16	51.5	13	67.0
	19	51.0	14	66.0
	20	47.5	–	–
	Average	49.25	Average	66.5

Table 22 showed the performance increment gained by the 12.7 mm tube bank over the 9.5 mm tube bank; the 12.7 mm tube bank performed at an average 33 % better than the 9.5 mm tube bank for the natural cooling mode and 28 % for the forced cooling mode. The 12.7 mm tube bank performed better consistently across the temperature, energy, and condensation metrics.

Table 22 also showed that for the 9.5 mm tube bank, the average condensation rate was 37 g/h and 52 g/h for the natural and forced cooling modes, respectively. The average condensation rate for the 12.7 mm tube bank was 49.25 g/h and 66.5 g/h for the natural and forced cooling modes, respectively. The maximum condensation rate was 65 g/h and 67 g/h for the 9.5 mm and 12.7 mm tube banks respectively; both occurred under forced cooling mode. The dynamic mass profiles of the tube banks show the same pattern as the heat sink, as shown in Figure 34. The condensate yield shows that 12.7 mm tube bank, forced > 9.5 mm tube bank, forced > 12.7 mm tube bank, natural > 9.5 mm tube bank, natural.

The tube banks performed less effectively compared to the heat sink heat exchanger. The 9.5 mm and 12.7 mm tube banks gave maximum condensation rates of 65 and 67 g/h compared to a maximum rate of 97 g/h for the heat sink. However, the 9.5 mm and 12.7 mm tube banks are a fraction, 28 % and 37 % respectively, of the heat sink surface area. Thus, on an area basis, the tube banks outperformed the heat sink heat exchanger by a factor of two.

4.3.3 Heated Water Bath Comparison

Objective 1 of the research paper, which called for characterising the performance of the external condensers was met by using the heated water baths as a control environment. The insights observed and discussed in Section 4.3 will be used to anticipate the performance of the external condensers when attached to the active solar stills. The active solar still experiments will be discussed in Section 4.4.

The summary of the heated water bath data analyses is shown in Table 23.

Table 23: Comparison of the heated water bath data analyses

Condenser (cooling mode)	Surface area (m^2)	$\Delta T_{humid\ air}$ (°C)	Mass yield ($g.hr^{-1}$)	Yield per area ($g.hr^{-1}.m^{-2}$)	UA ratio ($W.K^{-1}$)	Energy efficiency (%)
		Max	Max	Max	Avg	Avg
Heat sink (natural)	0.171	1.5	50.0	292	0.4	7.0
Heat sink (forced)	0.171	13.2	97.0	567	9.4	17.0
9.5 mm tube bank (natural)	0.0481	5.5	42.5	884	28.9	2.5
9.5 mm tube bank (forced)	0.0481	7.1	65.0	1,351	32.9	3.7
12.7 mm tube bank (natural)	0.0641	2.5	51.5	803	5.01	5.3
12.7 mm tube bank (forced)	0.0641	3.3	67.0	1,045	10.7	5.2

Figure 38 shows the performance of the different external condensers used with the heated water bath. Using the heat sink heat exchanger under forced cooling mode as the baseline, the heat exchangers were compared across condenser surface area, maximum yield, maximum yield per unit area, UA ratio, and energy efficiency.

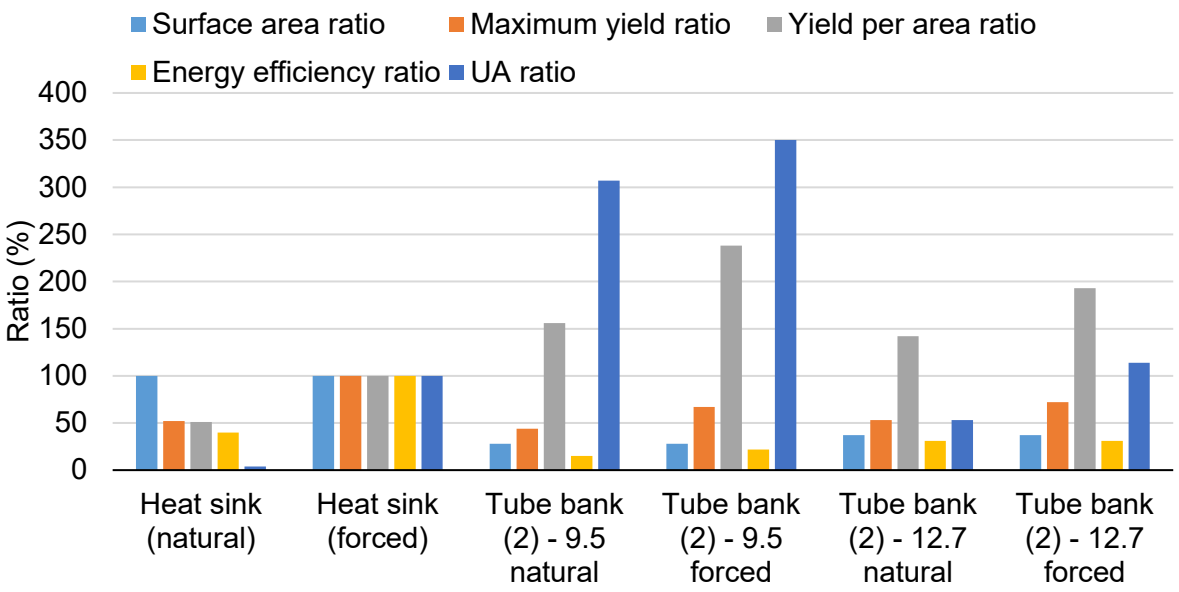

Figure 38: Performance analysis of the external condensers

The natural cooling heat sink was less effective than the baseline, performing at 50 % capacity when compared across the maximum yield and yield per area metrics. The 12.7 mm tube bank showed a stronger performance of the tube bank against the baseline. This was further confirmed by the substantially higher yield per area value; 142 % and 193 % yield per area capacity for the natural and forced cooling scenario, respectively. The same trend was observed for the 9.5 mm tube bank. Figure 38 showed that forced cooling performed better than natural cooling; also favouring energy efficiency, and the 9.5 mm tube bank performed better than the 12.7 mm tube bank; although showing a marginal difference in energy conversion, the 9.5 mm tube bank showed significantly better overall heat transfer rate of ~3 times when comparing the forced cooling scenario.

Ranking the heat exchangers in descending order gives:

1. 9.5 mm tube bank, forced cooling.
2. 12.7 mm tube bank, forced cooling.
3. 9.5 mm tube bank, natural cooling.
4. 12.7 mm tube bank, natural cooling.
5. Heat sink, forced cooling.
6. Heat sink, natural cooling.

The tube bank was more favourable than the heat sink. Figure 38 showed the 9.5 mm tube bank to perform better than the 12.7 mm tube bank based on the yield per area metric and overall heat transfer coefficient, however, the 12.7 mm tube bank gave better steady state heat transfer. The 9.5 mm and 12.7 mm tube banks, both under forced cooling mode, were recommended for the active solar still experiments. How the tube banks performed when attached to the active solar still will be investigated in Section 4.4. Following on from Sections 4.1 and 4.3, the active solar still will be fitted with a single pane glass cover surface and either of a forced cooled 9.5 mm or 12.7 mm tube bank attached as the external condenser.

4.4 Active Solar Still Experiments

The active solar still experiments informed on which solar still performed better on a condensate yield, energy efficiency, and cost basis; the active solar still or the basin solar still.

4.4.1 Effects of Disturbance Variables

4.4.1.1 Ambient Conditions

Similar to Section 4.2.1, although ambient can have a significant effect on the basin solar still performance, no correlations were investigated due to the constantly changing ambient. The active solar still analyses were performed on datasets that experienced clear, ambient weather conditions.

4.4.1.2 Seasonal Variation

The active solar still experiments were only run in the summer. Due to the lack of seasonal data, no conclusion can be made on how seasonal variation might affect the performance of the active solar still.

Marais (2018) showed that there was no seasonal variation during the year 2018. winter months were less cloudy and summer months were often cloudier but with higher solar intensity, reducing any potential for seasonal effects. The active solar still would most likely have experienced the same phenomenon of no seasonal variation.

4.4.2 Baseline Experiments

Still variation 3, which was Marais' (2018) best performing passive solar still, was used as the benchmark solar still against the active solar stills experiments. Table 24 shows the performance of the benchmark solar still (Marais, 2018) while Table 25 shows the baseline comparison of the reference solar still (still variation 3 design) and active solar still (still variation 4 design). The active solar still was run with no fluid circulation or heat exchanger fitted to the still. However, it should be noted that the active solar still is equipped with a double pane glass cover and the reference still with a single pane glass cover.

Table 24: Benchmark solar still (still variation 3) performance (Marais, 2018)

Day	Benchmark yield	Benchmark efficiency
297	1.29 kg	27.1 %
298	1.25 kg	27.2 %
299	1.24 kg	28.4 %
302	1.20 kg	26.4 %
303	1.18 kg	26.2 %
304	0.726 kg	24.6 %
Average	0.968 kg	26.7 %

* Marais' (2018) data is used as a benchmark and not a direct comparison

Table 25: Performance analysis for baseline comparison

Day	Ref. still yield	Active still yield	Increase in yield	Ref. still efficiency	Active still efficiency
3	1.26 kg	0.91 kg	-28 %	34 %	25 %
4	1.80 kg	0.88 kg	-51 %	41 %	20 %
5	1.31 kg	0.74 kg	-44 %	33 %	30 %
Average	1.46 kg	0.84 kg	-42 %	36 %	25 %

Baselining showed that there was a significant performance difference between the reference still and active solar still. The active solar still showed reduced yield and energy efficiency when compared to the reference still; the active solar still produced 42% less condensate and showed an 11% efficiency gap when compared to the

reference still. The underlying reason for the performance difference between the reference and active solar stills is due to the higher heat retention (insulation effect) of the double pane glass, reducing the condensate collected and energy efficiency of the active solar still. It is also possible that some baseline performance difference is introduced from how still variations 3 and 4 were assembled six months apart.

Figure 39 showed the energy balance analysis of the reference and active solar stills. Cover surface and body conductive losses were a similar magnitude across the reference solar still and active solar still – an average of 41% and 49%, respectively. The major differences of energy losses were across the base, condensate, and unaccounted energy. The reference still showed more base radiative losses (18% and 6%, respectively) due to the use of single pane glass cover while the active solar used double pane glass cover. The reference still showed more condensate losses, as shown by Table 25. The active solar still also showed larger unaccounted energy (31% and 14%, respectively).

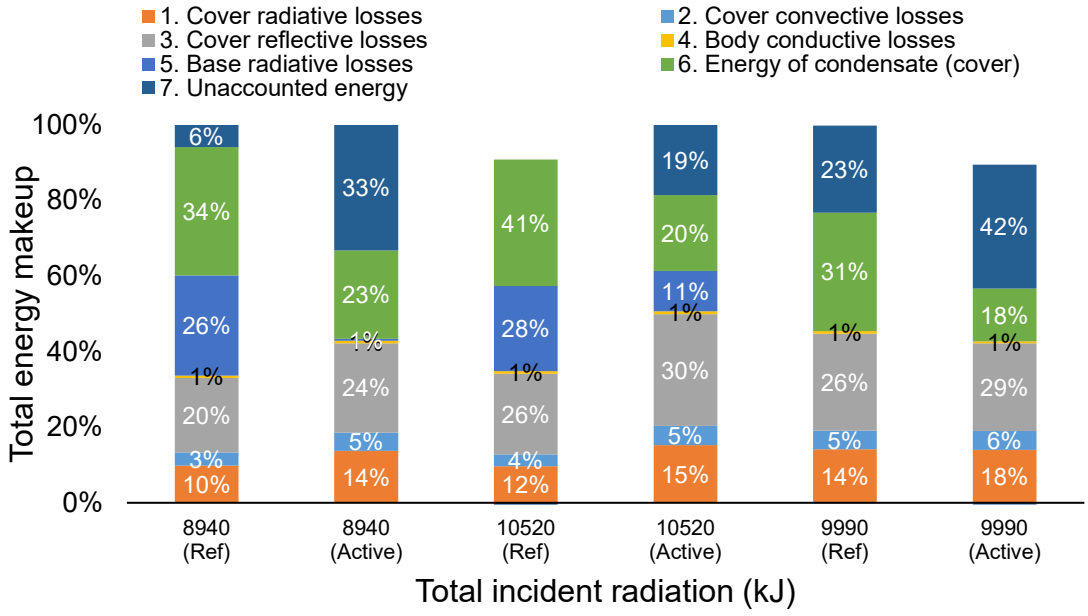

Figure 39: Energy balance analysis for baseline comparison

Figure 40 showed the cover surface temperature profiles while Figure 41 showed the water temperature profiles. The slight variance of 7 °C (peak of 49 °C for the reference solar still and 55 °C for the active solar still) in the cover surface temperature profiles matched the similar magnitude of cover losses in the energy balance analysis. With a

lower cover surface temperature, the driving force for evaporation and condensation was increased on the reference still compared to the active solar still.

Although the active solar still had a higher peak, the reference solar still peaked at ~11h00 – three hours earlier than the active solar still. The reference solar still gradually lost cover surface temperature when compared to the active solar still which had a higher rate of cover surface temperature loss.

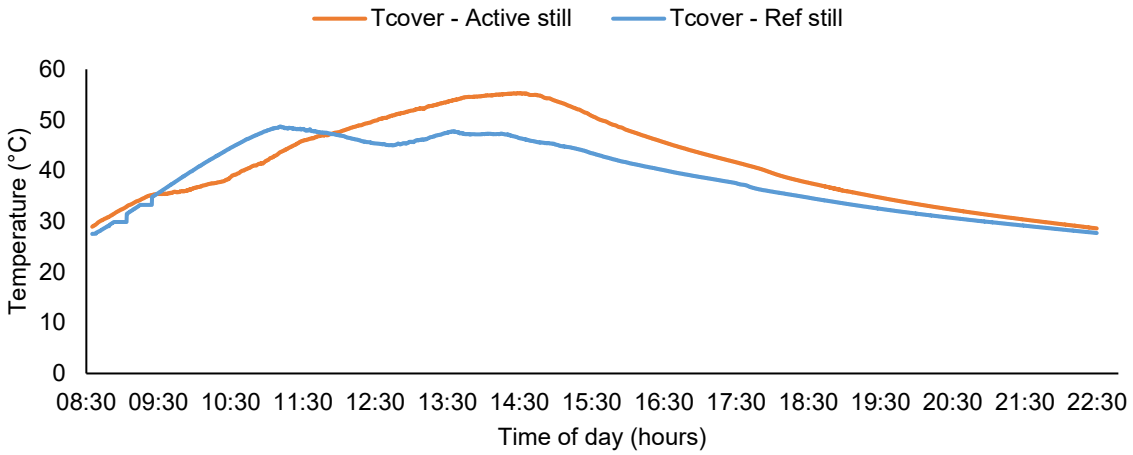

Figure 40: Cover surface temperature profiles for baseline comparison; sensor 11 referenced from Figure 21

The driving force is also dependent on the water temperature of the solar stills. Figure 41 showed that the reference and active stills both reached high water temperatures of 64 °C and 75 °C, respectively. This kept the driving force high and favoured high rates of evaporation and condensation.

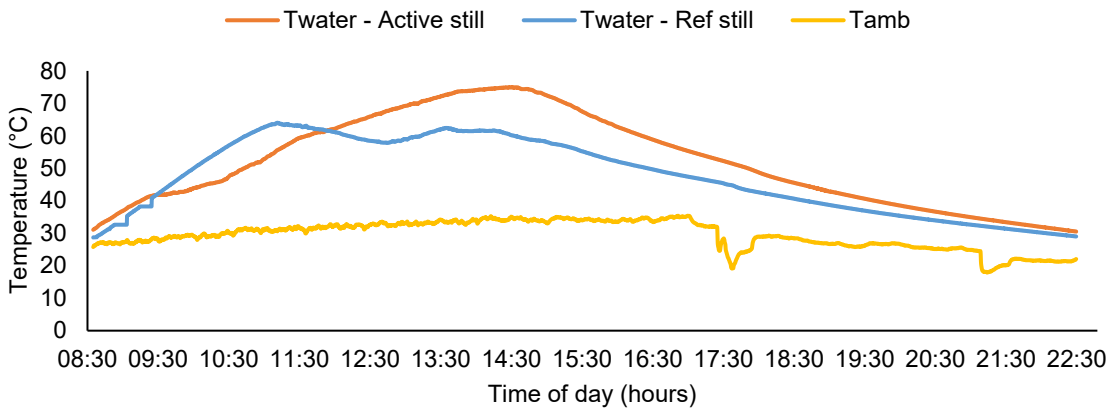

Figure 41: Water temperature profile for baseline comparison; sensor 6 referenced from Figure 21

4.4.3 Active Solar Still performance

The average row of Table 25 was used for baseline corrections between the reference still and the active solar still performance comparison. Table 11, from Section 3.2.4, showed three unique experimental cases where the three modes of circulation – water, humid air, and humid air and water – were run for the external condenser, under forced cooling. The type of external condenser was redundant for the water only circulation mode.

4.4.3.1 Circulation mode – Water

Figure 42 showed the cover surface and water temperature profiles of the reference and active solar still.

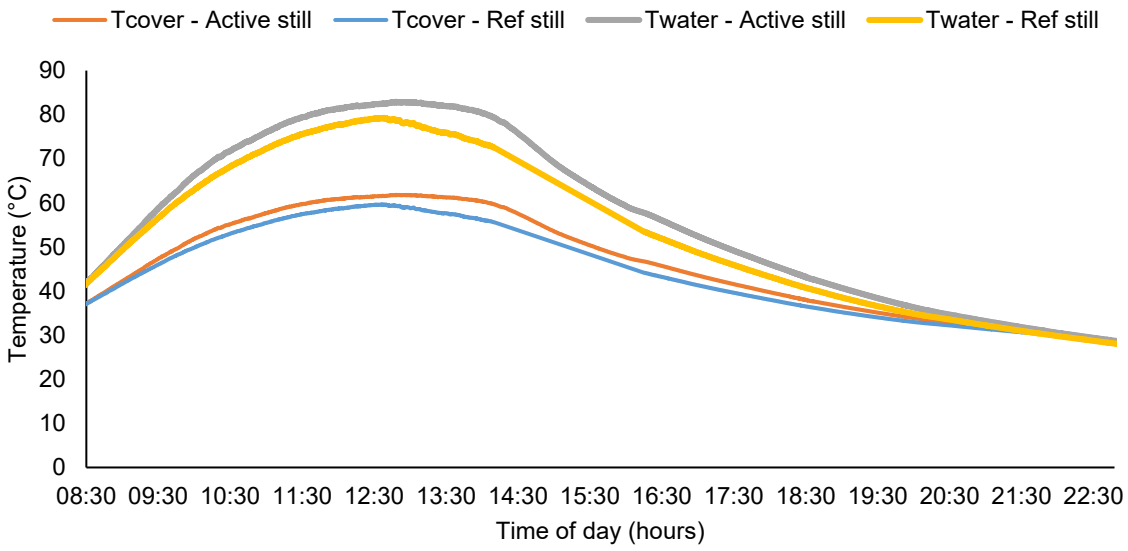

Figure 42: Cover surface and water temperature profiles; sensor 12 referenced from Figure 21

The peak water temperature of the active solar still was 4 °C higher than the reference case. This was detrimental to the performance of the active solar still as a high water temperature meant an accumulation of energy in the back wall and base of the active solar still. The water circulation mode was implemented to reduce the high back wall temperatures, however this objective was not met. This might have been due to the circulation of higher than usual water temperatures due to the limited presence of an evaporation and condensation in the active solar still. The water temperature from the reference still peaked at 73 °C while the active solar still water temperature peaked at 83 °C.

Figure 43 shows the energy balance of the water circulation mode. Body conductive losses increased by 4 % between the reference still and active solar stills; this correlates to the increase in water temperatures shown by Figure 42. The water circulation mode resulted in an increase in body losses and cover losses. However, it should be noted that there is little direct irradiance onto the back wall of the still during the time it was tested for. Perhaps an increase in water temperature can be observed if the same experiment is run during the winter season.

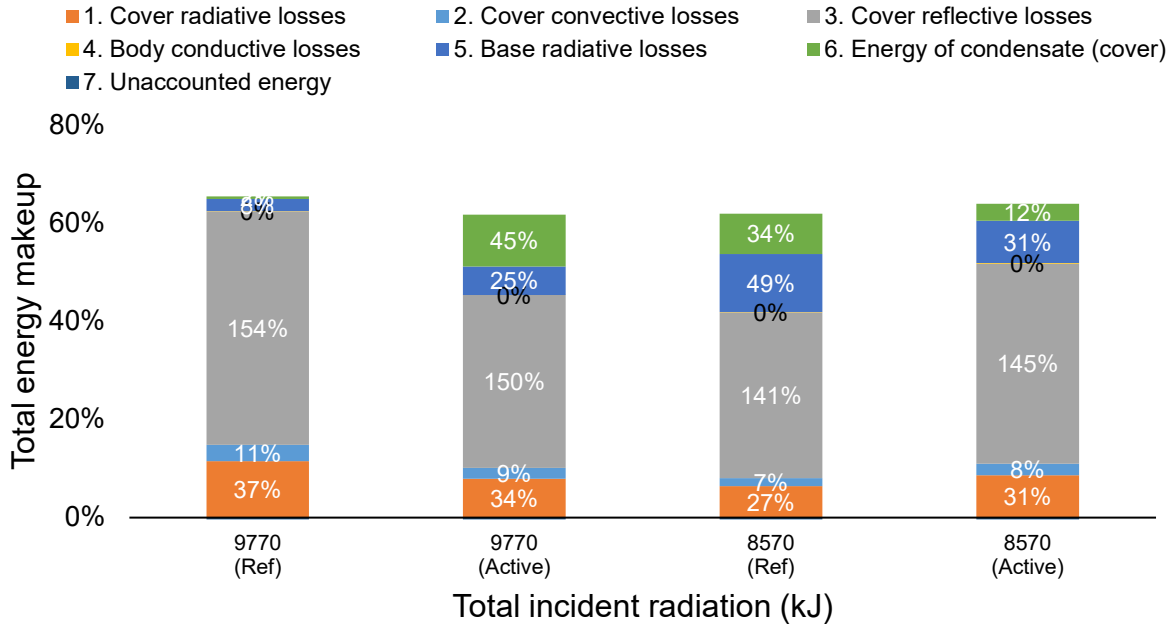

Figure 43: Energy balance profiles of water circulation mode

The yield profiles were shown in Figure 44. The cover surface of the active stills showed very low levels of condensate formation with a total yield of 0.07 kg. The reference still performed normally; condensation rates in the reference still showed a total yield of 1.84 kg, greatly outperforming the active still by 27 times. Multiple runs indicated a similar observation. The equipment was functioning properly during the trials and no leaks were detected upon inspection. The introduction of water circulation increases heat transfer on the back wall of the still and is most likely the cause of the increased heat losses through this was. It should also be noted that the trials were conducted during the summer months and the angle at which solar radiation impinges on the surface is very close to 0°.

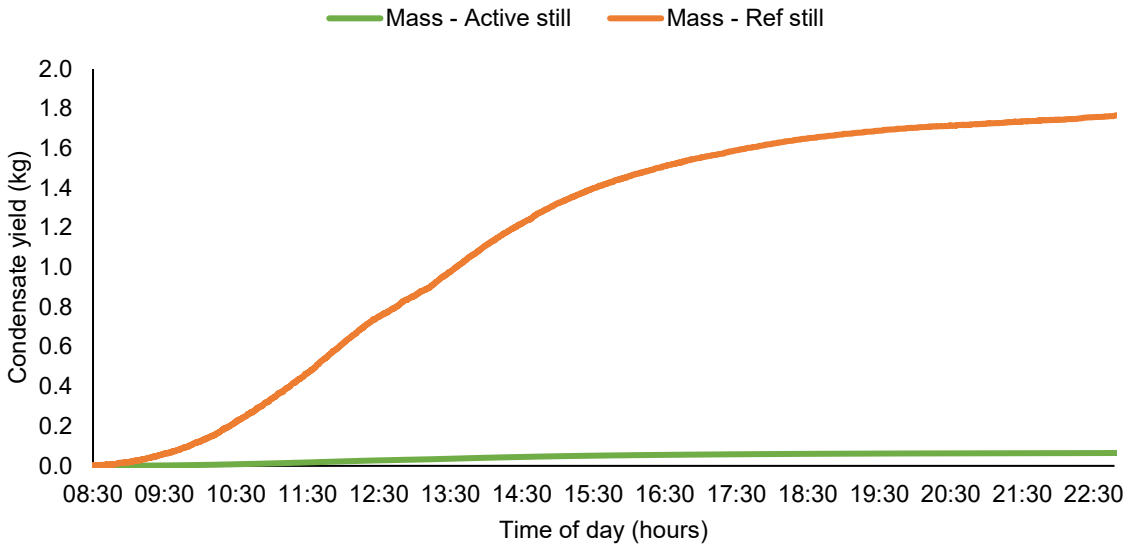

Figure 44: Yield profiles of water circulation mode; sensor referenced from Figure 21

Table 26 shows the condensate yields of the reference and active solar still under the water circulation mode. Table 26 also shows the corrected yield increase and the energy efficiencies of both stills.

Table 26: Comparison of condensate yield and still efficiency

Day	Ref. still yield	Active still yield	Increase in yield	Cor. yield increase*	Ref. still efficiency	Active still efficiency
4	1.84 kg	0.07 kg	-96 %	-54 %	45 %	2 %
4	1.23 kg	0.90 kg	-27 %	15 %	37 %	27 %
Average	1.54 kg	0.48 kg	-68 %	-19 %	41 %	14 %

* Corrected yield increase – performance contribution of water circulation, excluding active solar still performance contribution

The active solar still produced less condensate yield and converted less useful energy when compared to the reference still which showed higher condensation rates (1.54 kg and 0.48 kg, respectively) and higher energy utilisation (41 % and 14 %, respectively); there was low useful energy available for condensation in the active solar still.

The temperature driving force between the water and cover surface temperature profiles were shown by Figure 45. For most of the day, the condensation ability of the single pane glass and double pane glass existed – peaking during midday at 19°C and 21°C, respectively. The lack of evaporation was created by the insulation effect of the double pane glass and the water circulation in the active solar still – water circulation

meant the water body of the active still was limited in converting absorbed solar radiation or latent energy into evaporation energy.

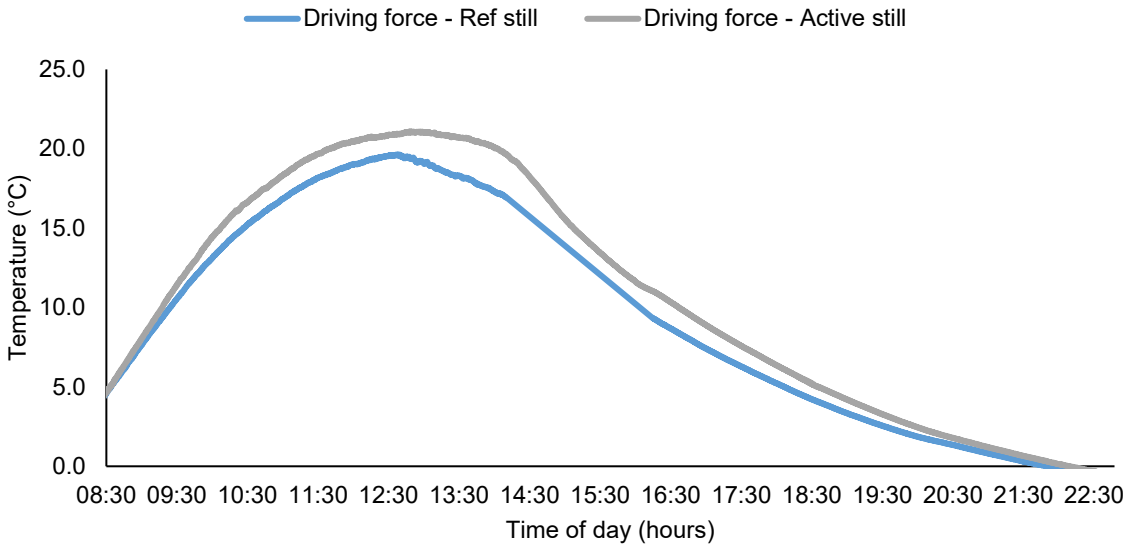

Figure 45: Dependency of condensate production on the driving force for evaporation

The water circulating mode in the active solar stills created a scenario where evaporation became limited, and the insulation effect of the cover surface was too strong to create a driving force for condensation. This significantly affected condensation and energy performance of the active solar still. The water circulation mode didn't meet the objective of reducing the back wall temperature. The water circulation mode was excluded from further experimentation which meant Objective 5(b) (reduce energy accumulation of the back wall) was not met.

4.4.3.2 Circulation mode – Humid Air

Before the humid air circulation mode was fully implemented on an active solar still with a heat exchanger, a trial run with no humid air circulation was tested – due to the failure of the active solar still under water circulation mode to reduce the back wall temperature. This observation suggested that the humid air circulation mode could also cause a performance deterioration in the active solar still.

Figure 46 showed the cover surface and water temperature profiles of the reference and active solar stills on the humid air trial run.

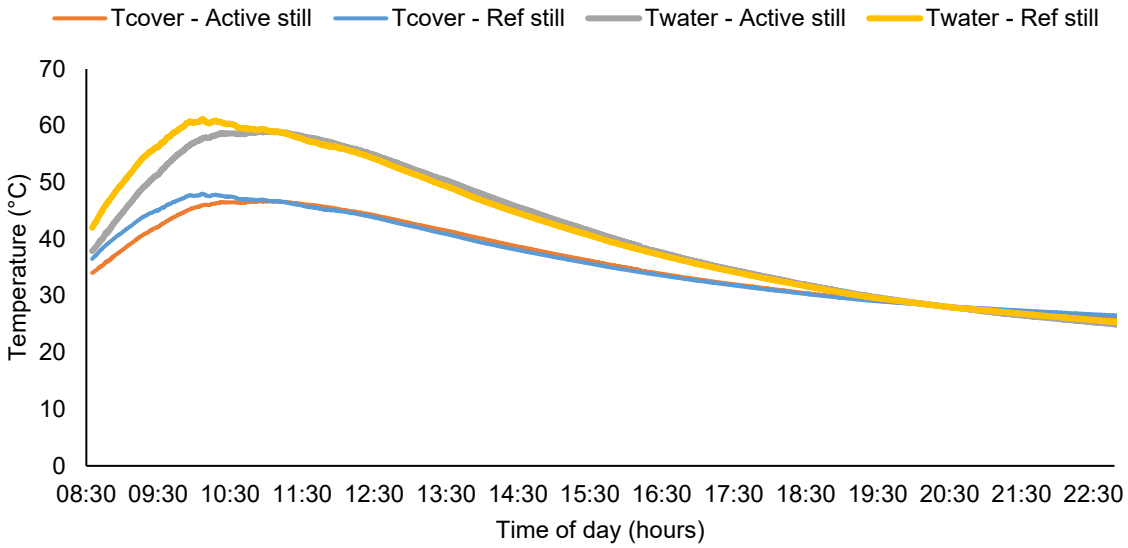

Figure 46: Cover surface and water temperature profiles; sensor 12 referenced from Figure 21

The reference still and active solar still showed similar cover surface and water temperature profiles – with the cover surface and water temperatures peaking at 48 °C and 61 °C, respectively. Simultaneously, Figure 47 showed the heat sink heat exchanger inlet air accumulated energy [during the day] while the outlet air remained steady at 30 °C – this indicated that energy was either lost through the heat exchanger body or as condensate.

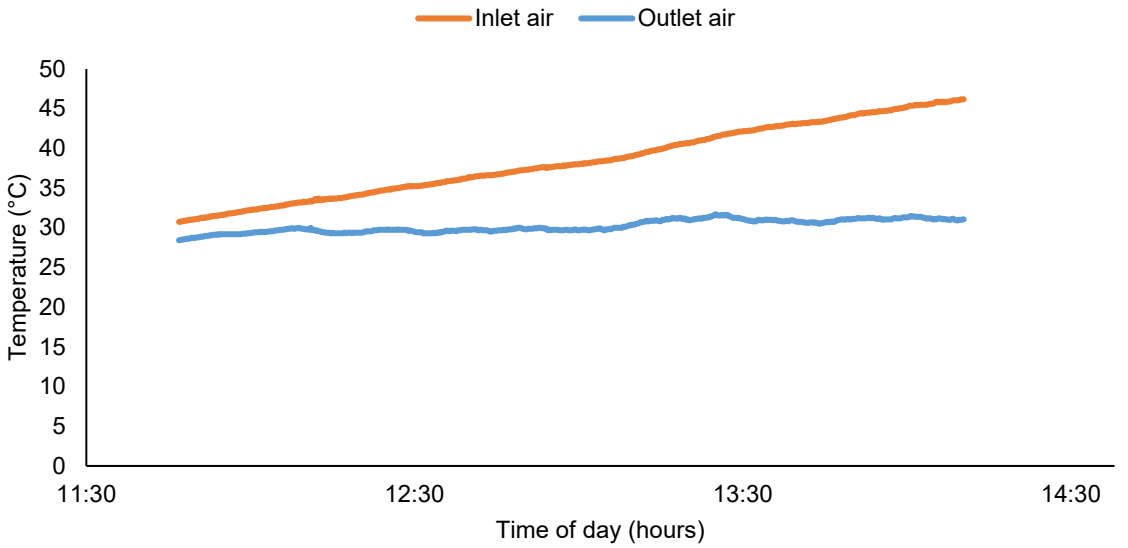

Figure 47: Heat sink heat exchanger inlet and outlet air temperature profiles; sensor 12 referenced from Figure 21

The yield profiles in Figure 48 showed that condensate lost from the heat exchanger was 6 % compared to the condensate lost from active solar still – 0.02 kg of condensate was recovered from the heat exchanger. The heat exchanger converted a minimal amount of humid air energy into condensate energy indicating poor performance of the heat exchanger setup – with no form of circulation.

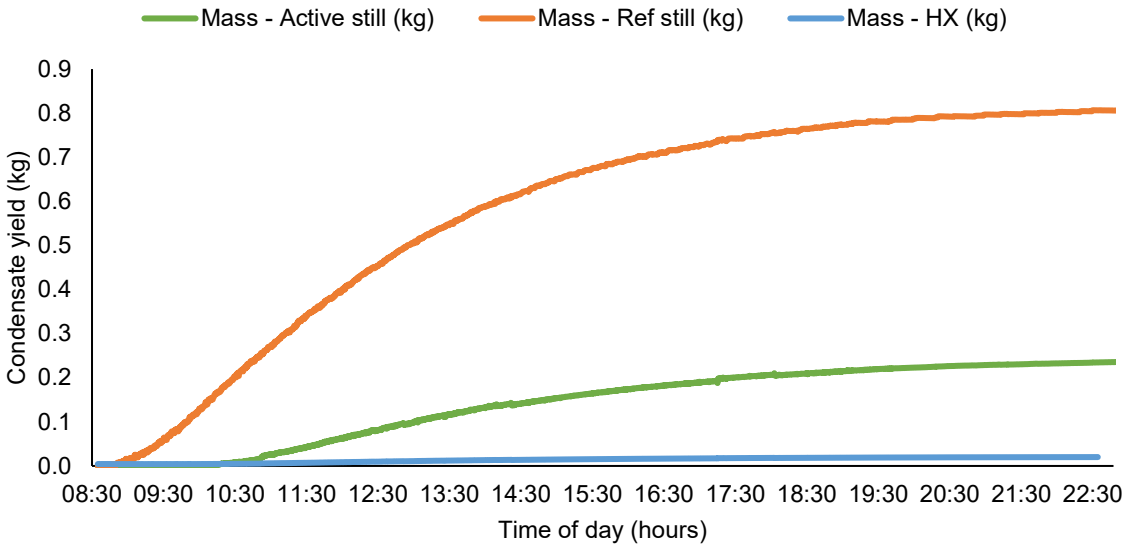

Figure 48: Yield profiles of humid air trial run (no form of circulation)

The low conversion of the heat exchanger meant that the major loss of energy was through the heat exchanger body to ambient, as shown in Figure 49. The 2 °C and 3 °C increase of ambient temperature around the heat exchanger and the back wall, respectively, indicated the absorption of energy lost from the heat exchanger.

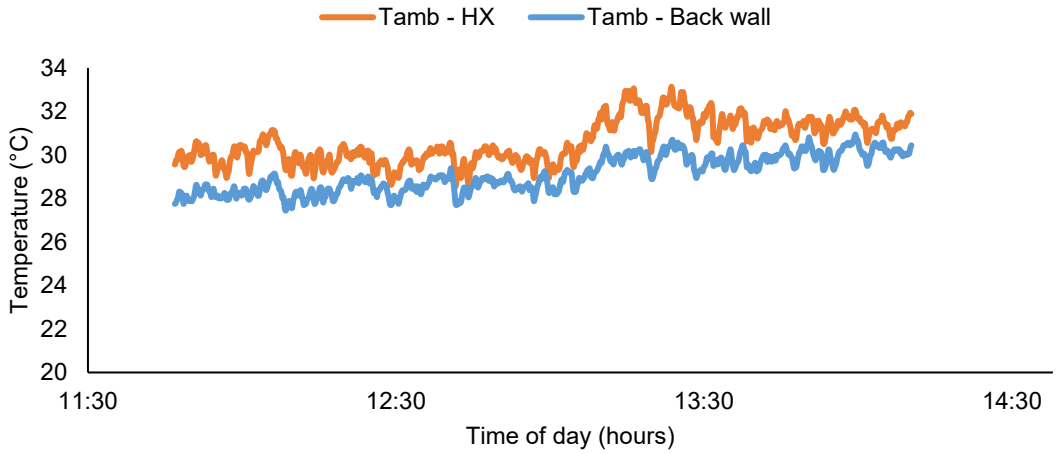

Figure 49: Ambient temperature profiles of humid air trial run (no humid air circulation)

In this scenario, implementing humid air circulation will increase heat losses across the heat exchanger (due to the heat exchanger's low energy conversion rate) and reduce the potential energy conversion of the active solar still – a water circulation scenario of the active solar still with no heat exchanger resulted in 0.90 kg of condensate collected (Table 26) while fitting the heat exchanger onto the active solar still with no form of circulation reduced the condensate collected to 0.33 kg (Figure 48). The humid air circulation mode was excluded from further experimentation.

4.4.3.3 Circulation mode – Humid Air and Water

Due to the poor performance of the water circulation (Figure 44 of 4.4.3.1) and the anticipated poor performance of the humid air circulation (Figure 48 of 4.4.3.2), experiments on the humid air and water circulation mode were not conducted. The lack of field testing of the active solar stills with external heat condensers attached meant that Objective 2 and Objective 3 were not met.

4.4.4 Life Cycle Cost Analysis

The energy conversion of the active solar still with humid air and water circulation would compromise the overall condensate collection rate of the active solar with no return on investment seen on the fluid flow equipment. The life cycle cost analysis was excluded due to the poor performance of the active solar stills.

Table 27 and Table 28 showed the bill of materials for the reference still and the active solar still (water circulation mode), respectively. The total fabrication cost, including labour, was R 1,810 for the reference still and R 2,523 for the active still. The VAT exclusive cost was reported as the initial cost in Table 29.

Table 27: Bill of materials for the reference solar still

Component	Material	UOM	Quantity	Rand/unit	Cost (R)	%
Walls	Extruded polystyrene	m^2	0.58	166.80	96.74	5 %
Cover surface	Single pane glass	m^2	0.51	259.00	131.69	7 %
Absorber	PVC Textile	m^2	1.01	34.66	35.09	2 %
Insulation	Extruded polystyrene	m^2	0.58	166.80	97.14	5 %
Wooden body	ShutterPly	m^2	1.38	113.63	156.90	9 %
Metal frame	Aluminium	m	10.1	56.77	573.40	32 %
Sundries	Various		1	418.82	418.82	23 %
Subtotal					**1,509.80**	
Labour		hour	2	150.00	300.00	17 %
Total (excl. VAT)					**1,809.80**	**100 %**
Total (incl. VAT)					**2,081.27**	

*Life cycle of the reference solar still is taken as a range between 5 and 10 years

Table 28: Bill of materials for the active solar still

Component	Material	UOM	Quantity	Rand/unit	Cost (R)	%
Reference solar still cost (excl. labour)	Various	–	–	–	1,509.80	38 %
Cover surface (ref still)	Single pane glass	m^2	0.51	259.00	-131.69	–
Cover surface (active still)	Double pane glass	m^2	0.51	518.00	263.37	10 %
Water pump	Various	unit	1	200.00	200.00	8 %
Sundries (ref still)	Various		1	418.82	-418.82	–
Sundries (active still)	Various		1	500.00	500.00	20 %
Subtotal					**1,922.60**	
Labour		hour	4	150.00	600.00	24 %
Total (excl. VAT)					**2,522.60**	**100 %**
Total (incl. VAT)					**2,900.99**	

*Life cycle of the active solar still is taken as a range between 5 and 10 years

The active solar still and reference solar still were assumed to have the same lifespan as both stills were continuously exposed to ambient conditions and high operating temperatures of the solar stills. Although the active solar still had multiple moving parts which might need frequent maintenance, frequent maintenance compared to complete still replacement would not affect the lifespan of the active solar still. The only difference would be the increased maintenance and salvage costs of the active solar still.

Table 29 compared the economic feasibility of the best performing active and reference solar stills, assuming a lifespan scenario of 10 years.

Table 29: Life cycle cost comparison of the reference and active solar stills

	Reference solar still	Active solar still
Unit cost of distilled water		
Annualised cost (R/l)	**0.52**	**2.20**
Area available for condensation (m^2)	*0.51*	*0.51*
Annualised cost per unit area	*1.02*	*4.33*
Still performance		
Average Productivity ($L.day^{-1}$)	2.50	0.82
Daily efficiency (%)	36.0	14.0
Interest rate (%)	11.75	11.75
Lifecycle (years)	10.0	10.0
Annual runtime (%)	75.0	75.0
Annual water productivity (L)	684	224
Life cycle cost analysis		
Initial cost (P)	**R 1,810**	**R 2,523**
Capital recovery factor (CRF)	0.175	0.175
First annual cost (FAC)	R 317	R 441
Sinking fund factor (SFF)	0.058	0.058
Annual salvage value (ASS)	R 9.10	R 10.8
Annual maintenance cost (AMC)	R 47.55	R 66.15
Annual cost (AC)	**R 355**	**R 494**
Market price of distilled water	**R 5.20/l**	**R 22.00/l**

The annualised cost per litre was R 0.52/l and R 2.20/l for the reference and active solar stills, respectively, where the annualised cost for the active setup was ~1.4 times more expensive than the reference solar still. This increased cost was due to the active still having a lower productivity level than the reference still but with increased capital and operational costs. The items used to convert the reference still into an active still were reasonably cost-effective. However, frequent maintenance increased the operational cost of the active solar still compared to the reference still by ~R 140 per

year. A 40 % cost increase and a 67 % drop in condensate productivity made the active solar still with water circulation mode unfavourable for water production. While the annualised water cost for the active solar still of R 2.20/l was cheaper than market rates of R 4.40/l, it was not cheaper than the municipal rate of 0.67 c/l. The active solar still did not meet Objective 4.

By varying the lifespan between 5 and 10 years, the cost per litre range for the active still was R 3.32/l to R 2.20/l while it was R 0.78/l to R 0.52/l for the reference still. The reference still fell in the R 0.20/l to R 2.00/l range indicating it was an economically feasible method of water production (Esfahani, et al., 2011; Malaiyappan & Elumalai, 2015; Tiwari, et al., 2008; Ibrahim, et al., 2015; Kumar, et al., 2016). The active solar still produced a respectable cost range but was still economically unfeasible. The full range of the cost per litre of water was shown in Figure 50, clearly showing the effect of extending the lifespan of the still beyond the 5-to-10-year range.

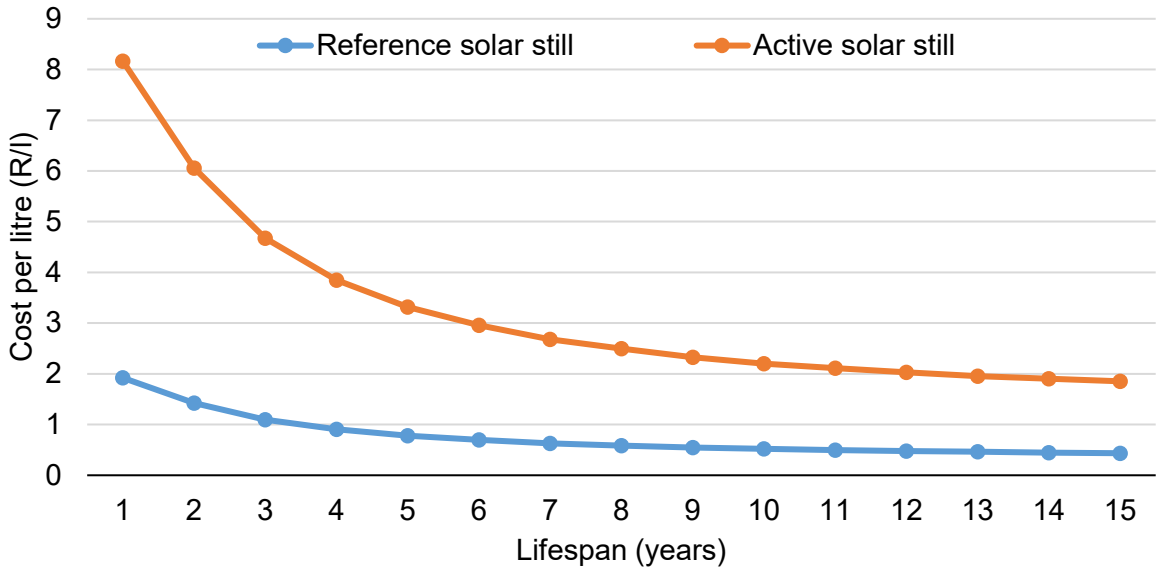

Figure 50: Annualised unit cost per litre range of water production

At all times, the cost per litre for the reference still was cheaper than the cost per litre for the active still. Extending the lifespan from 1 to 5 years for the reference and active stills gave a 59 % price reduction from R 1.92/l to R 0.78/l for the reference still and from R 8.17/l to R 3.32/l for the active still. From 5 to 10 years, a price reduction of 34 % was seen, and from 11 to 15 years, the price reduction was 16 %. There is great value in improving the lifespan of the solar stills beyond 10 years, but any efforts towards this should be weighed against the cost investment required and the potential

productivity improvements. As a precaution against diminishing returns, the lifespan should be capped at 15 years; at a lifespan of 100 years, the cost of water is R 0.36/l for the reference still and R 1.53/l for the active still. This translates to a 17 % price drop for the active still at the cost of adding 85 years to the lifespan compared to a price reduction of 77 % seen for a 15-year lifespan.

4.4.5 Active Solar Still Comparison

Table 30 summarised the results of the active solar still experiments. Table 30 included the total surface area of the active solar still for analyses, i.e., the active solar still with its respective external condenser. The stand-alone area of the still was 0.51 m^2 while the heat sink and the 12.7 mm tube bank surface areas were 0.171 m^2 and 0.0481 m^2, respectively.

Table 30: Comparison of the active solar still data analyses

Case	Mode of circulation	Total still surface area (m^2)	Initial cost (R)*	Yield rate ($L.day^{-1}$)	Yield per area ($L.day^{-1}m^{-2}$)	Energy efficiency (%)	Cost per litre (R/l)
				Max	Max		
Reference still	No circulation	0.51	1,810	2.50	4.91	36.0	0.52
1	Water	0.51	2,523	0.82	1.61	14.0	2.20
2	Humid air	0.56	Excluded from experimentation				
3	Humid air and water	0.56	Excluded from experimentation				
Benchmark solar still	No circulation	0.51	1,945	1.30	2.40	26.0	1.25

* Initial cost is dependent on the mode of circulation, i.e. Case 1 initial cost has water pump cost included and labour cost increased by two hours

Figure 51 showed the performance comparison of the active solar, including the average energy efficiency. The active solar stills were compared across the cover surface area, initial cost, maximum yield per unit area, energy efficiency, and the annualised water production cost as shown in Table 30. The benchmark solar still (Marais, 2018) was included in Table 30 for a complete comparison.

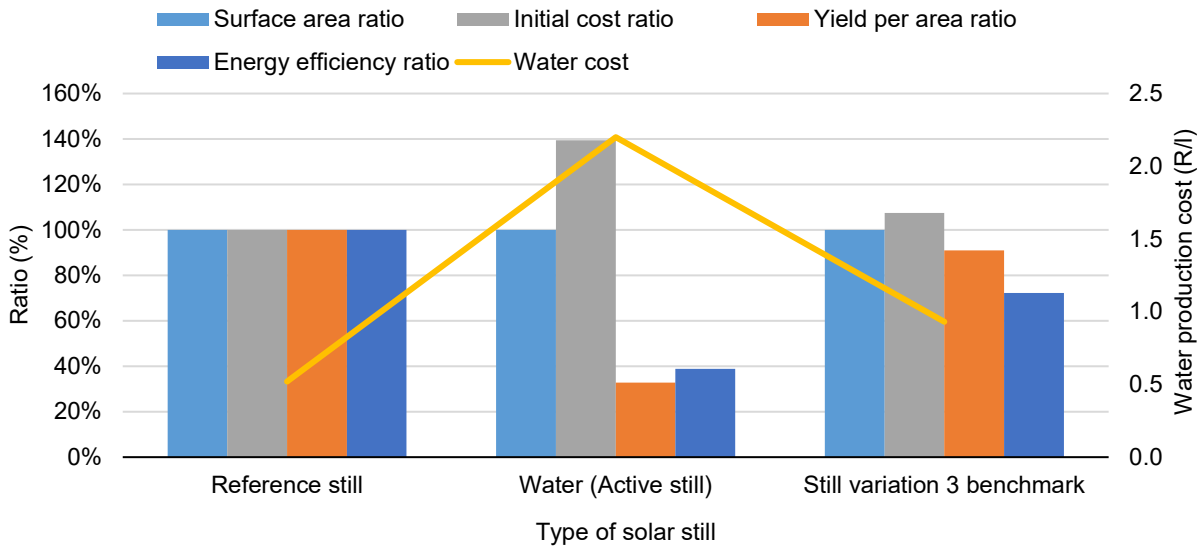

Figure 51: Performance analysis of the active solar still

Using the reference still as the baseline, the active solar still used 100 % of the surface area, was 40 % more costly, and managed a 33 % yield per area performance and a 40 % energy efficiency performance. The water production cost of the active solar still was the most expensive annualised cost at R 2.20/l, ~R 1.70/l more expensive than the baseline.

The baseline also performed better than the benchmark solar still; the benchmark was 7 % more expensive, 8 % less productive, and 30 % less energy efficient. The water production cost for the benchmark solar still was R 0.93/l; ~R 0.40/l more expensive than the baseline.

The reference solar still was the best performing design of a small-scale solar desalination of water.

5. Conclusions and Recommendations

5.1 Still Performance

The polystyrene solar stills were used to compare the performance between a PMMA cover surface and the single and double pane glass cover surfaces. The single and double pane glass cover surfaces produced condensate at a rate of 4.58 $L.day^{-1}.m^{-2}$ and 2.38 $L.day^{-1}.m^{-2}$, which was 275 % and 95 % better than the PMMA surface (1.22 $L.day^{-1}.m^{-2}$), respectively. The thin film condensation of the glass panes meant more solar radiation entered the basin, a minimal amount of condensation was lost from drop back into the still, and less energy lost through the glass cover. The cost comparison also favoured the glass panes, a cost of R 259 per m^2 for the single pane glass and R 518 per m^2 for the double pane glass compared to R 974 per m^2 for the PMMA. Accounting for a spare glass cover, the single and double pane glass cover surfaces was approximately 47 % cheaper than the PMMA. The double pane glass was the better option as it outperformed the PMMA and was more energy efficient than the single pane glass (4 % higher water temperatures than the single pane glass). The double pane glass cover surface successfully met all the objectives of the cover surface experiments.

The heated water bath experiments characterised the performance of the heat sink and tube bank heat exchangers according to the condensate recovery, energy efficiency, convection cooling mode, and cost. The heat sink, with a fan attached to imitate a forced convection cooling system, was used as the baseline. The baseline performed twice better than under natural cooling mode; forced convection produced more condensate than natural convection due to the high temperature gradient maintained between the humid air and the condenser surface.

The 9.5 mm tube bank performed at 44 % and 67 % maximum yield capacity under natural cooling and forced cooling, respectively, while only using 28 % of the baseline surface area. The 12.7 mm tube bank used 37 % of the baseline area and performed at 53 % and 69 % maximum yield capacity for the natural and forced cooling cases, respectively.

This showed that both sets of tube banks gave higher condensate yields across a smaller surface area. The effect of the forced convection scenario increased condensation rates by 52 % and 30 % for the 9.5 mm tube bank and the 12.7 mm tube bank, respectively. The 9.5 mm tube bank under forced cooling performed better than the 12.7 mm tube bank under forced cooling when compared on a yield per surface area basis. The 9.5 mm tube bank performed 2.4 times better than the baseline while the 12.7 mm tube bank performed 1.8 times better.

On an energy basis, the heat sink had an energy efficiency of 5 % for the natural cooling case and 12 % energy efficiency for the forced cooling case. The forced convection cooling made more energy available (5,233 vs 4,622 kJ) and more energy was lost as condensate (499 vs 226 kJ), leading to higher yields; this was also observed for the tube bank. The 9.5 mm tube bank recorded an energy efficiency of 1.9 % and 2.8 % for the natural and forced cooling mode, respectively. The 12.7 mm tube bank also recorded an energy efficiency of 4 % for the natural and forced cooling modes. For the tube bank heat exchanger, the cooling mode had no effect on the efficiency performance of the tube bank. Although the efficiency performance of the tube banks was lower than the heat sink performance, the tube bank experiments made more energy available into the system compared to the heat sink experiments; 6,580 kJ for the 9.5 mm tube bank and 6,171 kJ for the 12.7 mm tube bank compared to 5,568 kJ for the heat sink. On an overall heat transfer coefficient basis, the 9.5 mm tube bank under forced cooling showed better overall heat transfer (~3 times better) which was surprising given that the 12.7 mm tube bank had showed more consistent and higher heat transfer rates throughout the tube banks experiments.

The heat sink and the 12.7 mm tube bank heat exchangers, both under forced cooling, were recommended for experimentation on the active solar still. Although the 9.5 mm tube bank was not recommended, preliminary testing on the active solar still showed that the 12.7 mm tube bank maintained a superior performance over the 9.5 mm tube bank.

The active solar still experiments only tested the water circulation mode due to the anticipated poor performance of the humid air circulation mode and the humid air and water circulation mode – low condensate recovery and increased energy losses if

humid air fluid circulation was enabled. Under the water circulation mode, evaporation was limited and severely reduced the condensation ability of the solar still – 1.61 $L.day^{-1}.m^{-2}$ of condensate was produced on average. The energy efficiencies dropped from 36 % in the reference solar still case to 14 %. This confirmed the dominating effect that the absence of evaporation had in the water circulation scenario.

The reference solar still also performed better than the benchmark solar still (Marais, 2018). The annualised production cost of the reference solar still was ~58 % cheaper than the still 3 benchmark (R 0.52/l and R 1.25/l, respectively) and 40 % more energy efficient. The reference still gave the best heat and mass dynamics for a basin solar still.

While the reference solar still originally had a performance advantage over the active solar still, performance of the active solar still continued to drop off as the external condenser was fitted and circulation modes were changed between water circulation mode and humid air circulation mode. The external condenser drew a substantial amount of energy from the basin still, only managing to convert a small portion into condensate – the external condenser wasted too much heat energy. Additionally, the insulation effect of the double pane glass on the active solar still meant less energy was lost as condensate than could have been realised if a single pane glass was used.

5.2 Cost Analysis

The cost analysis considered the still production cost, the labour used, the annual production cost, and the annual still productivity to calculate the annualised unit cost per litre of distilled water for the best performing reference still and active solar still cases.

The lifespan used for the reference still and active still (water circulation) was assumed to be between 5 and 10 years, the interest was 11.75 %, and the annual still runtime was assumed at 75 %. The cost difference between the reference still and the active still was the labour involved and the devices used to enable fluid flow; the reference case and active case cost R 1,810 *(excl. VAT)* and R 2,523 *(excl. VAT)*, respectively. With a daily condensation rate of 2.86 $L.m^{-2}$ for the reference still and 0.94 $L.m^{-2}$ for

the active still, the annual cost was R 355/l for the reference still and R 494/l for the active still. The cost per litre range for the reference still and the active still was R 0.78/l to R 0.52/l and R 3.32/l to R 2.20/l, respectively. The reference still range represents a feasible method of water production. Even as the active solar still fell in the economically unfeasible cost range – it achieved its target by being cheaper than water market rates of R 4.40/l; the water production cost didn't meet the municipal water rate of 0.67 c/l. All other financial information is shown in Table 29.

5.3 Recommendations

Although the basin solar still outperformed the active fluid flow version, it is recommended to retry the active fluid flow experiments with several operational and design changes suggested below.

It would be beneficial to investigate the active solar still under seasonal effects in future research. This is because seasonal experiments were not run in this research and Pretoria's weather patterns continue to change from the last few years, most likely due to climate change. Understanding future weather patterns might give insights into useful features the solar stills should be equipped with.

The cost per litre range of the active solar still was higher than the reference still but was not far off from the feasible range. One of the levers that can be used to improve this cost factor is to improve the lifespan of the active still beyond five years but not more than 15 years. This can be done through a redesign of the active solar still and the use of more durable, cost-effective material. The cost of the still can also take a holistic perspective by including the positive effect of a reduced environmental burden from using a renewable source of energy. This will give an accurate impact of the solar still beyond an immediate Rand value.

It would be beneficial to investigate the trade-off between adding more external condenser area and increasing energy loss in the still. There exists an optimum where the condensation area used will allow the maximum latent energy to be lost without sacrificing overall still performance.

Using a process control mechanism across the active solar still could optimise performance and extend the operational lifecycle of the solar still. The control mechanism would consider abnormal operations (start-up and shutdown of fan and water pump) and normal, steady state operations according to the time of day and process conditions (such as solar radiation intensity, relative humidity, and water temperature).

The active solar still investigations can be enhanced by performing an exergy analysis in addition to the energy analysis. The exergy analysis will determine potential areas of improvement with emphasis on energy flow and conversion, and material usage. This will put the focus on converting more available energy into useful energy in addition to implementing an energy recycle process.

It is recommended to investigate the corrosion effect of fluid flow across the external heat exchangers. Understanding the effectiveness of the heat exchanger while exposed to corrosion could help mitigate against, or indicate poor performance, as well as help improve the lifespan or maintenance frequency of the active still.

It is recommended to use big data tools such as PowerBI or Qlik to develop a deeper understanding of the datasets. Using a visualisation tool like PowerBI could give a complete view of the system and allow hidden correlations to be discovered. This could be very valuable in the redesign and optimisation of the active solar still.

References

Abdallah, S., Badran, O. & Abu-Khader, M., 2008. Performance evaluation of a modified design of a single slope solar still. *Desalination,* Volume 219, pp. 222-230.

Ahsan, A. et al., 2013. Life cycle cost analysis of a sustainable solar water distillation technique. *Desalination and Water Treatment,* Volume 51, pp. 7412-7419.

Ali, H., 1993. Effect of forced convection inside the solar still on heat and mass transfer coefficients. *Energy Conversion and Management,* 34(1), pp. 73-79.

Bar-Cohen, A. & Rohsenow, W., 1984. Thermally optimal spacing of vertical, natural convection cooled, parallel plates. *Journal of Heat Transfer,* 106(1), pp. 116-123.

Bhardwaj, R., ten Kortenaar, M. & Mudde, R., 2013. Influence of condensation surface on solar distillation. *Desalination,* Volume 326, pp. 37-45.

Bhardwaj, R., ten Kortenaar, M. & Mudde, R., 2015. Maximised production of water by increasing area of condensation surface for solar distillation. *Applied Energy,* Issue 154, pp. 480-490.

Brooks, M. et al., 2015. SAURAN: A new resource for solar radiometric data in Southern Africa. *Journal of Energy in Southern Africa,* Volume 26, pp. 2-10.

Çengel, Y. A. & Ghajar, A., 2015. *Heat and Mass Transfer.* 5th ed. Singapore: MCGraw-Hill Education (Asia).

Checkers, 2021. *Bottled water.* [Online] Available at: https://www.checkers.co.za/c-2276/All-Departments/Drinks/Bottled-Water [Accessed 19 March 2021].

City of uMhlathuze, 2021. *City of uMhlathuze tariffs.* [Online] Available at: https://www.umhlathuze.gov.za/images/TOC_2022.pdf [Accessed 9 October 2021].

Dehghan, A., Afshari, A. & Rahbar, N., 2015. Thermal modelling of exergetic analysis of a thermoelectric assisted solar still. *Solar Energy,* Volume 115, pp. 277-288.

Emad, A., 2014. Evaluation of single slope solar still integrated with evaporative cooling system for brackish water desalination. *Journal for Agricultural Science,* Volume 6, pp. 48-58.

Esfahani, J., Rahbar, N. & Lavvaf, M., 2011. Utilisation of thermoelectric cooling in a portable active solar still - an experimental study on winter days. *Desalination,* pp. 198-205.

ESMAP, 2020. *Global photovoltaic power potential by country,* Washington, DC: World Bank.

Estahbanati, M. et al., 2016. Theoretical and experimental investigation on internal reflectors in a single-slope solar still. *Applied Energy,* Volume 165, pp. 537-547.

Farooquee, A., 2017. *Revisiting the rural energy challenge in developing countries.* [Online] Available at: https://jia.sipa.columbia.edu/online-articles/revisiting-rural-energy-challenge-developing-countries [Accessed 22 March 2021].

Fath, H. & Elsherbiny, S., 1993. Effect of adding a passive condenser on solar still performance. *Energy Conversion and Management,* 34(1), pp. 63-72.

Fath, H. & Hosny, H., 2002. Thermal performance of a single-sloped basin still with an inherent built-in additional condenser. *Desalination,* Volume 142, pp. 19-27.

Feilizadeh, M. et al., 2016. Effects of water and basin depths in single basin solar stills: An experimental and theoretical study. *Energy Conversion and Management,* Volume 122, pp. 174-181.

Feilizadeh, M. et al., 2017. Optimisation of geometrical dimensions of single-slope basin-type solar stills. *Desalination,* Volume 424, pp. 159-168.

Fernández, J. L. & Chargoy, N., 1990. Multi-stage, indirectly heated solar still. *Solar Energy,* 44(4), pp. 215-223.

GreenCape, 2019. *Water: market intelligence report 2019.* [Online] Available at: https://www.greencape.co.za/assets/Uploads/WATER-MIR-2019-WEB-01-04-2019.pdf [Accessed 17 March 2021].

Grimshaw, D. & Lewis, S., 2010. *Solar power for the poor: facts and figures.* [Online] Available at: https://www.scidev.net/global/features/solar-power-for-the-poor-facts-and-figures-1/ [Accessed 22 March 2021].

Hassan, H. & Abo-Elfadl, S., 2017. Effect of the condenser type and the medium of the saline water on the performance of the solar still in hot climatic conditions. *Desalination,* Issue 417, pp. 60-68.

Ibrahim, A., Allam, E. & Elshamarka, S., 2015. A modified basin type solar still: experimental performance and economic study. *Energy,* Volume 93, pp. 335-342.

Ibrahim, A. & Elshamarka, S., 2015. Performance study of a modified basin type solar still. *Solar Energy,* Issue 118, pp. 397-409.

Jamil, B. & Akhtar, N., 2017. Effect of specific height on the performance of a single slope solar still: an experimental study. *Desalination,* Volume 414, pp. 73-88.

Jones, A., Lackey, L. & Lindsay, K., 2014. Effects of wind and choice of cover material on the yield of a passive solar still. *Desalination and Water Treatment,* 52(1-3), pp. 48-56.

Kabeel, A., Omara, Z. & Essa, F., 2014. Enhancement of modified solar still integrated with external condenser using nanofluids: An experimental approach. *Energy Conversion and Management,* 46(4), pp. 493-498.

Khalifa, A., Al-Jubouri, A. & Abed, M., 1999. An experimental study on modified simple solar stills. *Energy Conversion Management,* Volume 40, pp. 1835-1847.

Klöckner, W. & Büchs, J., 2011. *Comprehensive biotechnology.* 2 ed. s.l.:Pergamon.

Ko, J. et al., 2017. Hydrophilic surface modification of poly(methyl methacrylate)-based ocular prostheses using poly(ethylene glycol) grafting. *Colloids and Surfaces B: Biointerfaces,* pp. 158; 287-294.

Kuik, O., Lima, M. & Gupta, J., 2011. Energy security in a developing world. *WIREs Clim Change,* Volume 2, pp. 627-634.

Kumar, A., Anthony, P. & Zaidi, M., 2014. Distillate water quality analysis and economics study of a passive solar still. *Recent Research in Science and Technology,* 6(1), pp. 128-130.

Kumar, R., Esakkimuthu, G. & Murugavel, K., 2016. Performance enhancement of a single basin single slope solar still using agitation effect and external condenser. *Desalination,* pp. 198-202.

Lawrence, S. & Tiwari, G., 1990. Theoretical evaluation of solar distillation under natural circulation with heat exchanger. *Energy Conversion and Management,* 30(3), pp. 205-213.

Mahian, O. & Kianifar, A., 2011. Mathematical modelling and experimental study of a solar distillation system. *Journal of Mechanical Engineering Science,* 225(5), pp. 1203-1212.

Malaiyappan, P. & Elumalai, N., 2015. Single basin and single slope solar still: various basin material thermal research. *J. Chem. Pharm. Sci.,* pp. 48-51.

Marais, H. L., 2018. *Experimental optimisation of a simple basin solar still; improved heat loss management and evaporation rate,* Pretoria: University of Pretoria.

MIT, 2017. *Water security in developing countries.* [Online] Available at: http://12.000.scripts.mit.edu/mission2017/water-security-in-developing-countries/ [Accessed 22 March 2021].

Monowe, P., Masale, M., Nijegorodov, N. & Valisenko, V., 2011. A portable single-basin solar still with an external reflecting booster and an outside condenser. *Desalination,* 280(1-3), pp. 332-338.

Purvis, K., 2016. *11 ideas for urban water security in developing countries.* [Online] Available at: https://www.theguardian.com/global-development-professionals-network/2016/jun/27/11-ideas-urban-water-security-developing-countries [Accessed 22 March 2021].

Rabhi, K. et al., 2017. Experimental performance analysis of a modified single-basin single-slope solar still with pin fins absorbers. *Desalination,* Volume 416, pp. 86-93.

Rahbar, N. & Esfahani, J., 2013. Productivity estimation of a single-slope solar still: theoretical and numerical analysis. *Energy,* Volume 49, pp. 289-297.

Rahmani, A., Boutriaa, A. & Hadef, A., 2015. An experimental approach to improve the basin type solar still using an integrated natural circulation loop. *Energy Conversion and Management,* Volume 93, pp. 298-308.

Reddy, M. et al., 1983. Performance of a multiple-wick solar still with condenser. *Applied Energy,* Volume 13, pp. 15-21.

Sethi, A. & Dwivedi, V., 2013. Exergy analysis of double slope active solar still under forced circulation mode. *Desalination and Water Treatment,* 51(40-42), pp. 7394-7400.

Singh, H. & Tiwari, G., 2004. Monthly performance of passive and active solar stills for different Indian climatic conditions. *Desalination,* Volume 168, pp. 145-150.

Sol Plaatje Municipality, T., 2021. *Kimberley Sol Plaatje municipal rates & tariffs for 2021/22.* [Online] Available at: https://www.kimberley.org.za/kimberley-sol-plaatje-municipal-rates-tariffs-for-2021-22/ [Accessed 9 October 2021].

South African Government, 2015. *Government on water scarcity and drought.* [Online] Available at: https://www.gov.za/speeches/government-water-scarcity-and-drought-13-nov-2015-0000 [Accessed 21 September 2021].

Srivastava, P. & Agrawal, A., 2014. Economics of a high performance solar distilled water plant. *International Journal of Research in Engineering and Technology,* 3(2), pp. 283-285.

Statista, 2021. *Distribution of households in urban and rural South Africa in 2019, by household size.* [Online] Available at: https://www.statista.com/statistics/1114300/distribution-of-households-in-urban-and-rural-south-africa-by-household-size/ [Accessed 9 October 2021].

Tiwari, G., Dimri, V. & Chel, A., 2008. Exergetic analysis of passive and active solar stills,. *International Journal of Exergy - Int J Exergy,* 5(3).

United Nations, 2015. *The human right to water and sanitation - media brief.* [Online] Available at: https://www.un.org/waterforlifedecade/pdf/human_right_to_water_and_sanitation_media_brief.pdf [Accessed 9 October 2021].

Webb, R. & Kim, N., 2005. *Principles of enhanced heat transfer.* New York: Taylor & Madison Group.

Welty, J. R., Rorrer, G. L. & Foster, D. G., 2015. *Fundamentals of momentum, heat and mass transfer.* 6th ed. Singapore: John Wiley & Sons.

Wohlgemuth, N., 2006. *Energy security and renewable energy in least developed countries.* [Online] Available at: https://www.osti.gov/etdeweb/servlets/purl/20840462 [Accessed 22 March 2021].

World Bank, 2017. *Water resources management.* [Online] Available at: https://www.worldbank.org/en/topic/waterresourcesmanagement [Accessed 22 March 2021].

World Bank, 2020. *Solar resource maps of Africa.* [Online] Available at: https://solargis.com/maps-and-gis-data/download/africa [Accessed 1 October 2021].

World Bank, 2021. *South Africa - World Bank data.* [Online] Available at: https://data.worldbank.org/country/south-africa [Accessed 9 October 2021].

Xie, G. et al., 2015. Experimental and numerical investigation on a novel solar still with vertical ripple surface. *Energy Conversion and Management,* Volume 98, pp. 151-160.

Zukauskas, A., 1972. Convection heat transfer in cross flow. In: *Advances in heat transfer.* New York: Academic Press, pp. 93-106.